The Ring Screw

Modelling, Development and Evaluation of a Novel Screw Transmission

E.Heijmink

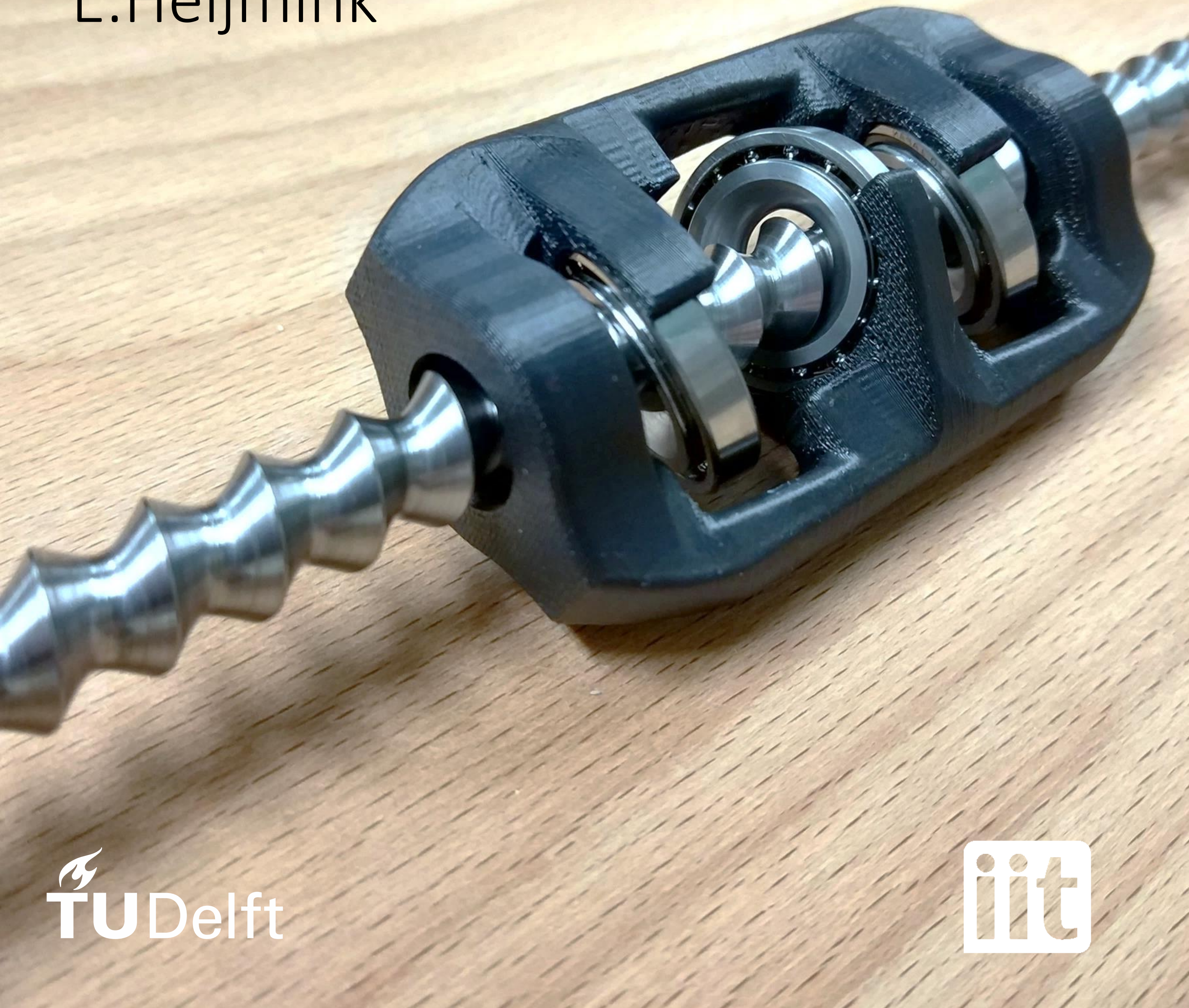

The Ring Screw

Modelling, Development and Evaluation of a Novel Screw Transmission

by

E. Heijmink

to obtain the degree of Master of Science
at the Delft University of Technology,
to be defended publicly on Friday August 10, 2018 at 14:00.

Student number:	4096274	
Project duration:	September 1, 2017 – August 10, 2018	
Thesis committee:	Prof. dr. ir. M. Wisse,	TU Delft, supervisor
	Ir. W. van de Sande,	TU Delft, coach
	Prof. dr. ir. H. Vallery,	TU Delft
	Ir. J.J.M. Driessen,	Italian Institute of Technology
External Supervisor:	Prof. dr. R. Featherstone,	Italian Institute of Technology

This thesis is confidential and cannot be made public until 15th *April 2019.*

An electronic version of this thesis is available at `http://repository.tudelft.nl/`.

TU Delft

Preface

The work presented in this thesis is the result of a collaboration between the Italian Institute of Technology (IIT) the Delft University of Technology. This project started with a casual chat with Roy Featherstone. He directly full enthusiasm explained al ins and out of his newest invention the ring screw. Quickly we both came to the conclusion that this idea should be developed but more importantly, this would make a great master project. With the help of Martijn Wisse, this project became my graduation project.

A lot of knowledge and support on the technical side of the research was available at IIT where in 5 months the main the research, including the development, and experiments, have been performed. The Delft University of Technology offered input, structure and support to make convert this work into the currently presented thesis.

This thesis is submitted for the Master of Science degree in Mechanical Engineering at the Delft University of Technology. The research and its results are presented in a scientific paper that is part of this thesis. The appendices contain more in-depth descriptions of the designs of both the prototypes and experimental setup as well as providing background information to the presented results.

E. Heijmink
Delft, August 2018

Acknowledgments

First, I would like to thank my main supervisor Roy Featherstone for his enthusiasm in working together on the ring screw project. Your high expectations, eye for detail and conviction lifted this project to a new level, while the long conversations about science, technology and history, lifted my general knowledge to the next level. Without your time and dedication this thesis, the results and my enthusiasm about the ring screw would not be the same.

Thanks to Josephus Driessen for the many discussions we had on the project, robotics, and Italians. These discussions led to a faster and deeper understanding of this topics. On top of that your feedback on my mechanical designs and my final thesis led to much better results.

I want to thank my supervisors in Delft, Werner van der Sande, Martijn Wisse and Patrice Lambert for making me able to graduate on this project. Especially the many meetings with Werner made me able to structure my work, make the right decisions and improve the project. Whereas Martijn showed me the strong and weak points of the work very efficiently.

Furthermore, I want to thank all members of the Haptics lab for giving me a graduation home before, in-between and after my 5 month stay in Italy. The great workplace, with the kipknak lunches, climbing sessions, pranks, awesome people and shared struggles made me enjoy working on my thesis, even when there was only writing left. Without this home my graduation would have been tougher and less memorable.

I also would like to thank Elisah Sneep for her patience, support and feedback during the whole project. You were always there for me when I needed it the most

Last but not least I want to thank my parents for their endless support, faith and feedback during my graduation and the whole of my study period.

E. Heijmink
Delft, August 2018

"Simplicity is the ultimate sophistication"

LEONARDO DA VINCI

CONTENTS

I Introduction 1

II The Ringscrew concept 2
- II-A Overview 2
- II-B Theory 2

III Theoretical performance 4
- III-A Selection of performance metrics 4
- III-B Velocity 4
- III-C Maximum thrust force 5
  - III-C.1 Preload 6
- III-D Efficiency 6
- III-E Optimal parameters selection 7

IV Prototype Development 8
- IV-A Functional prototype 8
- IV-B Nut 9
  - IV-B.1 Requirements 9
  - IV-B.2 Nut design concepts 10
- IV-C Selected nut design 11

V Experimental Design 12
- V-A Experimental Method 12
- V-B Experimental Setup 12
  - V-B.1 Setup design 12
  - V-B.2 Setup validation 12

VI Results 14
- VI-A Efficiency 14
- VI-B Thrust force 15
- VI-C Maximum velocity 15

VII Discussion 16
- VII-A Discussion of the results 16
- VII-B Comparison with existing technologies 16
- VII-C Future work 17

VIII Conclusion 17

References 17

Appendix I: Visualisation contact line 19

Appendix II: Screw rod and rings of the functional prototype 20

Appendix III: Details nut design of the functional prototype 23
- III-A Nut for experimental evaluation 23
- III-B Nut for product development 26

Appendix IV: Concepts experimental setup 28

Appendix V: Detailed results bearing friction experiments 31
- V-A Influence of heat on the bearing friction 31
- V-B Bearing friction 31

Appendix VI: Results ring screw velocity experiment 33
- VI-A Resonance of screw rod 33
- VI-B Ring screw operation at 16500 RPM 34

Appendix VII: Extra data efficiency experiments 35

Appendix VIII: Mechanical details experimental setup 46

Appendix IX: Electronics experimental setup 68

The Ring Screw:
Modelling, Development and Evaluation of a Novel Screw Transmission

Elco Heijmink

Abstract— **Rotational electric actuators are the most popular choice for actuation in modern day automation. These actuators are commonly used in combination with a transmission system. In this paper, the development of a new rotational to linear transmission technology, called the ring screw, is described, and its real-world performance is evaluated experimentally. The ring screw consists of freely rotating rings that constrain a rod to a screwing motion. The line contact between those rings and the rod allows for perfect rolling, resulting in a highly efficient screw transmission. The theoretical performance of the ring screw for the metrics *maximal velocity, maximal thrust force* and *mechanical efficiency* are explored analytically. Based on these performance metrics, this paper presents a method to find the optimal design parameters when the desired properties are provided. A prototype was evaluated in a custom developed test rig. In these experiments the ring screw is proven to be able to operate at $15,000RPM$ and deliver $750N$ with an efficiency of 90%. The ring screw operates at more than double the speed possible with other screw transmissions such as a ball screw, with the same high efficiency.**

I. INTRODUCTION

Many actuator technologies have been developed over the last several decades and are now available for modern day robotic designers. These actuator types involve systems such as pneumatic, electromagnetic or fluidic actuators [2]. Of all these actuation types, rotational electric motors are used the most used in modern machines. These motors are mainly used because of their high efficiency, scalability, power density and their ease to control [3].

The optimal performance of these rotational electric motors is typically at high angular velocities with a low torque output [4], whereas most machines require the opposite properties of low angular velocities at high torques[5]. This is especially the case in systems with a limited joint range like robotic systems. The optimal performance is limited by the maximum torque of the actuator, which needs to accelerate the mass of the system, rather than the maximum speed of the actuator. To this extent most rotational electric motors are used in series with a transmission.

Besides the decrease of the speed to increase the torque, transmissions are often used to translate the orientation of the motion. This translation of the motion can be used to gain more design freedom of motor placement. This freedom can be used to improve the looks or protection of the system [6], to reach a desired weight distribution [7], [8] or to generate a linear motion with a rotational actuator [9], [8].

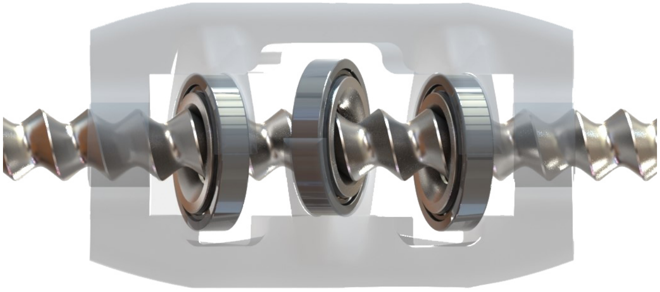

Fig. 1. The ring screw mechanism. The three rings rotate freely inside ball bearings. The nut holding the bearings in place is shown translucent. The rings make a line contact with the rod that allows for perfect rolling.

Driven by this high demand, a large number of transmissions have been developed for rotational electric actuators. However these transmissions still limit the performance of most robotic systems[10]. Whereas the rotational electric actuators have a much higher power density and efficiency than an average mammalian skeletal muscle, most robotic system lose up to half of this power density and efficiency due to imperfect transmission mechanisms [11]. Thus, new transmissions should be developed.

The performance limitation can most clearly be observed in high force applications like in a locomotion task. These systems often have a high power throughput and strongly contribute to the energy losses in the system [12]. Therefore, energy efficiency is often a prominent design criterion for these systems [13], [14], [15], [16]. For these high power applications, harmonic drives and ball screws are commonly selected [5]. Given the typically low efficiency of the harmonic drive, the ball screw seems like the optimal candidate, being the only efficient high power solution. Unfortunately, its limited operation speed will prevent most rotational electric actuators from being used on the most efficient speed, resulting in a lower efficiency as well [8].

Despite the limited operation speed, typically around 4000RPM, a ball screw offers a unique set of benefits compared to other transmissions [8]. In addition to its high efficiency up to 95% [17] it is able to generate high thrust forces of multiple kilonewtons [18]. Ball screws can be made backlash free by preloading the mechanism. Furthermore a high reduction ratio can be achieved through the selection of a small pitch. A mechanism like a ball screw without the speed limitation can therefore create a wide range of new possibilities.

Faculty of Mechanical Engineering, Delft University of Technology, Delft, The Netherlands `E.Heijmink@student.tudelft.nl`

*Patent Pending [1]

This work presents such a mechanism, called the ring screw, based on a theoretical concept developed by Dr. Featherstone. The ring screw mechanism is a newly invented device that performs the same function as a ball screw but with improved theoretically performance. The operating principle of this device is that the screw rod makes contact with freely rotating rings inside a nut, which constrain the rod to make a screwing motion relative to the nut. Unlike any previous mechanism involving rotating rings and a screw rod [19], [20], this new mechanism has been designed, so that the contact between each ring and the rod is a theoretically perfect rolling line contact. It's expected that this mechanism will allow much higher rotational speeds and achieve higher a efficiency than any other screw transmission.

This thesis expands on the work of Dr. Featherstone, with the description of the nut needed to create a functional ring screw. The rings and screw rod described in the previous work allow for a perfect rolling line contact, but the nut, holding the rings while applying a preload wrench, is needed to ensure this perfect rolling line contact.

This thesis aims to identify the real-world performance of this ring screw mechanism. For the evaluation of this performance, a prototype, with representative performance, needs to be developed. Therefore, in this thesis the influence of design parameters on the performance is investigated. Based on this influence, design parameters have been selected and a prototype has been developed. For the measurement of the performance, an experimental setup was designed to evaluate the efficiency of screw transmissions at high speeds. The internal energy loss of this setup is experientially evaluated to allow for accurate efficiency measurements. A wide range of experiments measuring the performance of both the developed ring screw and a standard ball screw were performed using this setup.

The main scientific contribution of this work is the analysis of the theoretical performance, development and detailed testing of the first operational prototype. This is conduced for a new mechanism having significant potential commercial value, in order to determine whether or not the real device lives up to its theoretical potential. The results are useful to prove the correctness of the theoretical background as well as boosts market interest to continue development of the ring-screw mechanism on an industrial scale.

This thesis is structured as follows. In section II, the ring screw concept is described. This section introduces the ring screw, the working principle and the theory behind it. Section III, presents an analytical representation of the theoretical performance of the ring screw. These results give insight into the relation between the design parameters and performance. In section IV, the development of the ring screw prototype used for experimental evaluation is described. Extra focus is given to the development of the required nut. Section V, elaborates on how to measure the performance of the developed prototype. The development of a custom test rig to assess this performance is described. Section VI presents the results of the experimental evaluation of the ring screw prototype. Finally the work is discussed and concluded in sections VII and VIII.

II. THE RINGSCREW CONCEPT

This section describes and explains the working principle and logic behind the ring screw concept. The ring screw concept is preceding this thesis and previously described in an internal invention disclosure written by Dr. Featherstone. For this section only minor edits were made to this internal document. Therefore the whole of this section should be credited to Dr. Featherstone. This section is added as background information necessary to understand the work presented in this thesis. Furthermore equations 11 to 18 and equation 21 were provided by Dr. Featherstone during the thesis work. All other work presented in this thesis is conducted by the first author.

A. Overview

Referring to Figure 1, the invention consists of a rod with a screw thread and a nut consisting of a housing containing a multiplicity of ball bearings, each carrying a ring on its inner race. The housing holds the bearings in fixed positions relative to each other, and the inner surfaces of the rings make contact with the screw thread of the rod. The rings are arranged in such a manner that when the rod is inside the nut each ring makes a perfect rolling line contact with the screw thread of the rod, and the rings collectively constrain the rod so that it can make only a screwing motion relative to the nut. The overall effect is that the rod can make a nearly frictionless screwing motion relative to the nut, thereby allowing a highly energy-efficient conversion between rotary and linear motion. Each ring makes perfect rolling contact with the rod along a straight line fixed in the nut—a different line for each ring. The line contacts can therefore transmit larger forces than point contacts. In order to achieve this property of a perfect rolling line contact, the mating surfaces of the rings and the rod must have a specific shape. Furthermore the rotation axes of the bearings must be both tilted and offset relative to the central axis of the rod by a specific amount as can be seen in figure 2.

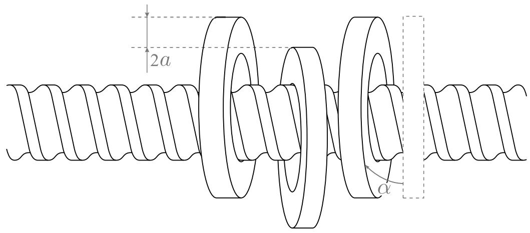

Fig. 2. Schematic representation of the rings screw mechanism. In this figure the ring offset a and tilt angle α relatively to the screw is clearly illustrated.

B. Theory

The ring screw is based on the idea that it is possible for a rotating part to make perfect rolling contact with a part that is making a screwing motion. A perfect rolling contact is one in which the relative velocity of the two contacting surfaces is zero at every point where the two surfaces touch. Thus, in theory, a perfect rolling contact exhibits zero frictional loss and zero friction-related wear.

Figure 3 shows the geometrical aspects of a perfect rolling contact between a ring and a screw rod. In this figure, the line Z_{ring} is the rotation axis of any one ring, the line Z is the central axis of the rod. These lines can be chosen anywhere as long as X is the unique common perpendicular line to Z and Z_{ring}. The point of intersection between X and Z is labelled O, and a Cartesian coordinate frame is placed here with axes X, Y and Z. Likewise, the point of intersection between X and Z_{ring} is labelled O_{ring}, and a Cartesian coordinate frame is placed here with axes X_{ring}, Y_{ring} and Z_{ring}, the axis X_{ring} being on the same line as X. The position of the ring relative to the rod is characterized by an offset distance a measured from O to O_{ring} and a tilt angle α measured about X in the direction shown. Note that O_{ring} marks the geometrical centre of the ring. Each ring in the nut will have a different O_{ring}.

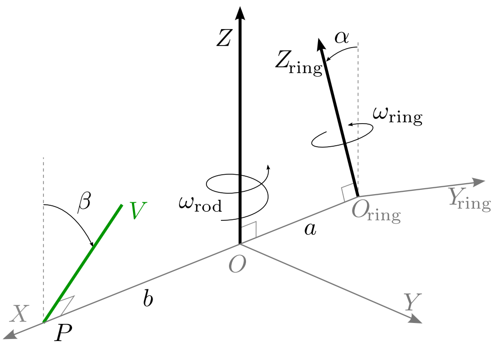

Fig. 3. Geometry of perfect rolling contact between a screw rod and a ring. Z and Z_{ring} respectively represent the central axis of the screw rod and a ring. The line V in space where perfect rolling between the screw rod and the ring is possible is shown in green.

If the rod is rotating at a rate of ω_{rod}, measured in radians per second, then the linear velocity of any point that moves with the rod is given by the formula

$$\mathbf{v}_{rod}(x,y,z) = \omega_{rod}\begin{bmatrix} -y \\ x \\ h \end{bmatrix} \tag{1}$$

where x, y and z are the coordinates of the point and h is the pitch of the screw thread measured in lead per radian. Likewise, if the ring is rotating at a rate of ω_{ring}, also measured in radians per second, then the linear velocity of any point that moves with the ring is given by the formula

$$\mathbf{v}_{ring}(x,y,z) = \omega_{ring}\begin{bmatrix} -\sin(\alpha)z - \cos(\alpha)y \\ \cos(\alpha)(x+a) \\ \sin(\alpha)(x+a) \end{bmatrix} \tag{2}$$

By equating these velocities, we find that there is a single line in space with the property that the velocities can match at every point along the line. This line is labelled V in Figure3. It intersects the line X at the point P, which is located at a distance b from O; it is perpendicular to X; and it is tilted by an angle β relative to Z, this angle being measured about X in the direction shown, which is opposite to the direction of measurement of α. For equation 1 and 2 to be equal, the five parameters h, a, α, b and β must satisfy the two equations .

$$\tan(\alpha) = \frac{h}{b} \quad \textit{and} \quad \tan(\beta) = \frac{h}{a} \tag{3}$$

and the condition for the velocities to match is

$$\frac{\omega_{ring}}{\omega_{rod}} = \frac{\sqrt{h^2+b^2}}{a+b} \tag{4}$$

Having found the one line in space where perfect rolling contact is possible, the next step is to design the inner surface of the ring and the outer surface of the rod, so that they make contact only along this line. In the case of the ring, the argument proceeds as follows: if the ring rotates about Z_{ring}, and yet always makes contact with the rod along V , then the surface of the ring must be the surface of revolution that is generated by sweeping V in a circle of radius $a+b$ around Z_{ring}. A surface of this kind is a well-known mathematical surface and is called a hyperboloid of one sheet. An example of such a surface is shown in Figure 4(a). The equation describing the inner surface of the ring is

$$x^2_{ring} + y^2_{ring} = (a+b)^2 + \tan^2(\alpha+\beta)\cdot z^2_{ring} \tag{5}$$

where X_{ring}, Y_{ring} and Z_{ring} are coordinates expressed in the coordinate frame located at O_{ring}, $a+b$ is the radius of the surface at its narrowest point, and $\alpha+\beta$ is the tilt angle of V relative to Z_{ring}. One consequence of Eq. 5 is that the design parameters must satisfy $ab > h^2$, which implies $\alpha+\beta < 90\,\text{deg}$, because if $ab = h^2$ ($\alpha+\beta = 90\,\text{deg}$) then the hyperboloid surface collapses to a plane with a hole in the middle, and the thickness of the ring drops to zero.

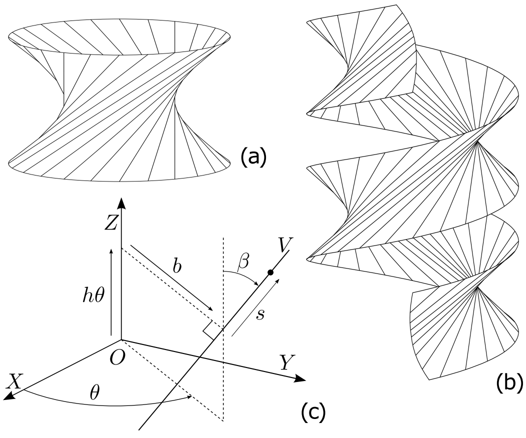

Fig. 4. Examples of a hyperboloid, constructed by sweeping contact line V around the ring axis Z_{ring} in a circle (a) and a helicoid constructed by sweeping contact line V around the ring axis Z in a helix (b), and the definition of the coordinates θ and s used to describe the helicoid surface of the screw rod (c).

Applying the same reasoning to the rod, we can see that the outer surface of the rod must be the surface of revolution that is formed by sweeping the line V around Z in a helix of radius b and pitch h. The resulting surface is called a *oblique open ruled generalized helicoid* . It will be referred to here as a *helicoid*. An example of a helicoid is shown in Figure 4(b). The equation describing this surface is best expressed in terms of a pair of surface coordinates, θ the sweep angle of V, and s the location of a point on V, as shown in Figure 4(c). In terms of θ and s the equation of the surface, expressed in the coordinate frame associated with the rod, is

$$\begin{aligned} x &= b\cos(\theta) - s\sin(\beta)\sin(\theta) \\ y &= b\sin(\theta) + s\sin(\beta)\cos(\theta) \\ z &= h\cdot\theta + s\cos(\beta) \end{aligned} \tag{6}$$

Having now established the conditions for perfect rolling contact, and the necessary shapes of the screw thread in the rod and the inner surface of the ring, Figure 5(left) shows the precise location of the ring and the line of perfect rolling contact relative to the screw rod.

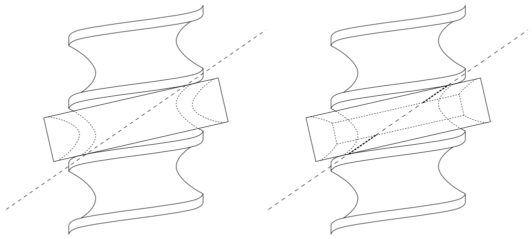

Fig. 5. Relative locations of screw rod, ring and line of perfect rolling contact (left), and cutaway ring making contact along two segments of the line of perfect rolling contact (right)

The upper portion of the line of contact allows the ring to exert a substantial axial force on the rod in the upward direction, and the lower portion allows the ring to exert a substantial axial force in the downward direction. However, the middle portion is not able to transmit substantial axial forces. It is therefore possible to cut away the innermost portion of the ring, as shown in Figure 5(right), thereby restricting the contact to the upper and lower portions of the line of contact, which are shown emphasised in the figure, without significantly reducing the ring's ability to transmit an axial force to the rod.

The purpose of this cut-away is to increase the range of parameters a, b, α, β and h that can be used by making feasible those designs that would not otherwise have worked because the ring does not clear the outer diameter of the screw rod on the opposite side to the line of contact.

III. THEORETICAL PERFORMANCE

The aim of this thesis is to identify the real-world performance of the ring screw mechanism described in the previous section. In order to develop a prototype of the ring screw and so to evaluate its performance, the influence of the design parameters on this performance has to be investigated first. Therefore this section illustrates interconnections between the theoretical transmission performance and design parameters, including geometric parameters, preload force and manufacturing limitations. The result is useful to predict the ring-screw performance in practical applications and therefore be a guideline in parameters selection.

A. *Selection of performance metrics*

Screw transmissions comparable to the working of the ring screw are widely used in industry. These devices include a lead screw, a ball screw and the less common roller screw. Accordingly, the results of this study should be comparable with studies on these devices in order to be able to make relevant claims about its performance. If we look at the properties of the existing screw technologies, it can be observed that they are commonly compared to the following properties. *Efficiency, thrust force (load capacity), operation velocity, cost, lifetime, accuracy* and *backlash* [17], [18], [21]. Table I shows a comparison between existing screw technologies and the expectations of the ring screw for these properties.

TABLE I
COMPARISON OF SCREW TECHNOLOGIES [17], [18], [21]

screw tech.	lead screw	ball screw	roller screw	ring screw
efficiency	$< 50\%$	90%	$< 90\%$	90%
thrust force	low	medium-high	very high	medium
velocity	slow	medium	medium-high	very high
cost	low	medium	very high	medium
lifetime	low	high	high	unknown
accuracy	low	high	high	high
backlash	high	low-medium	low	low

The properties listed in Table I are commonly listed in screw comparisons and therefore considered the most important properties of a screw transmission and therefore most relevant for evaluation in this work. The properties lifetime and accuracy strongly depend on the manufacturing quality while the cost depends on manufacturing quantity. Therefore the comparison of these properties between a fully developed product and a first prototype will yield a biased result. The ring screw has to be preloaded to be able to work, and so will be backlash free by design, this will be elaborated on in subsection III-C.

Concluding, this work will investigate the performance of the ring screw considering the performance parameters *efficiency, maximum thrust force* and *maximum velocity*.

B. *Velocity*

The first performance criterion, needed for comparison of the ring screw with alternative screw transmissions, is the maximum operating velocity. Due to the low amount of moving parts the maximum velocity is only limited by the equipped ball-bearings and the resonance frequency of the screw. The maximum velocity of the equipped ball-bearing is often given by the manufacturer. Using the rotational velocity relation between the rings and the screw we find that the speed limit caused by the ball bearing can be expressed as

$$\omega_{rs,max} = \omega_{bearing,max} \cdot \frac{a+b}{\sqrt{h^2+b^2}} \tag{7}$$

where $\omega_{rs,max}$ is the maximum rotational velocity of the ring-screw, $\omega_{bearing,max}$ is the maximum velocity of the equipped ball-bearing and a, b and h are geometry parameters defined in Section II. Since the maximum bearing velocity is often very high and $\frac{a+b}{\sqrt{h^2+b^2}}$ is always bigger than one, the speed is unlikely to be limited by the equipped ball bearings.

More likely the velocity of the ring-screw is limited by the resonance of the screw rod. This so- called critical speed is a speed limit in all other screw transmissions as well [22], however, these devices are often limited by other factors before resonance becomes relevant. Resonance caused by finite spindle stiffness and inertia can cause damage to the ring-screw itself and its surroundings. Therefore the maximum velocity should not exceed the natural frequency corresponding to the first eigenmode of the spindle. In fact, in most applications, it is advised to stay below approximately 80% of the critical speed as a safety margin to compensate for uncertainness[22].

The natural frequency of a uniform cantilever beam for free vibration can be calculated as follows [23]

$$w_n = K_n \sqrt{\frac{EI}{A\rho L^4}} \tag{8}$$

where w_n is the natural frequency in rad/s, L is unsupported length of the beam, E is the young's modulus, I is the second moment of area, ρ is the mass density and A is the area of the cross-section.

The value K_n depends on the number of the eigenmode and the constraints. Only the first eigenvalue is relevant since it has the lowest resonance frequency by definition. Figure 6 shows the K_1 for three constraint conditions.

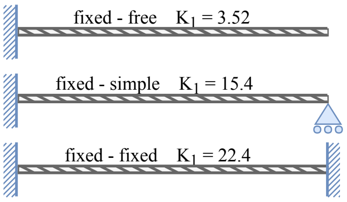

Fig. 6. The three considered screw constraints, where the grey bar represents the screw rod. The K values for the first eigenmode are indicated

The screw spindle can be approximated with a round profile. Therefore $I = \pi/4r^4$ and $A = \pi r^2$ are substituted where r is the inner radius of the screw. This results in

$$w_n = K_n \sqrt{\frac{Er^2}{4\rho L^4}} \tag{9}$$

Equation 9 gives a simplified representation of the critical speed. Both the screw rod is simplified to a straight rod and the effect of the nut on the rod is ignored. Since only the inner portion of the screw rod is considered both the extra stiffness and weight of the screw thread is ignored. It is expected that these two effects will be in the same order of magnitude and so can be ignored. If the nut would be considered the frequency would be lower due to the extra weight of the nut however the attachment of the load adds stiffness increasing the critical speed. Therefore it is expected that these effects can be ignored as well. Hence Equation 9 will give a reliable estimation of the frequency. Furthermore, a safety factor (FoS) of 80% is used as normally done in machine design to compensate for this simplification. Therefore the rotational velocity limit of the ring-screw caused by resonance can be expressed as

$$\omega_{rs,max} = FoS \cdot w_n \tag{10}$$

C. Maximum thrust force

The second performance criteria, needed for comparison of the ring screw with alternative screw transmissions, is the maximum operation thrust force the screw can deliver. To find this maximum thrust force the force at which the performance degrades is investigated. The working of the ring-screw strongly depends on the perfect rolling between the screw rod and the rings. To this extent the only contact has to be on the line defined in section II. If an external force breaks this contact, the perfect rolling cannot be ensured. Therefore the maximum thrust force can be defined as the force where the contact force on this line becomes zero. To find the at which magnitude of the thrust force this contact force becomes zero, the internal force of the mechanism have to be analysed. The ring screw is designed to have a specified contact between the rings and the screw rod, therefore the contacts are well known. The locations of the contacts together with the knowledge that there is no friction at the contacts allows us to get detailed insights on the internal forces of the mechanism. All forces point into into the screw and have to be perpendicular to the contact surface.

The forces that act on this contact line are action in line with the contact normal $\underline{s}$. To find this contact normal $\underline{n}(s)$ we define a point $p(s)$ on the contact line V on a distance s from the X-axis illustrated in Figure 7.

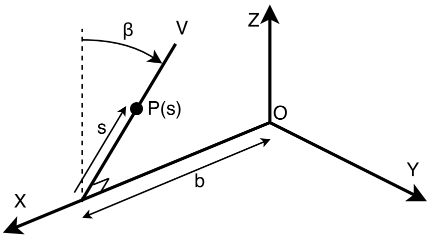

Fig. 7. Simplified description of the hyperboloid surface at $\theta = 0$ to describe of point $p(s)$

Using the coordinate system illustrated in Figure 7 the cartesian coordinates of point $p(s)$ can be found

$$p(s) = \begin{bmatrix} b \\ s \cdot \sin\beta \\ s \cdot \cos\beta \end{bmatrix} \tag{11}$$

To get the contact normal $\underline{n}(s)$ at point $p(s)$ we have to find two lines on the surface at the contact point. The first is line $V(s)$, where the second one is the screw helix $H(s,\theta)$ passing through point $p(s)$ described by equation 6. The derivative of lines $V(s)$ and $H(s,\theta)$ at $\theta = 0$ gives the slope at $p(s)$ of both lines.

$$\underline{V}(s) = \begin{bmatrix} 0 \\ \sin\beta \\ \cos\beta \end{bmatrix}, \qquad \underline{H}(s) = \begin{bmatrix} -s \cdot \sin\beta \\ b \\ h \end{bmatrix} \tag{12}$$

The cross product of these derivatives gives the contact nominal $\underline{n}(s)$ perpendicular to both the contact lines $\underline{V}(s)$ and the screw helix $\underline{H}(s,\theta)$

$$\underline{n}(s) = \underline{V}(s) \times \underline{H}(s) = \sin\beta \begin{bmatrix} h - \frac{ab}{h} \\ -s\cos\beta \\ s\sin\beta \end{bmatrix} \tag{13}$$

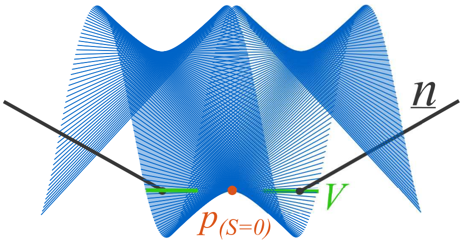

Fig. 8. Visualisation showing a contact normal $\underline{n}$ *(black)* that is perpendicular to both the contact line V *(green)* and the screw helix H *(blue)*. In this example $\underline{n}$ is shown for one ring at $s = 0.8L$ and $s = -0.8L$, with L the half-length of the contact line V.

Only the direction of the contact normal is relevant therefore the factor $\sin(\beta)$ can be dropped. This contact normal always points in to the screw rod ($h - \frac{ab}{h} < 0$). Note that we substituted equation 3 to replace $\frac{\cos\beta}{\sin\beta}$ with $\frac{a}{h}$.

By using the moment arm from the origin to the contact point we can find the spatial force corresponding to this normal.

$$\hat{f}(s) = \begin{bmatrix} \vec{OP} \times \underline{n} \\ \underline{n} \end{bmatrix} = \begin{bmatrix} s^2 \\ s \cdot \cos\beta(h - b(\frac{a}{h} + \frac{h}{a}) \\ -s \cdot h \cdot \sin\beta \\ h - \frac{a \cdot b}{h} \\ -s \cdot \cos\beta \\ s \cdot \sin\beta \end{bmatrix} \tag{14}$$

The contact line V of each ring is symmetrical around the X axis, so the spatial force of one ring is:

$$\hat{f}_{ring}(s) = \hat{f}(s) + \hat{f}(-s) = \begin{bmatrix} 2 \cdot s^2 \\ 0 \\ 0 \\ 2 \cdot (h - \frac{a \cdot b}{h}) \\ 0 \\ 0 \end{bmatrix} \tag{15}$$

1) Preload: To ensure that the rings will keep contact at the desired contact line a preload force is applied. According to equation 15 only linear preload force in the X direction and a torque around this X-axis have to be applied to ensure a correct contact. The relation between this linear preload force (f_{pl}) and torque (T_{pl}) around the axis of this linear preload force torque can be described as

$$T_{pl} = \frac{s^2}{h - \frac{a \cdot b}{h}} \cdot F_{pl} \tag{16}$$

Since the ring screw mechanism will consist of multiple rings on difference sides of the screw, it is interesting to look at the forces created by two rings opposite from each other, like the first two rings of figure 2. We find that the forces create moment around the Z axis and a force along the Z axis in line with the thrust force:

$$\hat{f}(s) + rot_z(\pi) \cdot \hat{f}(s) = \begin{bmatrix} 0 \\ 0 \\ -2sh\sin(\beta) \\ 0 \\ 0 \\ 2s\sin(\beta) \end{bmatrix} \tag{17}$$

The first thing to notice is that the resulting moment and force in Equation 17 cancel out if both halves of the ring (s and $-s$) transmit equal contact forces. Therefore if only preload applied there are no resulting forces. If an thrust force (Z axis) is added the contact force on one halve increased while the other decreases, up till the point where one contact force equals zero. The maximum thrust force (F_T) allowed on one ring before the contact is broken is therefore:

$$\max F_T = \frac{1}{2} \cdot \frac{s \cdot \sin\beta}{h - \frac{a \cdot b}{h}} \cdot F_{pl} \tag{18}$$

This linear dependence between the thrust force and preload suggests that an infinite preload would result in an infinite maximum thrust. However, the preload is limited by the loading limit of the used bearings and material stress of the screw rod as a consequence of the preload.

D. *Efficiency*

The third performance criteria, needed for comparison of the ring screw with alternative screw transmissions, is the efficiency. To define the theoretical efficiency of the mechanism we have to identify the energy losses in the mechanism. These energy losses will mainly occur in moving contacts. The contact between the rings and the rod is by definition of the concept a perfect rolling contact. With the absence of any relative motion, there will be theoretically no friction between these parts. In practice, small deformations and production imperfections will result in an energy loss. Because no practical information is available these energy losses are assumed to be negligible. Moving contacts can be found in the ball bearings as well. Caused by the requirement to transfer both radial and axial forces in a compact design four-point contact ball bearings are used. These bearings induce higher friction than normal radial ball bearings and so this friction cannot be neglected, especially when high radial loads are applied. According to the manufacturer[24]. the friction on the bearings can be estimated by:

$$M_{friction} = f_{fr} \cdot F_{bearing} \cdot \frac{d_M}{2} \tag{19}$$

Where f_{fr} is a friction factor dependant on the type of bearing which is ranging from 0.002 to 0.0035 for the used bearings, $F_{bearing}$ is the radial and axial load on the bearing, and d_M is the mean bearing diameter. To calculate the energy loss, this friction torque should be multiplied by the rotational speed. The loading of these bearings depends on the preload and the thrust force derived by the screw mechanism. The preload will mainly generate a radial load, with a small axial force as a result of the torque. The thrust force will mainly generate an axial load on the bearings with a small radial load caused by the angle of the rings. The loading on the bearings can be calculated using equations 20

$$\begin{aligned} F_{Bearing}^{Radial} &= F_{pl} + F_T \cdot \sin(\alpha) \\ F_{Bearing}^{Axial} &= T_{pl} \cdot \frac{D}{2} + F_T \cdot \cos(\alpha) \end{aligned} \tag{20}$$

Where D is the diameter of the bearing and α is the tilt angle of the rings.

Due to the preload, the bearings are already loaded when no force is transmitted through the transmission. The friction generated by this preload is present when there is no power transmitted trough the mechanism (when the thrust force is zero). In this case, an input power is needed to operate the system while the output power is zero, therefore the efficiency in this no loading case is zero. When loading is added the friction torque is linearly correlated with the thrust force as can be derived from equation 19. As a result, the energy loss from the preload will become less significant with an increasing thrust force, this can be seen the almost horizontal energy loss line in Figure 9. Therefore a higher efficiency is expected at higher thrust forces. Since the rotational speed is linearly related to both the energy loss in the bearings and the output power, a constant efficiency is expected over the whole speed range.

An example of an efficiency profile is given by Figure 9, with $\alpha = 0.3rad$, $F_{pl} = 200N$, $D = 24mm$ and a pitch of $h = 6mm$. For the power calculation a rotational screw rod speed of $800RPM$ is used. This figure shows the increasing efficiency with an increasing thrust force

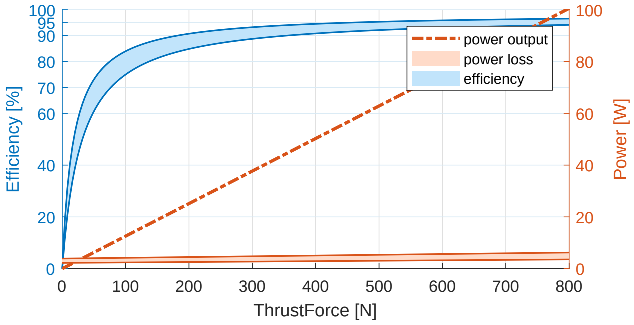

Fig. 9. The expected efficiency is between the 80% and 96% for the relevant thrust range. Lower efficiencies should be expected at low thrust forces due to low power throughput and constant friction caused by the preload.

From Figure 9 we can see that on the relevant operation range an efficiency between 80% and 96% can be expected. This efficiency is in the same range as the state of the art ball- and roller screw transmissions [24].

E. Optimal parameters selection

Using the found relations between design parameters and the performance of the ring screw, this section defines how the parameters of the ring screw should be selected. The first parameters that have to be selected are the geometry parameters of the ring-screw concept described in Section II. These parameters are the offset and tilt of the ring a and α the tilt angle of the contact line β, the radius of the screw hyperboloid b and the pitch h. Most of these parameters like the tilt and offset of the ring and contact line give no intuitive insight in the resulting screw transmission and its performance. Therefore a way to define these parameters using more intuitive inputs is desired.

First, the desired input parameters have to be defined in order to find a method to define these geometry parameters. The first thing screw transmissions are selected on is the pitch h and the outer diameter R_2 of the screw, giving already two input parameters. To be able to materialise the screw, a minimum ridge d width is required. On top of that, a minimal clearance clr between both the outer and inner diameter of the rod and de inner diameter of the ring is required to allow for manufacturing margins. This totals to four desired input parameters.

We have now introduces eight parameters (5 geometry parameters + R_2, d and clr) of which four are desired inputs. By using the relation between the parameters we can reduce our parameters set. Both the geometry parameters α and β can be expressed in the other geometry parameters $(a, b$ and $h)$ using equations 3. Furthermore, the geometry parameter a can be calculated using the groove width and the groove profile. The groove width can be expressed as $gw = 2\pi \cdot h - d$. Using the X and Y representations of the cross-section of the groove used for manufacturing equalling the Y coordinate to the outer radius R_2 and the X coordinate to half of the groove width we can express the value of a as

$$a = \frac{h \cdot \frac{gw}{2} + h \cdot T}{b \cdot \tan(T)} \qquad with \qquad T = \cos^{-1}\left(\frac{b}{R_2}\right) \tag{21}$$

This results in the minimally required input parameters listed in Table II. From these parameters, parameter b is open and not intuitively to select. Therefore this parameter should be used to optimise the performance of the ring screw. Based on the previous subsection of this section, we find that the parameter b has no direct effect on the expected efficiency and maximum velocity, but has a direct effect on maximum thrust force. Therefore we can determine which value for b results in an optimal screw.

The maximum thrust force can be calculated using equation 18. All forces along a half contact line can be replaced by a force, 10% from each end of the line. Therefore we can simplify this equation by substituting $s = 0.9 \cdot L$ where L is the length of a half contact line.

TABLE II

MINIMALLY REQUIRED INPUT PARAMETERS FOR SCREW GEOMETRY

parameter	symbol	defined by
Pitch	h	screw requirements
Outer diameter	R_2	screw requirements
ridge width	d	manufacturing limits
minimal clearance	clr	manufacturing limits
hyperboloid radius	b	open

$$F_T = \frac{1}{2} \cdot \frac{0.9L \cdot \sin(\beta)}{\left|h - \frac{a \cdot b}{h}\right|} \cdot F_{pl} \tag{22}$$

The length of a half contact line can be expressed as $L = \frac{\sqrt{R_2^2 - b^2}}{\sin\beta}$. Substituting this results in:

$$F_T = 0.45 \cdot \frac{\sqrt{R_2^2 - b^2}}{\left|h - \frac{a \cdot b}{h}\right|} \cdot F_{pl} \tag{23}$$

From this equation, we can draw the conclusion that the radius of the helical hyperboloid b can indeed be used to change the maximum thrust force of the ring screw. The optimal screw performance occurs when the maximum thrust force is as high as possible. If the denominator of equation 23 equals zero this thrust force per unit of preload will reach zero. This is at the point where:

$$\left|h - \frac{a \cdot b}{h}\right| = 0 \qquad \Rightarrow \qquad a \cdot b = h^2 \tag{24}$$

However, this value of b will result in an infeasible solution with a zero ring thickness. To find a feasible value for b the relation between the thrust force per unit of preload and the parameter b outside this point is investigated. Figure 10 shows the max thrust force per unit of linear preload force as a function of b where $h = 6mm/rev$ and $R_2 = 5mm$ are kept constant.

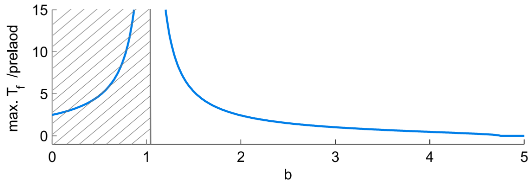

Fig. 10. The relation between, max thrust force per unit of linear preload force and the free parameter b, grows to infinity at the point where $b = \frac{h^2}{a}$. Therefore b should be selected as close to this value as physically possible. In the marked area the ring thickness is negative and so the solution is infeasible.

This graph clearly shows the peak to infinity at the at the edge of the infeasible area. However, it can be observed as well that the closer we get to this condition the higher the max thrust force per unit of linear preload force. Next to the max thrust force the value b also influences the width of the ring and so, is limited by the fact that the ring surface should not intersect with the bearing that holds the ring. Figure 11 shows the effect of b on the shape of the ring and the max thrust force per unit of linear preload force again with $h = 6mm/rev$ and $R_2 = 5mm$.

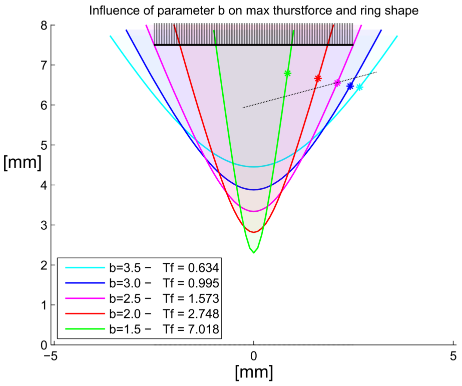

Fig. 11. Crossections of rings with different values of b. The solid black line represents the inner bearing edge of a 5x15mm bearing, the dotted line a 55° line with a min. distance of 0.8mm to the bearing and the stars represent the outer radii of the ring surfaces R_4.

The surface of the rings make contact with the rod up till an outer radius R_4, indicated with a star in Figure 11. After this point, the surface can deviate from the prescribed shape. Making an angle outwards from this point, increases the minimal wall thickness and so allows for, a more ideal, lower value of b. While bigger angles increase the wall thickness more, they also make production more difficult. If an angle of 55° is selected and a minimal wall thickness of 0.8mm, $b = 3$ would best value in the example of Figure 11

As can be derived from equation 23 the maximum thrust force can also be increased by increasing the preload. However, as can be concluded from equation 19 an increased preload will result in lower efficiency and therefore should be kept as low as possible.

IV. PROTOTYPE DEVELOPMENT

This section aims to identify the challenges to develop a functional prototype of the ring screw mechanism. This starts with designing the screw rod and rings by setting requirements for the parameter selection guideline presented in Section III. Followed by the development of the nut that constrains the rings while applying the preload.

A. Functional prototype

In this subsection, a functional prototype for an example application is designed. This gives an insight in how the parameter relation derived in section III can be used to design the ring screw mechanism. While at the same time illustrate how the prototype used for experimental evaluation is developed. The example applications is selected to be representative for a future real ring screw application. In the example application, the screw should be able to deliver forces up to $800N$ and reach a rotational velocity of $15,000RPM$ while the efficiency should be maximized. The outer radius R_2 and the pitch h of the screw are respectively set to be $10mm$, and $6mm/rev$. The combination of this pitch and rotational speed will result in a maximum linear speed of $1.5m/s$ The limitations from our manufacturer *PST group* are a minimum ridge width of 0.4mm and a manufacturing margin of $0.1mm$ which is the standard fine class for this dimensions. Therefore for the worst case scenario, the clearance needs to be $0.2mm$.

From these parameters, we can derive the radius of the helical hyperboloid b. For machinability, a minimum wall thickness of the ring is desired to be $0.8mm$. Following the method of Section III-E we find $b = 3mm$ to be the optimal value that still fits a standard bearing with an inner diameter of 15mm and a width of 5mm as can be seen in Figure 11. Using these five input parameters and the parameter relations presented in Section III-E the remaining parameters needed to design the mechanism can be found. These parameters are presented in Table III.

TABLE III

SCREW PARAMETERS OF FUNCTIONAL PROTOTYPE

Parameter	**Symbol**	**Value**	**Unit**
Pitch of screw	h	0.955	rad/mm
Outer radius of the screw	R_2	5	mm
Distance between adjacent grooves	d	0.4	mm
Clearance	clr	0.2	mm
Radius of the helical hyperboloid	b	3	mm
Ring offset	a	0.880	mm
Ring tilt	α	0.308	rad
Contact tilt	β	0.826	rad
Inner radius of the screw	R_1	3.187	mm
Inner radius of the ring	R_3	4.337	mm
Outer radius of the ring contact	R_4	6.473	mm
Half-length of the line contact	L	5.439	mm

Four rings are used instead of the minimal required three rings to achieve a constant loading on all contact lines and bearings. Therefore each ring should be able to produce at least 200N of thrust force for the ring screw to be able to deliver $800N$ of thrust force. Using Equation 23, it follows that a linear preload of $199N$ is required to guarantee contact at the preferred contact line.

These contact forces have to be transferred over a contact line of only $3.3mm$. To minimize deformations that lead to energy loss in at this contact line material selection is relevant for its performance. A material that allows for a high surface hardness is preferred. The SEA 8620 steel alloy can be case-hardened up till $62HRC$, while being easy to machine to high precision and having proper mechanical properties, making it the good material for the ring screw.

The thrust force will be transferred to from the rings to the nut through the bearings. Following Equation 20, this will result in high axial forces on the bearings. At the same time, a minimal bearing with is beneficial for the performance of the ring screw, as elaborated in Subsection III-E. Miniature four point contact bearings are therefore the optimal choice. For example the SBN Q1802 bearings with a width of only 5mm. Both the maximal axial load and maximal speed are higher than needed for this example application.[24]

The speed will be limited by the critical speed of the screw rod. With the geometry of the screw rod fixed by the parameters listed in Table III this can only be influenced by the length and fixtures of the screw rod. Since a longer rod will be beneficial for high-speed experiments this length should be maximized. For the fixtures, the ”fixed - simple” solution shown in Figure 6 is selected, to maximize the screw length while not over-constraining the screw. Over-constraining the screw, like in the case of a ”fixed-fixed” solution, can influence the efficiency measurements and is therefore not selected. Using these screw fixtures and the material properties of the used SEA 8620 steel alloy we find that a screw length of $250mm$ will result in a critical speed of $1980rad/s$. With a mentioned safety margin of 20% following industry standards, we can be confident that the critical speed is above the desired maximum speed of $15,000RPM$.

Now that all design parameters are known the screw rod and rings of the ring-screw could be designed. The final design following the design parameters described above can be found in appendix II.

B. Nut

Besides the above described screw rod and rings, a nut is required to make the ring-screw mechanism functional. The nut is not described in the previous work presented in section II. Therefore this subsection first analyses the requirements of the nut whereafter designs are proposed and evaluated. Special focus is given to the implementation of the preload.

1) Requirements: The nut should fulfil three functions. Keeping the rings in the right orientation and transfer the power and facilitate the preload in the system. This last requirement makes the design complicated since the pre-load wrench at each contact between the rod and a ring should follow Equation 15. Next to these requirements, the nut is preferred to be as compact as possible and be easy to mount on the rod.

a) Ring arrangement: Where a minimum of three rings is required to limit the screw rod to a screwing motion relative to the rings, this will result in an uneven spread of the preload and so thrust force on the rings, therefore four rings are used. An alternating orientation of the rings (Figure 12(b)) will result in a smaller bending moment on the rod. However this will still result in an uneven distribution of the preload forces, since for static equilibrium the sum of the moments should be zero but the moment arms differ. Following this logic, a sorted arrangement (Figure 12(c)) is the most optimal solution.

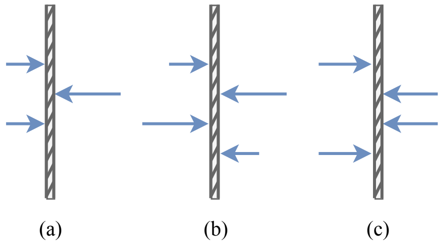

(a) (b) (c)

Fig. 12. The use of 3 rings (a) would result in an uneven loading of the rings. Adding one ring asymmetrical (b) would create the same problem due to the zero moment requirement. Therefore a symmetric loading using 4 rings (c) is most optimal.

b) Degrees of freedom rings: The rings should be held in the correct orientation by the nut. Variation from this correct orientation will change the contact between the rings and the screw rod, and will thus introduce sliding. This sliding would take away most of its advantages of the ring-screw mechanism confirming the importance of the orientation of the rings. From equation 17 we can derive that only one linear force and a torque around the same axis is needed to apply the preload, requiring only three contact points, one for the linear force and two for the torque (Figure 13(a)). When a thrust force is added, this introduces a linear force on the contact line V at an angle with respect to the rings. This angled force will simultaneously push the ring down sideways (Figure 13(b)). If the contact points to apply the preload torque are applied on the contact line V only 5 contact point are required (Figure 13(c)). Positioning this torque contacts in line with the contact line V compensates the downwards force of the thrust (yellow in Figure 13(b)) while preventing any resulting moment from this same thrust force. Those constrains allow the ring to rotate freely in the clockwise direction and move away from the linear thrust force, allowing the contact between the ring and screw rod to self-align.

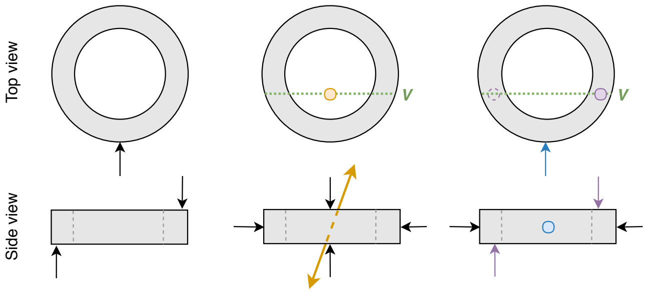

(a) Preload (b) Thrust force (c) Required constraints

Fig. 13. Applying the preload only requires three contact points on the ring(a), while counter acting the bidirectional thrust force (yellow) requires four contact points(b). Positioning the preload torque contacts on the contact line V (c) allows to minimally constrain the rings while being able to apply the preload and contracting the thrust force.

2) Nut design concepts: Applying the required preload wrench while keeping the nut compact can be done in many ways resulting in different combinations of advantages and disadvantages. Four compact ways of applying the preload are designed and evaluated, these concepts are summarised in Figure 14.

a) Milled nuts: The first two concepts make use of a highly accurate and stiff nut structure like milled aluminium. Due to the accurate and stiff structure, it can be assumed that the angle of the bearing and so of the ring is correct. Therefore only the linear preload force indicated in blue in Figure 13 has to be applied. The preload torque (purple), that results from this linear force can be counteracted with ridged surfaces. The use of a stiff milled frame allows for a highly accurate result but is not an economic solution. Furthermore milling had design restrictions resulting in a less compact solution than when 3D-printing is used.

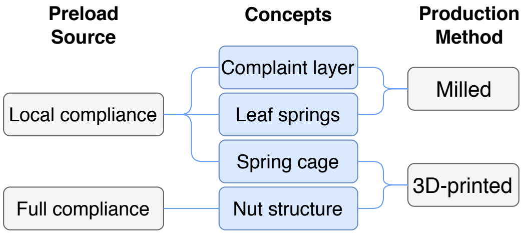

Fig. 14. Four concepts are designed and evaluated. Three of these concepts use a local compliance to apply the required preload wrench. The last concept uses the full compliance of the nut structure to apply the preload. For this concepts two production methods are used each having their own advantages.

Compliant layer: The first concept is a layer of compliant material that get compressed when the screw rod is inserted. A compact nut design for this prototype allows only for a small compliant layer, for instance, $5mm$ by $12mm$ resulting in a surface of $A = 60mm^2$. To generate the previously defined preload of $199N$ a surface pressure of $3.33MPa$ is required. If a layer of $1mm$ is used and the desired compression is $0.1mm$ the desired compression modules of Elasticity for the material is $CME_{des} = 3.33/0.1 = 33.3MPa$ with a compression strength of at least $3.33MPa$.

Using the compliant material gives a compact solution and if rubber is used increases the damping of the nut and so reducing resonance related problems. However the compression force is strongly dependant on the shape of the sheet and are less predictable.

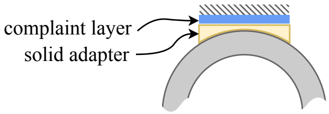

Fig. 15. First preload option, a compliant material gets compressed due to insertion of the rod and so applies a linear preload on the ring.

leaf springs: The second considered concept to apply the preload is the use of leaf springs. Due to the limited space in the compact nut, the leaf springs have to be small. For instance the width $B_{spring} = 6mm$ and a length of $L_{spring} = 13.5mm$. This small spring length and the required preload force of $199N$ results in high stresses in this springs. Therefore INOX 1.4310 with a high stress limit of $E = 1350Mpa$ is selected. The relation between deflection and applied force of a leaf spring supported from both sides is given by equation 25.

$$f_c = \frac{F \cdot L_{spring}^3}{48 \cdot E \cdot I_{yy}}, \qquad with \qquad I_{yy} = \frac{B_{spring} \cdot t^3}{12} \tag{25}$$

Where t is the thickness of the leaf spring and f_c is the deflection at the centre of the spring. Since we have a desired deflection of 0.1mm and a desired force of $199N$ we can rewrite this formula to find the required thickness of the springs to equation 26

$$t = \sqrt[3]{\frac{F \cdot L_{spring}^3}{4 \cdot E \cdot f_c \cdot B_{spring}}} \tag{26}$$

To limit the maximal material stresses two stacked plates are used instead of one thick plate. This results in two plates with a thickness of $t = 0.8mm$ with a maximal material stress of $\sigma = 527.3MPa$ far below the stress limit of the spring material.

The use of the springs will result in a very accurate and predictable preload and therefore take more advantage of the potential of the milled nut to be predictable than the compressed material concept.

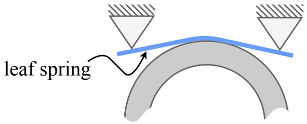

Fig. 16. Second preload option, a leaf spring gets bent due to the insertion of the screw rod and so applies a linear preload on the ring.

b) 3D printed nut: The last two concepts the use of a 3D printed nut structure. Using 3D printing the generation of the preload can be integrated resulting in a monolithic design. Doing so a very compact, simple and economic design can be achieved. However 3D printing techniques are less accurate than milling and have a higher surface roughness, accordingly correct location of the bearings cannot be guaranteed. Therefore unlike when an accurate stiff nut is used this concept should allow movement of the bearings in the torsional direction (purple in Figure 13) to allow for self aligning following Equation 17.

Spring cage: The third option is the use of a spring cage that holds the rings. he rings are suspended in spring cages creating the force equilibrium given by Equation 17. The approach is very similar to the leaf springs used in the milled nut. The very limited space and high forces make the use of plastic springs infeasible, therefore printing in titanium is selected. The printable version of Ti-6Al-4V has a Young's modulus of around $E = 112GPa$ and Yield stress of around $\sigma = 1022MPa$ [25]. Using Equation 25 and the minimum thickness limit for titanium 3D printing of $0.8mm$ results in the design shown in Figure 17.

This design has a spring at the back of the bearings to apply the linear preload, leaf springs in the torsional direction to counteract the preload torque and allow for self-aligning. Furthermore the design has supports that allow for small motions in the direction of the screw axis in order to get an even load distribution over all bearings.

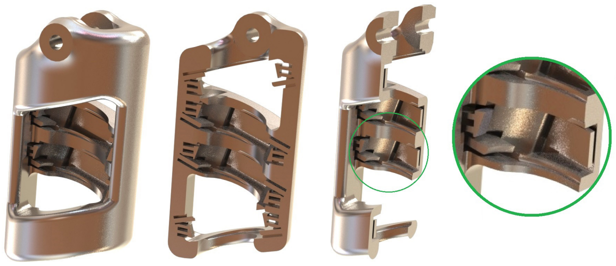

Fig. 17. Third preload option uses a spring cage, integrated in the structure, that holds the bearing in place. This spring cage allows for self aligning of the rings and so compensates 3D printing inaccuracies.

c) Fully compliant nut structure: In last evaluated option the whole structure of the nut is used as a spring to apply the preload. The nut is designed to be a little to small so when the screw rod is inserted the nut exactly applies the desired preload wrench on the rings as a response. Since the shape of the nut is too complex to be modelled analytically a finite element analysis (FEA) is used to model the deformations and stiffness of the nut. For this design, nylon-12 is selected as printing material because of its high printing accuracy, low price, good elastic properties and high strength. Using FEA, the deformations of the initial nut design caused by the preload wrench, are calculated as can be seen in Figure 18. From this deformations, the displacements of the rings are calculated to define the required ring offset before insertion of the screw rod. The nut is designed to have all offsets around $0.2mm$, to be less influenced by inaccuracies while still to allow for easy insertion of the rod.

While using the complete nut structure as a spring to generate the preload is less predictable than when local deformations are used, this results in a more compact design. Furthermore for the local deformations more advanced printing materials are required like titanium resulting in a much less economic solution than when the common nylon is used. Therefore the nut designed using a FEA takes the best advantage of the 3D print production method.

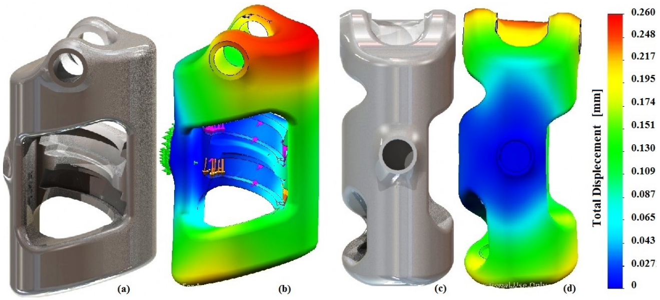

Fig. 18. The preload is applied due to deformation of the whole nut structure. A FEA is used to identify which deformations result in the required preload wrench. This plot shows the deformations due to the preload wrench (purple arrows in Figure b) with the track roller hole as the fixed point (green arrows in Figure b). The nut is designed to have deformations around 0.2mm at this preload wrench.

C. Selected nut design

All described preload methods fulfil the requirements and therefore would be suitable solutions. However on other factors dependant on the applications advantages and disadvantages can be found between the solutions. While the use of a stiff and accurate nut like in the first two solutions allow for high predictability of the actual preload, the solutions exploiting 3D printing would result in a more compact and economical solution.

To test the performance of the ring screw in an experimental setting as done in this thesis, predictability is important to get accurate and repeatable results. Therefore the milled nut using leaf springs for the preload is strongly preferred for the experiments presented in this thesis. However from a product perspective and so for future development, a more compact and economic nut has clear advantages. Therefore both the milled nut with leaf springs and a nylon 3D printed nut are selected and materialised.

V. EXPERIMENTAL DESIGN

This section describes the experimental design used to evaluate the performance of the prototype developed in section IV. Furthermore the development and validation of the experimental setup are described in this section.

A. Experimental Method

To evaluate the real-world performance of the ring screw, the performance metrics, maximum operation speed, efficiency and maximum thrust force, of the developed prototype will be evaluated. Therefore the developed prototype will be subjected to the following experiments.

To evaluate the real-world performance of the ring screw, the performance of the developed prototype is being evaluated. The following experiments are conducted to find the performance metrics maximum operation speed, efficiency and maximum thrust force.

a) Maximum velocity: The maximum speed is limited by the resonance of the screw and the maximum rotational speed of the equipped ball bearings as explained in section III. The maximum speed of the ball is provided by the manufacturer and so only the resonance frequency has to be verified. The first resonance mode of the screw is designed to be above $15,000RPM$, this will be experimentally verified. Next to that, the screw transmission is operated at its designed speed of $15,000RPM$ to find any unexpected failure modes. Due to the maximum acceleration of the motor, limited by the motor controller driving it, in combination with the limited screw length, no efficiency measurements could be performed at the speed of $15,000RPM$. However this speed can be reached by accelerating over the full length with a high deceleration at the end when reaching the end stops.

b) Efficiency: While the maximum operation speed of the system is quite evident, based on the working of the ring-screw, the theoretical high efficiency depends on the perfect rolling contact in all conditions. Hence a high efficiency above 90% would be strong evidence that the theory and assumptions used for development are correct. The efficiency used in these experiments is $\frac{PowerOut}{PowerIn}$, where the $Power$ is the mechanical power. It is predicted that the energy loss will mainly occur in the bearings holding the rings. Resulting in an efficiency profile as depicted in Figure 9 that is not influenced by the rotational velocity. To evaluate this efficiency profile, the efficiency should be measured in a wide range of loading cases. The experiments can be simplified by measuring the efficiency at a constant speed and force. This will cancel out the dynamic effects of the experiment. To filter out the mechanical vibrations and electrical noise, the speed, torque and force measurements are filtered with a zero delay 4th order Butterworth filter. The cut-off frequency for the velocity is at 10Hz while the cut-off for the force and torque is at 40Hz just below the mains hum.

c) Maximum thrust force: The maximum thrust force is defined at the point where the contact forces between the ring and rod are compromised. This point is expected to be around $800N$. After this point, the contact will shift from the desired line contact introducing sliding friction and so significantly lowering the efficiency. Therefore it will be evaluated if the efficiency stays constant up to such high thrust forces.

B. Experimental Setup

An experimental setup is developed to measure the performance using the experiments described in subsection V-A. This experimental setup should be able to operate at at least $15,000RPM$ for the maximum velocity experiments. Furthermore the setup should be able to load the screw with a linear load of $800N$. The more challenging metric is the measurement of the efficiency. The efficiency is expected to be up to 96% so accurate efficiency measurements is that identify a energy losses that are a fraction of this 4% is a must.

1) Setup design: The experimental setup is designed in the shape of a test rig, that allows for the testing of many different screw transmissions. In this work, the test rig is used to be able to compare the ring screw to a standardised ball screw. The test rig is designed to rotationally drive the screw while applying a linear load. A rotational electric motor with a maximal rotation speed of $16.700RPM$ is selected to drive the screw. To accurately measure the mechanical power input to the system, this motor is equipped with an encoder to measure the speed and a torque sensor measuring the reaction torque of the motor. More details on the selected electronics can be found in appendix IX.

The screw is loaded with a linear load to measure the efficiency and verify the maximum thrust force. Multiple test rig concepts with different load sources have been evaluated, see appendix IV. A design that allows for interchangeable loads with a damper as the main load has been selected. The damper will force the experiments to have the desired constant speed and force profile hence making the test rig easy to control. While the damper load has many advantages, it can not be used for back-driving experiments and does not allow for low forces at high speeds. Therefore constant force springs are selected as a secondary load to replace the damper in some experiments. To measure the output force, a load-cell is placed in series with the linear load. The resulting setup can be seen in Figure 19. More details can be found in appendix VIII.

To constrain the screw in the selected "fixed - simple" configuration illustrated in Figure 6, the screw rod is held by preloaded angular contact bearings on one side and a self-aligning bearing on the other side. A track roller is used to prevent the nut from rotating. This track roller is selected instead of a guide rail to minimise friction. However a linear guide is used to keep the load coaxial with the screw rod. This linear guide is placed after the force sensor and so does not influence the measurements.

2) Setup validation: The designed experimental setup aims to measure the efficiency of the ring-screw prototype

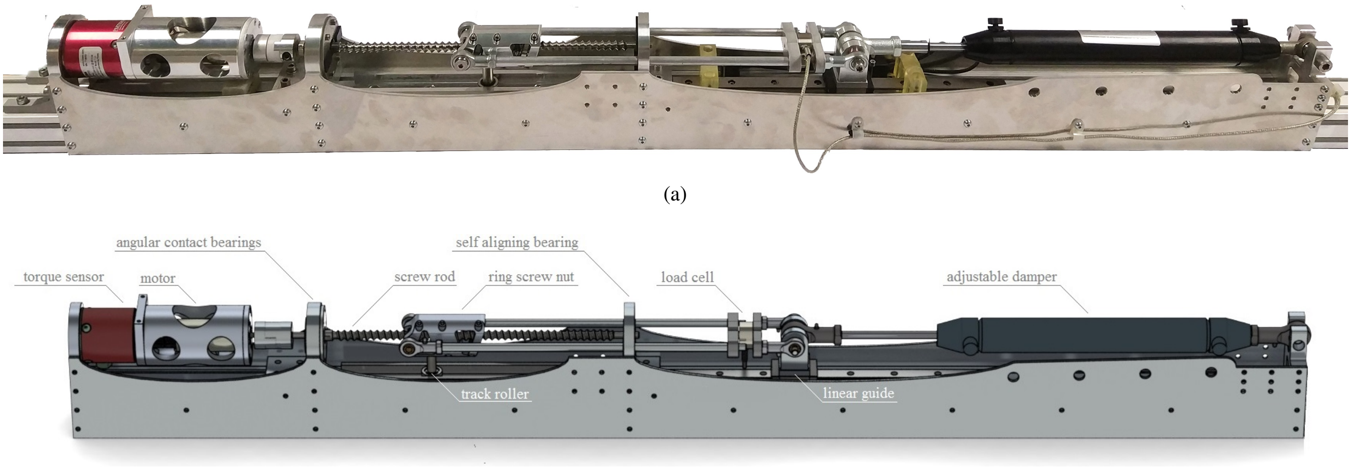

(a)

(b)

Fig. 19. The test rig, developed in this work to evaluate the performance of the ring screw. It's able to measure high efficiencies accurately while being able to generate load forces over $800N$ and rotational velocities over $15.000RPM$. a) The fabricated set-up with an hydraulic damper as load. b) Schematic representation of the test rig with various parts labelled.

with a high accuracy. If no external contact would be made between the force sensors, the efficiency can be calculated by dividing the output power by the input power. However contact is made at both ends of the screw and by the track roller. Preliminary experiments have shown that the energy loss due to the track roller and self-aligning bearing is negligible. However the energy loss in the preloaded angular contact bearings is significant. To be able to subtract this energy loss from the results the bearing friction should be identified.

According to the manufacturer of the thrust bearings, the friction torque of these bearings is mainly dependant on the axial loading, as can be seen from Equation 19. However a more accurate prediction can be made using Equation 27. Where A, B, C and D are the variables to experimentally define. F_{tb} Represents the axial load on the bearings and ω represents the rotational speed.

$$T_{friction} = A + B \cdot F_{tb} + C \cdot \omega + D \cdot F_{tb} \cdot \omega \tag{27}$$

To find reliable values for A, B, C and D the energy loss in these bearings should be measured over the whole operating range. For this purpose, the test setup is shown in Figure 20 is developed.

The bearing friction tester has the same driving assembly as in the final test rig described in subsectionV-B. It consists of and torque sensor and encoder to measure the mechanical input power. This assembly is driving two sets of angular thrust bearings, one set connected to the frame, in the same way as the final test rig, the other set connected to a weight. These weights are connected so that they both prevent the bearing from rotating while applying an axial load to both bearing sets. A wide range of loadings can be created by changing the weights. Since there is no other world contact it is assumed that all input energy is dissipated in the bearings. So, with the assumption that the bearing sets are identical, the energy loss in a set of bearings is half the input energy.

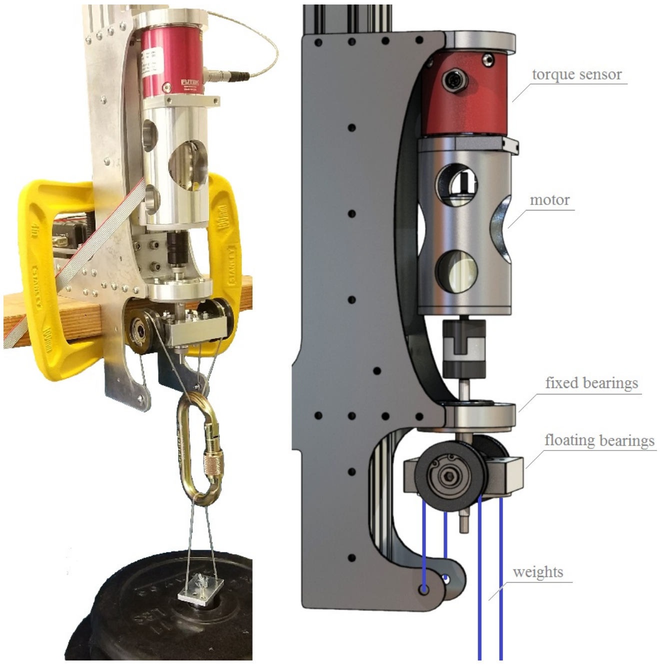

Fig. 20. Picture showing the developed test setup used to identify the friction losses in the thrust bearings.

Next to loading and speed, also temperature can have an influence on the friction of the bearings. Therefore the effect of heating during operation has been investigated. We found that the friction in the bearings decreases exponentially up to 30% from completely cooled till a steady state in around 5 seconds. To this extent, all measurements are performed after 5 seconds of running to get reliable results. More details can be found in appendix V-A

Bearing friction measurements have been performed 3 times for all loading conditions, with speeds ranging from $2000RPM$ up to $8000RPM$ and thrust forces from $1N$ up to $600N$. The value presented in Table IV are derived by fitting Equation 27 on the found data. It can be observed

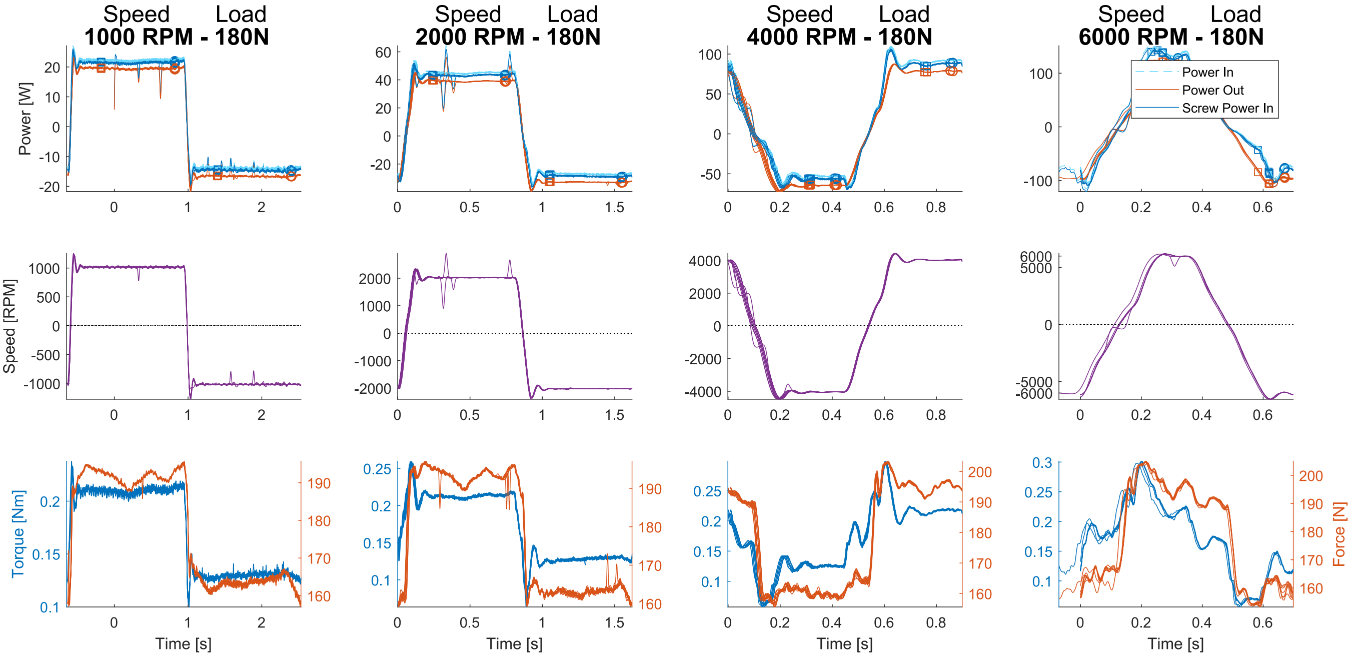

Fig. 21. Graph showing the raw data of four experiments (from left to right) determining the efficiency of the ring screw. Ten repetitions of each experiment have been aligned and plotted over each other without averaging. These experiments use the same constant force spring as a load but different velocities, as can be seen from the purple speed and orange force data.

that A, the constant friction induced by the preloading of the bearings and B, the friction related to the axial load, are most dominant as was expected based on the rough estimation from Equation 19. More details can be found in appendix V-B

TABLE IV

EXPERIMENTALLY FOUND PARAMETERS FOR EQUATION 27

A	B	C	D
$5.2 \cdot 10^{-4}$	$1.7 \cdot 10^{-5}$	$9.1 \cdot 10^{-8}$	$-9.4 \cdot 10^{-12}$

VI. RESULTS

This section presents the experimental results are presented. These results are measured using the developed prototype with the leaf spring nut described in section IV in the experimental setup described in section V-B. The next subsections present the found results from a sequence of experiments that have been performed order by the three performance metrics.

A. Efficiency

The efficiency of the screw in a wide range of loading cases is the most important measure to validate the correct working of the ring screw. Therefore the ring screw has been operated in a wide range of velocities up to $8000 RPM$ and loadings up to $750N$ using the damper load. Next to the damper, the constant force springs have been used to apply the forces up to $200N$ to allow efficiency measurements for both a forward and backward driven screw. The screw is accelerated and decelerated with $50.000\frac{RPM}{s}$ with a steady state at the desired velocity in-between. This is repeated 10 times for all load cases whereafter the data of the steady state is used to define the efficiency at that load case. An example of the raw data of four experiments can be seen in Figure 21.

In this figure, the raw data is presented form four load cases. In the top graph of Figure 21, the mechanical power output from the load side is shown in orange and in blue the power input from the motor side. A light blue line can be observed slightly above the dark blue line, where the light blue line represents the raw measured mechanical power. The dark blue line represents the mechanical power corrected for the friction experimental setup as described in subsection V-B.2. The middle graphs show the rotational speed of the screw, showing different velocities for the four experiments. It can be observed that, since the acceleration is kept constant, the steady state part is shorter at higher velocities. The bottom graphs show the reaction torque at the motor side in blue and the linear force at the load side in orange. In this graphs can be seen that the same constant force spring is used as a load for these four experiments. These springs deliver a static force of $180N$ and a direction dependent force of $\pm 20N$ caused by friction in the springs functioning as a load.

Important to notice is that, no averaging has been applied in Figure 21 but ten repetitions of each experiment have been aligned and plotted over each other. This can barely be seen due to the high similarity of the data, which proves the high repeatability of the experiments. This also shows that the oscillations in the linear force of the load are consistent and are similar in the different experiments. Hence it is expected that these oscillations are caused by irregularities

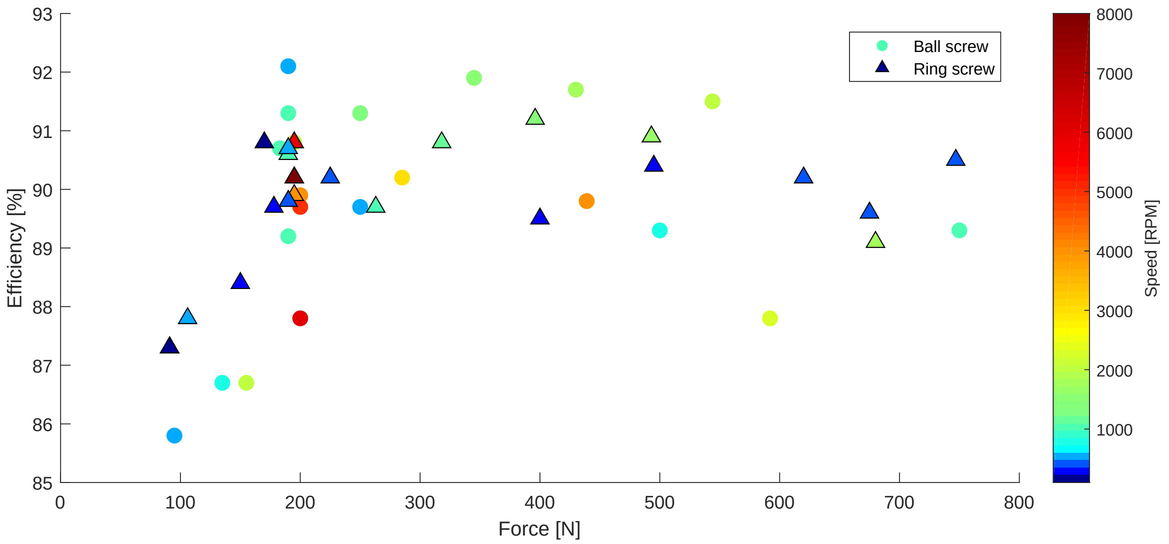

Fig. 22. The efficiency is between 85% and 93% for all loading conditions for both the ring screw (△) and ball screw (◯), where the low efficiencies are at low thrust forces. The efficiency of the ring screw is not influenced by the rotational speed, while the ball screw is. This can most easily be observed at a loading of $200N$ which contains most experiments.

in the rolling of the springs and the linear guide of the load.

A wide range of experiments has been performed in the same way as the experiment described above. Next to variation in the velocity as described above the load has been varied. To prevent the measurement from being influenced by the used measurement tool, a fair and accurate comparison can only be made if measured with the same tool. The used test rig is designed and developed specifically for this experiments and so no comparison data exist yet. To this extent closed comparable ball screw from SBN[24] is tested in the same scenarios for comparison reasons. The results of all these experiments are summarised in Figure 22 All efficiencies vary between 85% and 93% for both the ball screw and the ring screw. As expected from the theory we observe lower efficiencies at the low thrust forces around 100N.

B. Thrust force

In the thrust forces above $200N$, the efficiencies of the ring screw are all around and above the efficiency of 90%. This high efficiency indicates a correct working of the ring screw at thrust forces up to $750N$. Therefore the maximum thrust force of the ring screw prototype is above $750N$ as predicted. Since no experiments above this thrust force have been performed at higher thrust force up to a lower efficiency could be observed the exact maximum thrust force cannot be defined from this data.

C. Maximum velocity

From figure 22 it can be observed that, mainly on the $200N$ line, the efficiency of the ring screw is not influenced by the velocity while the efficiency of the ball screw goes down with an increasing velocity.

Even velocities up to $8,000RPM$ an efficiency of 90% for the ring screw can be seen. While this velocity is already double the rated velocity of a ball screw, the screw is expected to withstand operation velocities up to $15,000RPM$, limited by the resonance of the screw (the critical speed). To validate these, three experiments have been conducted as described in subsection V-A.

The first velocity experiment aims to find the critical speed of the screw in the normal "fixed - simple" configuration. The screw is slowly accelerated while potential visual and sensory resonances are monitored. No resonance was observed up to the maximum motor speed of $16,500RPM$, confirming the first resonance mode to be above this speed as predicted.

The second velocity experiment aims to find a defined value for the critical speed instead of a minimal value. Since the speed of the motor is limited the resonant frequency of the screw is decreased. This is done using the "fixed - free" configuration from Figure 6. As calculated in section III-B the frequency of the first resonance mode is expected to be around $3200RPM$ taking into account the extra screw length normally inserted in the self aligning bearing. The measured resonance can be observed around $3100RPM$, both visually and in the power consumed by the system based on sensor readings as can be seen in appendix VI-A. While the critical speed is 3% lower than the expected speed, this uncertainty was captured in the earlier mentioned safety margin of 20%.

The last experiment aims to find any other failure modes in the system. The ring screw has successfully been accelerated over the whole length of the screw up to a speed of $16,500RPM$ with a high deceleration at the end when reaching the end stops as can be seen in appendix VI-B. No damage or change in the measured performance caused by the high speed or impact was observed.

VII. DISCUSSION

The performance of the ring screw has been investigated both in theory and in practice. In this section, we discuss the results and the ring screw.

A. Discussion of the results

The experimental results show that the prototype has an efficiency of around 90% for all measured conditions with a variation of $\pm 2\%$. The measurements showed no considerable difference in the efficiency up to a thrust force of $750N$. Furthermore, the ring screw was successfully operated at $15,000RPM$.

A comparison is made between the experimentally found and the predicted performance we see that both the maximum thrust force and maximal operation speed meet the expected performance. However, the efficiency is slightly lower than predicted at higher thrust forces. This can be observed if the predicted (Figure 9) and measured (Figure 22) efficiency are compared. The measured efficiency is in and slightly above predicted range up to a loading of $200N$, after this point the measured efficiency remains constant around 90% while the predicted efficiency grows on to an efficiency of 96%. Since this difference is not present over the whole range, it is not a result of underestimated bearing friction. In that case, the efficiency would be lower at low thrust forces as well. It is expected that this extra energy loss is the result of imperfections in the geometry of the screw rod and rings. Imperfections in the geometry of any kind will make the contact between the screw rod and rings deviate from its ideal line, introducing sliding and therefore friction. Following the laws of friction, this energy loss becomes more dominant at higher contact forces. Thereby explaining the slightly lower than expected efficiency only at higher thrust forces. Therefore it is expected that a more accurate prototype would result in higher efficiencies especially at high speeds.

Based on the theory presented in section III-D it is expected that the efficiency of the ring screw is not influenced by the speed. This is in contrast with the knowledge that in similar devices like a ball screw the efficiency is negatively correlated with the operation speed [26]. The experimental results are shown in Figure 22 confirm both these expectations. These results show no correlation between speed and efficiency for the rings screw while a negative correlation can be observed for the ball screw. In Figure 22 this can be seen most clearly at a load of 200N. At this load, ball screw experiments can be found ranging from $500RPM$ up to $6,000RPM$ show this negative correlation . At the same loading, no relation between speed and efficiency for ring screw experiments ranging from $300RPM$ up to $8,000RPM$ has been found. . This result supports the argumentation that the ring screw is superior to the ball screw at high speeds.

Although the ring screw was successfully operated even above $15,000RPM$, the efficiency could only be accurately measured up to $8,000RPM$. This lower speed is a result of unexpected acceleration limitations caused by the electronics. However, since there is no correlation between the speed and the efficiency, it is expected that the efficiency remains around 90% up to its designed speed of $15,000RPM$.

B. Comparison with existing technologies

In this work, the ring screw is mainly compared to the ball screw mechanism while in Table I two other comparable devices are presented, the lead screw and the roller screw. The table already indicates that the ring screw will outperform the the lead screw on all selected performance metrics. Accordingly, the lead screw will not result in a useful comparison. The roller screw, on the other hand, is expected to outperform both the ball screw and the ring screw on some of the metrics. Nonetheless, the roller screw is barely used in industry, because of its exceptionally high retail price. A high-performance roller screw has a retail price, of 7× up to 20× the retail price of a ball screw, which makes it an unfavourable option. The production cost of a ring screw is expected to be around the price of a ball screw. This retail price is expected since the ring screw only consists of three unique parts that are not more complex than ball screw parts. Therefore the ball screw is the most relevant device to compare with the ring screw.

performance metrics: If the experimental results of the ring screw are compared with the results of the ball screw, shown in figure 22, we see similar efficiencies in all loading conditions. For these experiments, the first ever made functional prototype is used while the ball screw is already fully developed. The fact that the ring screw can keep up in this comparison is strong evidence that the technology is very interesting for future development. For example, the use of optimised low friction bearings will increase the efficiency of the ring screw mechanism.

The experimental results have shown that the efficiency of the ring screw and ball screw are comparable, the ring screw can reach much higher speeds while they are both able to push $750N$ of thrust force. However while this is close to the expected limit of the ring screw, the used ball screw is rated to deliver a dynamical load of $1450N$[24]. Therefore the ball screw is superior to the ring screw for high thrust force application.

other properties: The ring screw exploits a perfect rolling contact, what means an absence of sliding friction. Accordingly, the ring screw has the ability to run without lubrication unlike a ball or roller screw. This is a huge advantage in various applications, like applications in dusty, submerged or hygienic environments where the lead screw is currently the only option.

A limitation a ball screw mentioned by Roozing et al. [16] is the fragility against a non-coaxial loading. Only small moments are enough to damage the seals needed to force the balls in the return mechanism. While a non-coaxial loading will probably limit the performance of the ring screw by creating an uneven loading on the rings, this will result in a working configuration.

If the size of the nut of the ring screw prototype is compared with other screw transmissions like lead and ball screws a downside of the ring screw can be observed. Even the compact and lightweight 3D printed nut is significantly bigger size than competing devices. This size can be reduced by integrating the required ring surface in the inner ring of the bearing. For the prototype developed in this work, this can reduce the outer diameter of the bearing from $24mm$ to $17.5mm$ as depicted in figure 23.

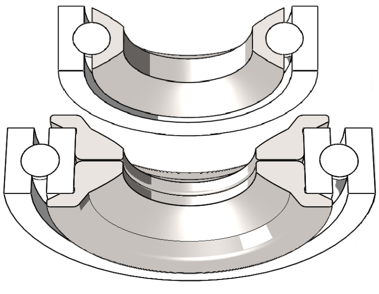

Fig. 23. Illustration showing the reduction of ring size when custom bearings are used. The bottom ring represents the current setup with the use of off the shelf bearings, where the top represents the ring size if custom bearings are used.

C. Future work

The listed speed limitation of the ball screw used in the experiments is $4,000RPM$, however the ball screw is tested up to $6,000RPM$ in this work. While this is 50% above the speed is given by the manufacturer, it does not directly break but results in noisy and inefficient operation with a higher risk of failure and wear [27]. Although the lower efficiency and high noise are not present in the ring screw at speeds up to $8,000RPM$ and the ring screw does not fail at $15,000RPM$, the wear and failure risk have not been addressed in this work.

Preliminary experiments at low force experiments showed no significant difference in the efficiency when operating the ring screw with and without lubrication. The rings and rod are both made out of steel and so the friction coefficient of the oiled and dry surfaces differ with a factor of 2. Accordingly, if friction was a noteworthy contributor to the energy loss a substantial difference in the efficiency would be observed. Therefore there is a strong indication that the contact between the rings and rod is indeed mainly a rolling contact. However, the data presented in Figure 22 indicates friction due to production errors at high thrust forces. Therefore more detailed experiments should be performed to quantify this effect. Moreover, experiments should be performed to verify the perfect rolling contact.

Furthermore, the effect of errors in the prescribed ring and rod surfaces should be addressed in future work. Experiments with very low preloads have shown that the preload is inconsistent during travel over the screw rod of the current ring screw prototype. These inconsistencies indicate undesired variations in the screw rod and so errors in the geometry. It is known that these errors will influence the resulting performance, but there is no information available on the correlation between the performance and surface errors. This will be an important topic for future development since production costs can be decreased if bigger tolerances are allowed in production.

VIII. CONCLUSION

The goal of this study was to develop a functional prototype and evaluate the performance of a novel screw transmission called the ring screw. The relations between design parameters and the theoretical performance of the ring screw are analytically found. The rings and rod of the functional prototype has successfully been developed, based on the identified relation. Two nut designs have been materialised, both maximising the degree of freedom of the rings to ensure correct contact between the rings and screw rod but using different manufacturing and preloading techniques. The first nut design is developed for the evaluation experiments in this thesis, therefore it's made accurate and predictable. The second nut is developed for future commercialising and so economic and compact.

For the evaluation of the performance of the ring-screw prototype a high precision test rig was developed. This test rig was successfully validated against a standard ball screw transmission. The efficiency of the ring screw was found to be around 90% in loading conditions up to $750N$ and $8,000RPM$, similar to the efficiency of state-of-the-art screw transmissions, such as ball screws. The predicted maximal rotation speed of $15,000RPM$ was reached while the efficiency remained constant at over $750N$ of thrust force, meeting the mechanism's theoretical potential.

This high rotational speed exceeds today's screw speed limits by more than a factor of two. Combined with other benefits including; high reliability, high efficiency, and lubricant-free operation, the ring screw has clear advantages over state-of-the-art screw transmissions. The ring screw therefore enables machine designs that were previously impossible, resulting in a significant commercial value.

REFERENCES

[1] Roy Featherstone. Linear drive mechanism of the screw and nut type with perfect rolling contact, August 15 2016. International Patent: PCT/IB2016/052739.

[2] B Huard, M Grossard, S Moreau, and T Poinot. Multi-model observer for position estimation and object contact detection of a flexible robotic actuator. pages 916–921, CEA, LIST, Interactive Robotics Laboratory, F-92265 Fontenay aux Roses, France, 2012.

[3] M Cempini, D Marconi, M Muscolo, M Moise, M Fantozzi, M Cortese, A Parri, T Yan, S Crea, F Giovacchini, F Posteraro, M C Carrozza, and N Vitiello. Relevance of Series-Elastic actuation in rehabilitation and assistance robotic: Two cases of study. pages 76–81, BioRobotics Institute, Scuola Superiore sant'Anna, viale Rinaldo Piaggio, 34, Pontedera, PI, Italy, 2015. Institute of Electrical and Electronics Engineers Inc.

[4] Maxon Motor. Products catalogue 18/19, 2018. https://www.maxonmotor.com.

[5] Serge Pfeifer, Anna Pagel, Robert Riener, and Heike Vallery. Actuator with Angle-Dependent Elasticity for Biomimetic Transfemoral Prostheses. *ASME Transactions on Mechatronics*, 20:1384–1394, 2015.

[6] B Zeng, S Fan, L Jiang, M Cheng, and H Liu. Design and control of an anthropomorphic prosthetic hand with a cosmesis. pages 926–930, State Key Laboratory of Robotics and System, Harbin Institute of Technology, Harbin, China, 2016. Institute of Electrical and Electronics Engineers Inc.

[7] Jan F Veneman, Rik Kruidhof, Edsko E G Hekman, Ralf Ekkelenkamp, Edwin H F Van Asseldonk, and Herman Van Der Kooij. Design and evaluation of the LOPES exoskeleton robot for interactive gait rehabilitation. *IEEE Transactions on Neural Systems and Rehabilitation Engineering*, pages 379–386, 2007.

[8] JJM Driessen. Machine and behaviour co-design of a powerful minimally actuated hopping robot. *master thesis, Delft University of Technology, Delft, The Netherlands.*, 2015.

[9] B Sun, C Xiong, Wenrui Chen, Q Zhang, L Mao, and Q Zhang. A novel design method of anthropomorphic prosthetic hands for reproducing human hand grasping. pages 6215–6221, Institute of Rehabilitation and Medical Robotics, State Key Lab of Digital Manufacturing Equipment and Technology, Huazhong University of Science and Technology, Wuhan, China, 2014. Institute of Electrical and Electronics Engineers Inc.

[10] Douwe Dresscher, Theo J A De Vries, and Stefano Stramigioli. Motor-gearbox selection for energy efficiency. In *IEEE/ASME International Conference on Advanced Intelligent Mechatronics (AIM)*, pages 669–675, 2016.

[11] Jee-Hwan Ryu. Twisted string actuation: State of the art, challenges and new applications. *IROS Workshop*, 2016.

[12] Ill Woo Park, Jung Yup Kim, Jungho Lee, and Jun-Ho Oh. Mechanical design of humanoid robot platform KHR-3 (KAIST humanoid robot - 3: HUBO). In *IEEE/RAS International Conference on Humanoid Robots (Humanoids)*, pages 321–326, 2005.

[13] S Seok, A Wang, M Y Chuah, D J Hyun, J Lee, D M Otten, J H Lang, and S Kim. Design principles for energy-efficient legged locomotion and implementation on the MIT Cheetah robot. *IEEE/ASME Transactions on Mechatronics*, 20:1117–1129, 2014.

[14] M R Tucker and K B Fite. Mechanical damping with electrical regeneration for a powered transfemoral prosthesis. pages 13–18, Clarkson University, Potsdam, NY 13676, United States, 2010.

[15] M Liu, P Datseris, and H Huang. Prototype for smart prosthetic legs-analysis and mechanical design, 2012.

[16] W. Roozing, Z. Li, G. A. Medrano-Cerda, D. G. Caldwell, and N. G. Tsagarakis. Development and control of a compliant asymmetric antagonistic actuator for energy efficient mobility. *IEEE/ASME Transactions on Mechatronics*, 21(2):1080–1091, April 2015.

[17] Travis Schneider. Which screw is best for you? *Parker Hannifin, www.parker.com*, 2015.

[18] Igor Gilkin. A critical look at acme, ball, and roller screws for linear motion. *Machine Design, http://www.machinedesign.com*, 2009.

[19] Osamu Sano. Movement transforming device and power steering apparatus, 2001. Google Patents, US Patent 6,244,125.

[20] Robert Gartner. Screw jack, 1989. Google Patents, US Patent 4,856,356.

[21] Tolomatic. Which screw, pricking the right technology. *Tolomatic, Inc, http://www.tolomatic.com*, 2006.

[22] Isel. Automation, from components to systems. Catalogue, https://www.isel.com/, 2017.

[23] Warren C Young and Richard G Budnyas. *Roark's formulas for stress and strain*. McGraw-Hill, 2017.

[24] SBN Waelzlager. High precision ball bearings. Catalogue, https://www.sbn.de/, 2017-2018.

[25] M. Benedetti, M. Cazzolli, V. Fontanari, and M. Leoni. Fatigue limit of ti6al4v alloy produced by selective laser sintering. *Procedia Structural Integrity*, 2016.

[26] George V Puiu, Dumitru N Olaru, and Vasile Puiu. Friction torque and efficiency in ball–screw systems. *Acta Tribologica*, 17:25–29, 2009.

[27] Chin-Chung Wei, Wei-Lun Liou, and Ruei-Syuan Lai. Wear analysis of the offset type preloaded ball–screw operating at high speed. *Wear*, 292:111–123, 2012.

[28] Brian Garret Ben Redwood Filemon Schöffer. *The 3D Printing Handbook: Technologies, design and applications*. 3D hubs, 2017.

APPENDIX I
VISUALISATION CONTACT LINE

This appendix shows a visualisation of the contact line between a ring and screw rod. The surface geometry of the ring and screw rod is such that this contact line allows for perfect rolling.

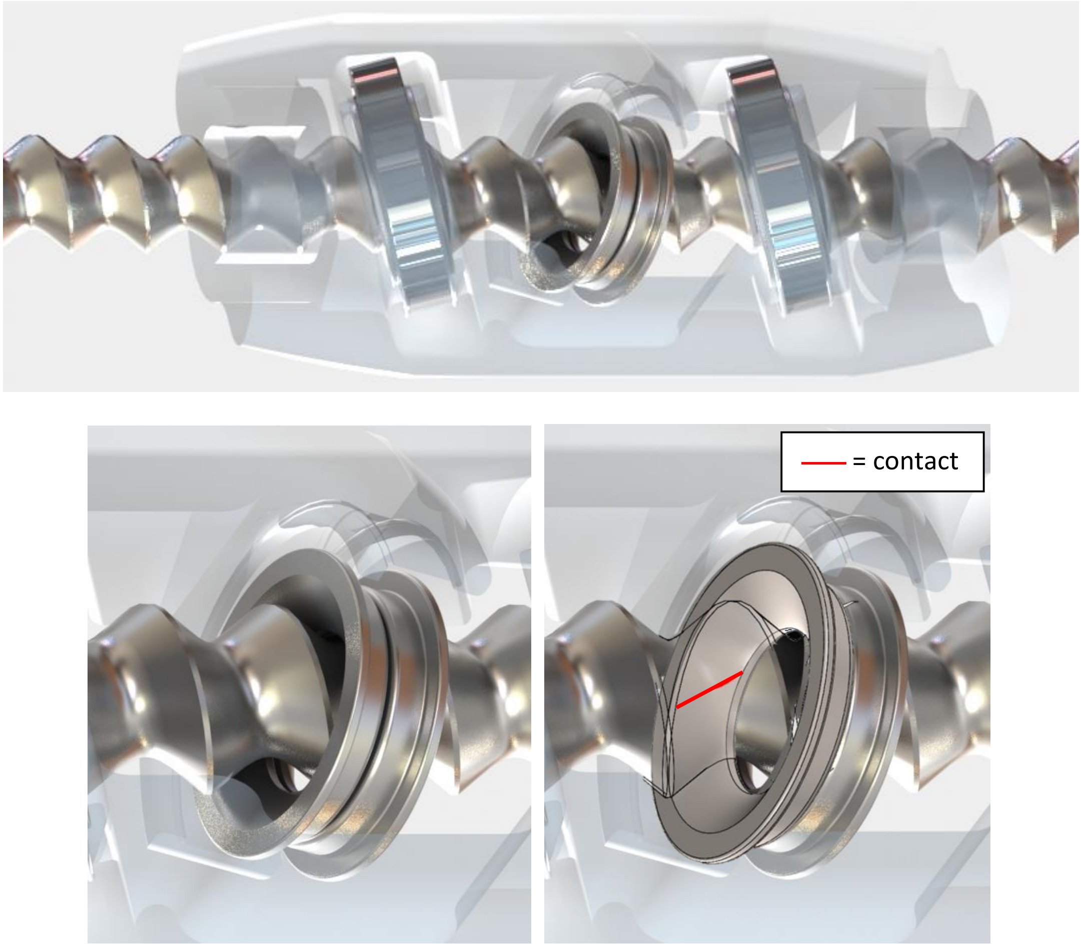

Fig. 24. visualisation of the contact line between a ring and screw rod. It can be seen that the line follows a straight line along the ring and rod surface. This straight line continues on the other side of the ring.

APPENDIX II
SCREW ROD AND RINGS OF THE FUNCTIONAL PROTOTYPE

This appendix shows the resulting designs for both the screw rod and rings for the functional prototype. Figure 25 shows a picture of the parts after machining. On the next two pages the engineering drawings made for manufacturing can be found, which contains all details and tolerances.

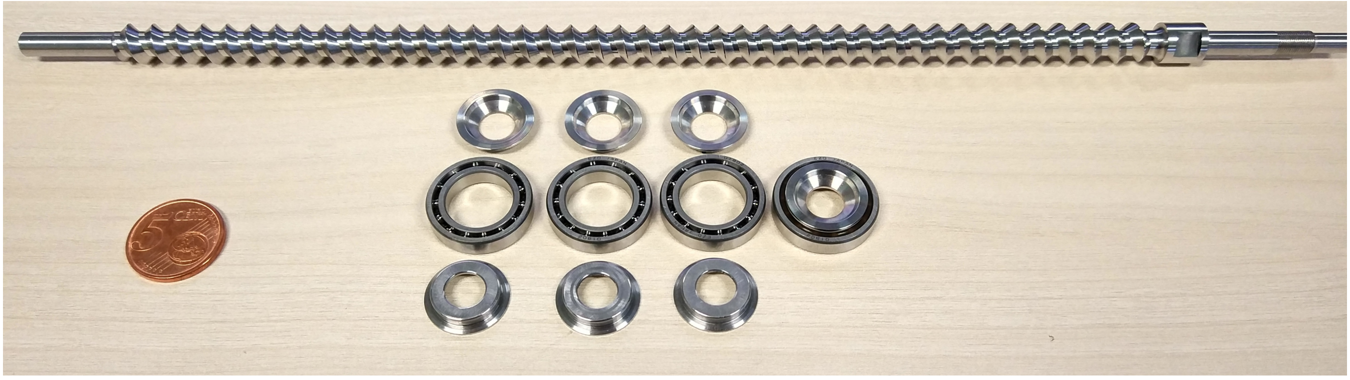

Fig. 25. The screw rod, rings and bearings for the functional prototype.

For the engineering drawings and thus for manufacturing a representation of the ring and rod surface on a plane is required. The 2D representation of the ring surface is found to be

$$Y = \tan(\alpha+\beta) \cdot \sqrt{\left(X + \frac{B}{2}\right)^2 + \left(\frac{a+b}{\tan(\alpha+\beta)}\right)^2} \tag{28}$$

Whereas the 2D representation of the grove surface of the screw rod is described by the following two equations

$$Radiaal = \frac{b}{\cos(\theta)} \tag{29}$$

$$Axial = h \cdot T - a \cdot \frac{b}{h} \cdot \tan(\theta) \tag{30}$$

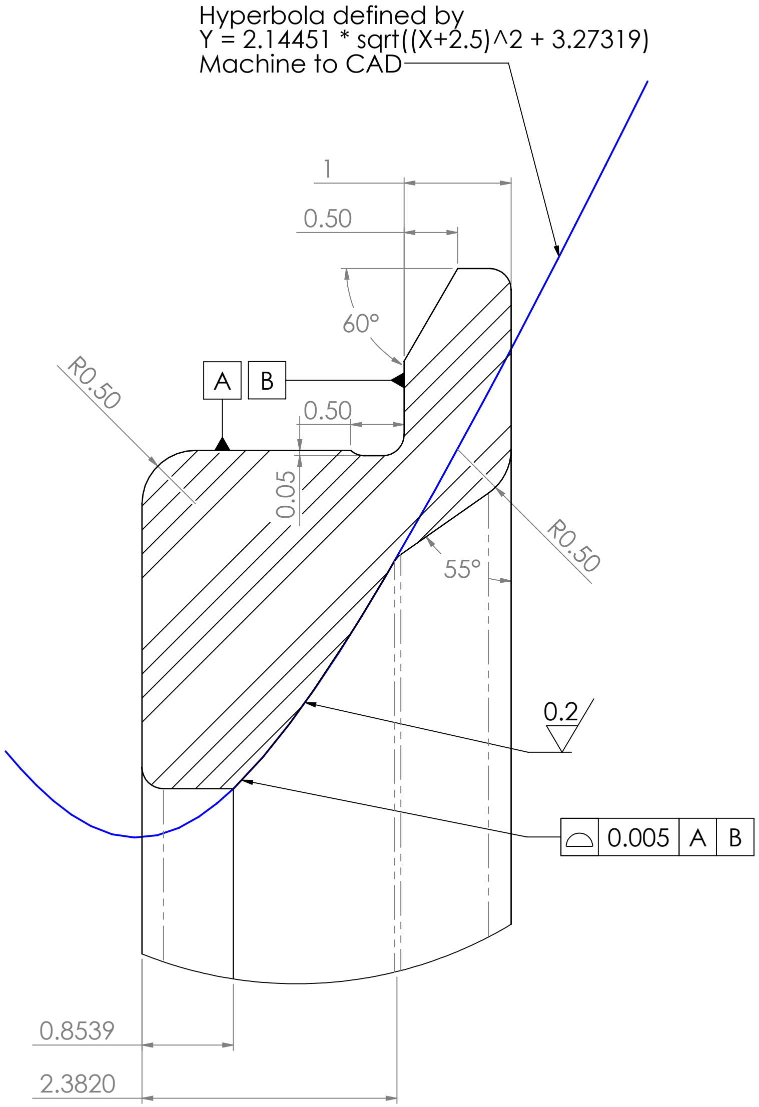
Hyperbola defined by
Y = 2.14451 * sqrt((X+2.5)^2 + 3.27319)
Machine to CAD
1
0.50
60°
A
B
R0.50
0.50
0.05
55°
R0.50
0.2
0.005
A
B
0.8539
2.3820

DETAIL B

SCALE 20 : 1

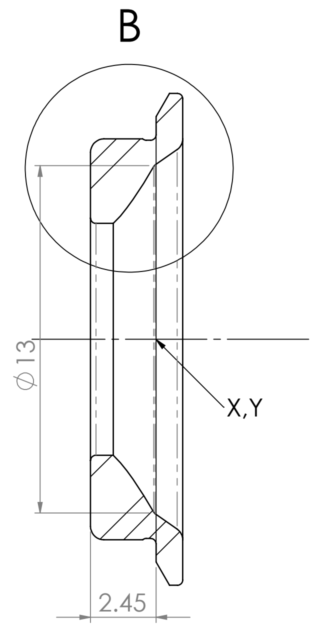

SECTION A-A

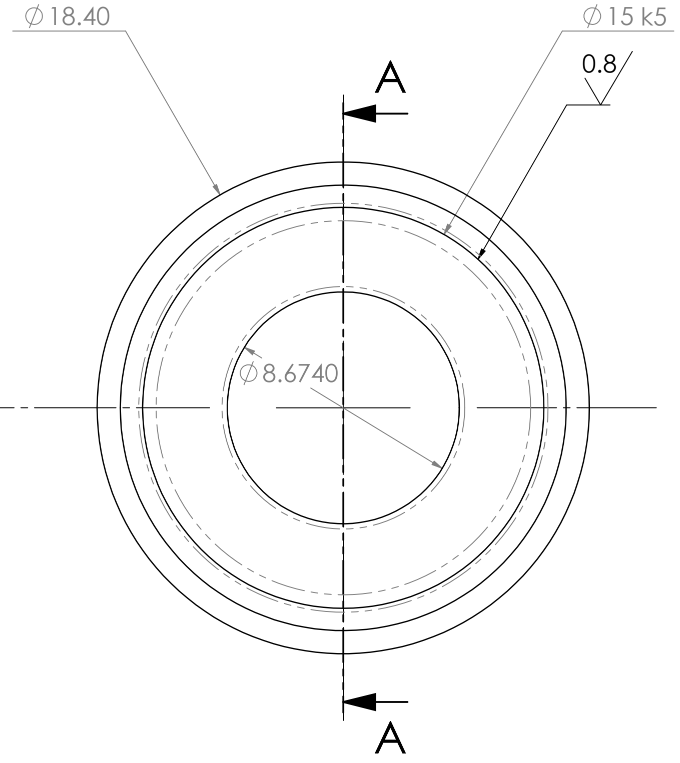
⌀18.40
⌀15 k5
0.8
A
⌀8.6740
A

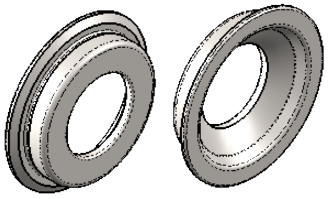

Pictorial Views

Scale 5:1		**Date** 22/08/2017	**Tolerances according to** UNI ISO 8015
Unit mm	**Mass** 3 gram		
Drawn E. Heijmink		**Model Ref.** RS0021A	**General tolerances UNI EN 22768-1 / 22768-2** Dimensional Tolerance class - f Geometric Tolerance class - H
Name Ring Screw Ring			**Roughness** 3.2
			Material Mat.: 1.6523 (20NiCrMoS2-2) Treatment: HEAT TREATMENT TO 60 HRC
IIT Italian Institute of Technology		formaat A3	**Undim. Rounds** R = 0.2 **Undim. Chamfers** 0.2 x 45

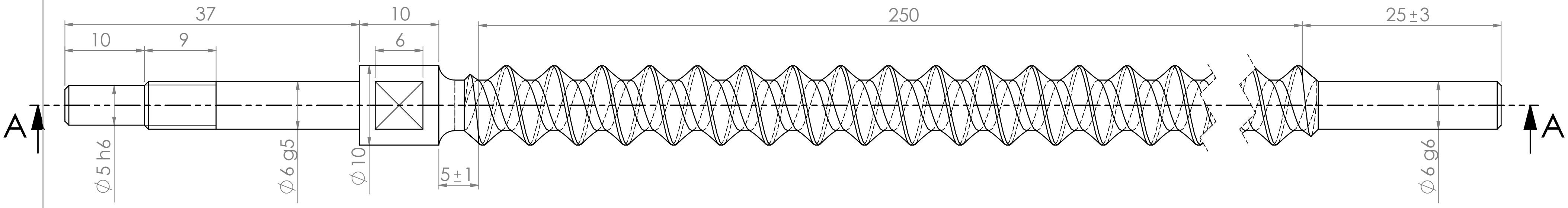
37
10
9
10
6
250
25±3
A
A
⌀5 h6
⌀6 g5
⌀10
5±1
⌀6 g6

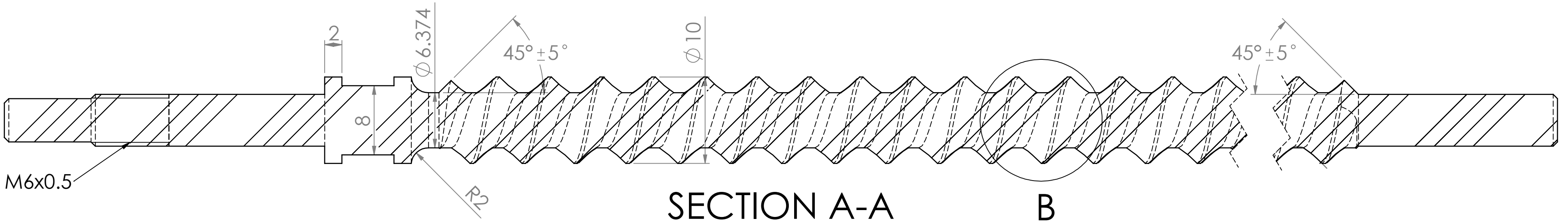
2
⌀6.374
45°±5°
⌀10
45°±5°
8
M6x0.5
R2
B

SECTION A-A

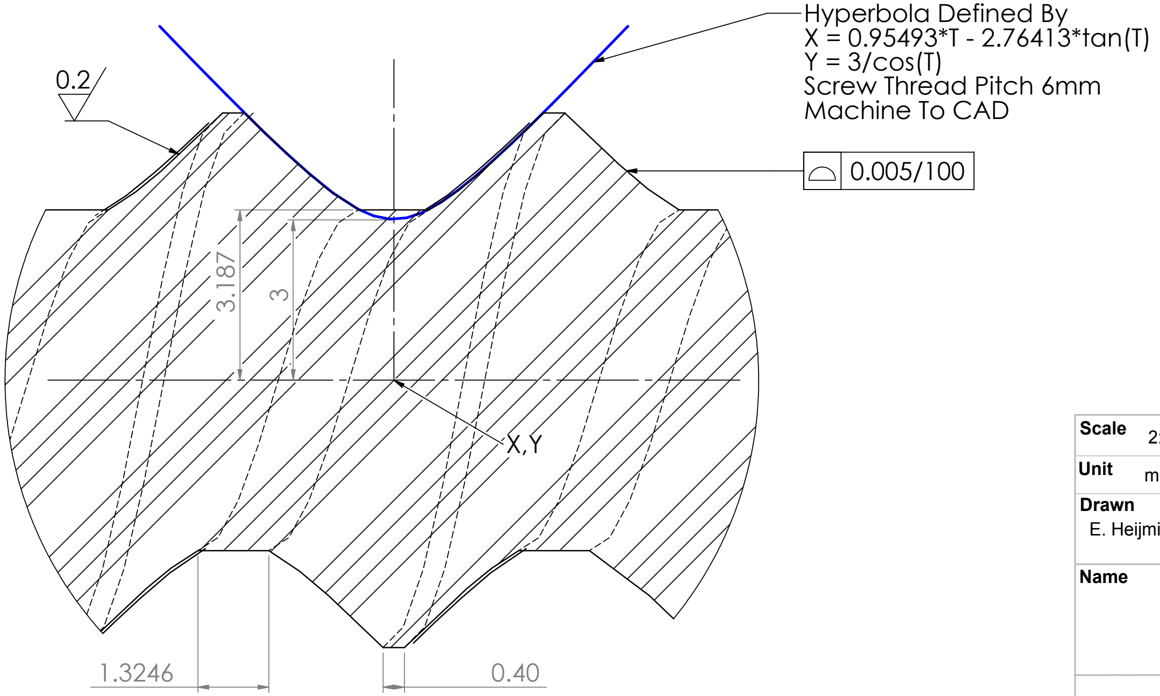
Hyperbola Defined By
X = 0.95493*T - 2.76413*tan(T)
Y = 3/cos(T)
Screw Thread Pitch 6mm
Machine To CAD
0.2
0.005/100
3.187
3
X,Y
1.3246
0.40

DETAIL B

SCALE 10 : 1

Pictorial view

Scale 2:1

Date 22/08/2017

Unit mm

Mass 117 gram

Drawn E. Heijmink

Model Ref. RS0022A

Tolerances according to
UNI ISO 8015

General tolerances UNI EN 22768-1 / 22768-2
Dimensional Tolerance class - f
Geometric Tolerance class - H

Name

Ring Screw Rod

Roughness 3.2

Material
Mat.: 1.6523 (20NiCrMoS2-2)
Treatment: HEAT TREATMENT TO 60 HRC

Undim. Rounds
R = 0.1

Undim. Chamfers
0.5 x 45

IIT
Italian Institute of Technology

formaat
A3

APPENDIX III
DETAILS NUT DESIGN OF THE FUNCTIONAL PROTOTYPE

This appendix shows the two materialised nut designs for the functional prototype. Pictures of the nut will be show as well as the engineering drawings used for manufacturing.

A. *Nut for experimental evaluation*

The first nut design is the design used in for experimental evaluation. This design uses leaf springs to apply the required preload between the screw rod and the rings as shown in Figure 16. Since this design consists out of two parts, locating pins are used to ensure a correct relative position. The metal design makes it possible to cut the screw tread , needed to attach the nut to the load and to each other, directly in the nut. Grooves around the bearing cut outs are added to improve machinability and reduce the effect of manufacturing inaccuracies.

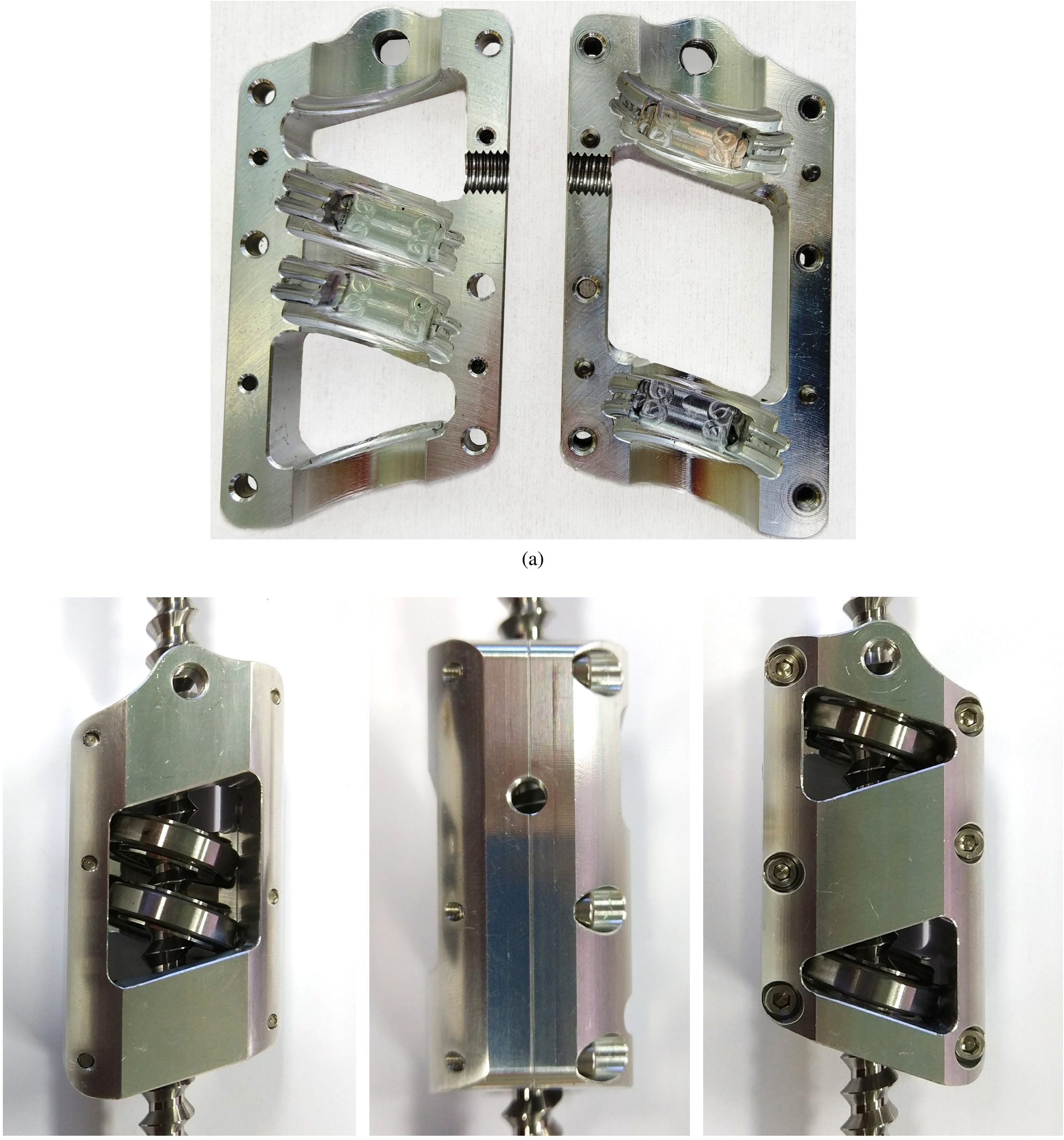

(a)

(b) (c) (d)

Fig. 26. The materialised nut design, used for experimental performance evaluation of the ring screw. (a) shows the inside of two nut halves, clearly showing the locating pins, seating for the leaf springs and screw thread used for the track roller.

(Front view)

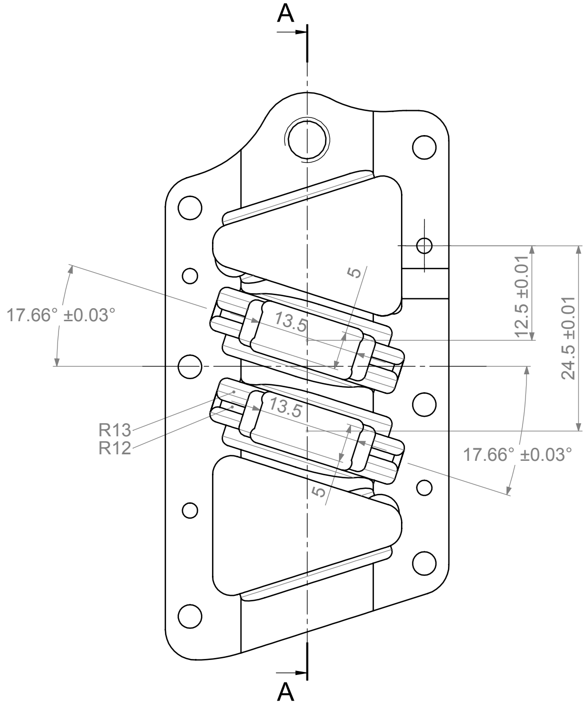
A
17.66° ±0.03°
5
13.5
12.5 ±0.01
24.5 ±0.01
13.5
R13
R12
17.66° ±0.03°
5
A

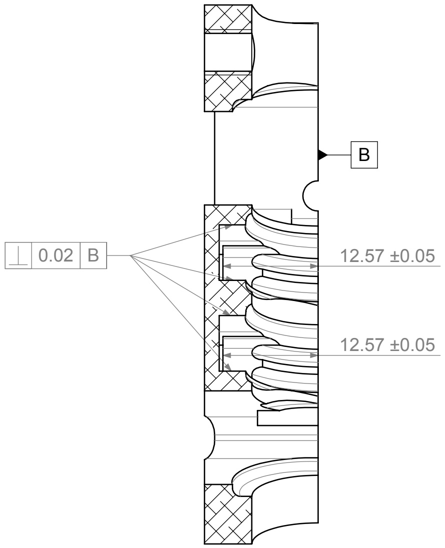
B
0.02 B
12.57 ±0.05
12.57 ±0.05

A-A

Location Pin holes and thread (front view)

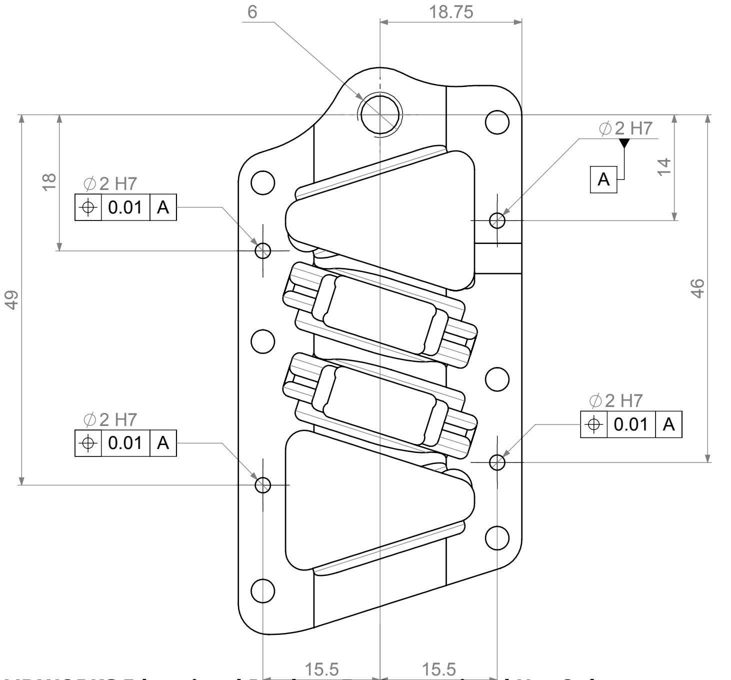
6
18.75
18
49
∅2 H7
0.01 A
∅2 H7
A
14
46
∅2 H7
0.01 A
∅2 H7
0.01 A
15.5
15.5

SOLIDWORKS Educational Product. For Instructional Use Only

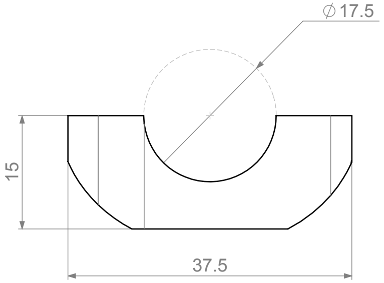

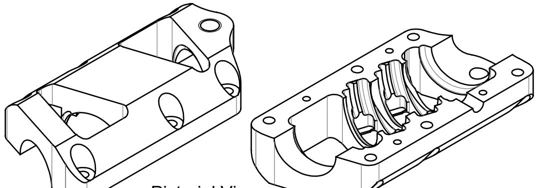

Pictorial Views

NOTES

#1- MACHINE TO MATH DATA (CAD)
This drawing only contains most important dimentions.

#2- REMOVE SHARP EDGES

Scale 2:1		**Date** 10/01/2018
Unit mm	**Mass** 44 gram	
Drawn E.Heijmink	**Part Number** RS3023A_M	

General tolerances UNI EN 22768-1 / 22768-2
Dimensional Tolerance class - **f**
Geometric Tolerance class - **H**

Name
RingScrew Nut Mid

IIT
Italian Institute of Technology

formaat A2

Roughness 1.6

Material
Material: Mat.: 7075-T6 (SN)
Treatment: None

Undim. Rounds
R = 0.2

Undim. Chamfers
0.5 x 45

(Front view)

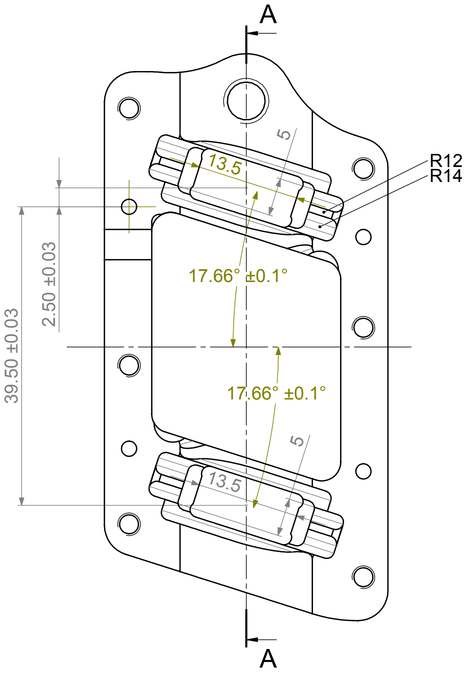
A
5
13.5
R12
R14
2.50 ±0.03
39.50 ±0.03
17.66° ±0.1°
17.66° ±0.1°
5
13.5
A

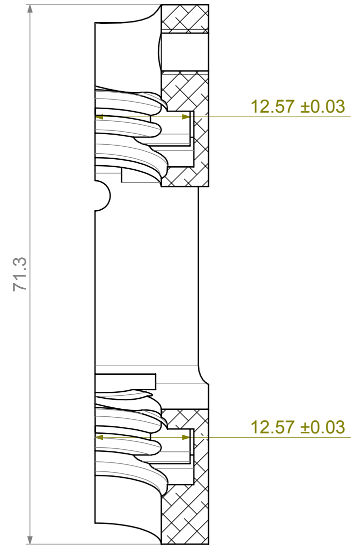
12.57 ±0.03
71.3
12.57 ±0.03

A-A

Location Pins and thread (front view)

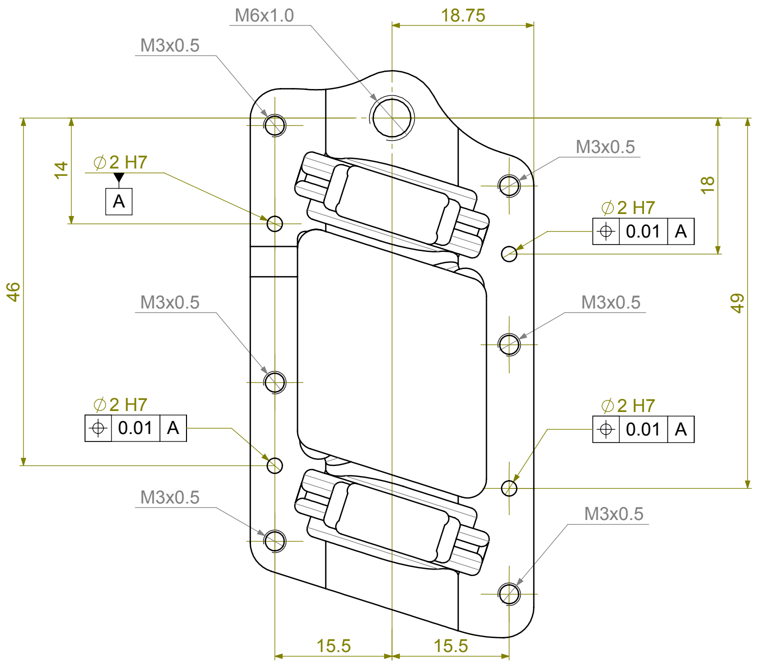
M6x1.0
18.75
M3x0.5
14
∅2 H7
A
M3x0.5
∅2 H7
⌖ 0.01 A
18
46
M3x0.5
M3x0.5
49
∅2 H7
⌖ 0.01 A
∅2 H7
⌖ 0.01 A
M3x0.5
M3x0.5
15.5
15.5

SOLIDWORKS Educational Product. For Instructional Use Only

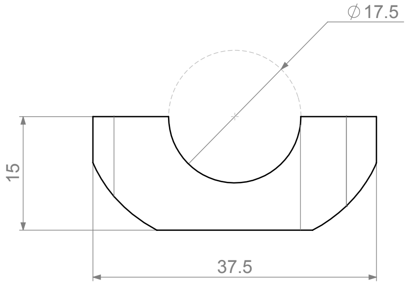

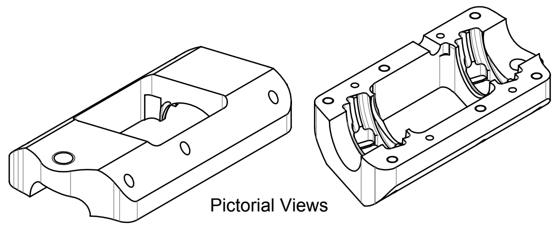

Pictorial Views

NOTES

#1- MACHINE TO MATH DATA (CAD)
This drawing only contains most important dimentions.

#2- REMOVE SHARP EDGES

Scale 2:1
Date 10/01/2018
Unit mm
Mass 43 gram
Drawn E.Heijmink
Part Number RS3023A_TB

General tolerances UNI EN 22768-1 / 22768-2
Dimensional Tolerance class - **f**
Geometric Tolerance class - **H**

Name
RingScrew Nut top

Roughness 1.6

Material
Material: Mat.: 7075-T6 (SN)
Treatment: None

Undim. Rounds
R = 0.2

Undim. Chamfers
0.5 x 45

formaat
A2

IIT
Italian Institute of Technology

B. Nut for product development

The second nut design is the design that shows the most potential for future commercializing of the ring screw. This design uses the deformation of the whole nut to apply the required preload between the screw rod and the rings. Caused by the complex structure of the nut, a FEM analysis is used to model this preload as can be seen in figure 18. The nut is printed out of Nylon-12 (PA12) powder using a 3D printing technique called Selective laser sintering (SLS). The use of SLS technique and PA12 material is chosen becouse it higher accuracy, strength and mechanical properties that are comparable (or sometimes even better) than the bulk material. [28] The nut is printed such that the printing layers are perpendicular to the main axis of the screw rod. In this way the stiffness of the material is equal in this planes and a little lower along the screw axis.

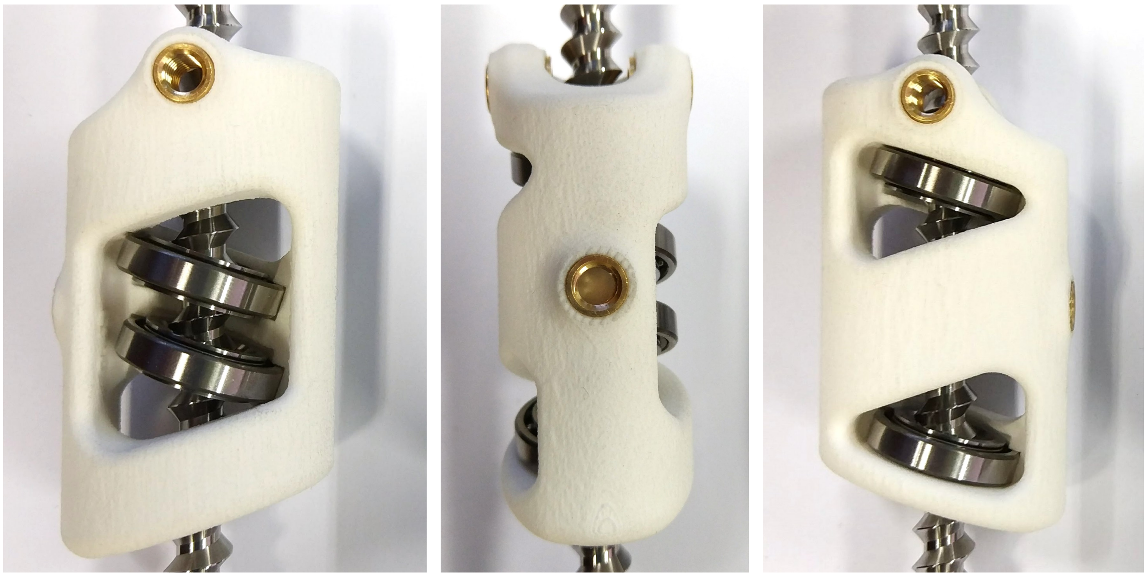

(a) (b) (c)

Fig. 27. The materialised nut design that shows the most potential for future commercializing of the ring screw. Copper screw thread inserts are used for connecting the load and the track roller.

Preload 0 N
Offset = 2x 0.879

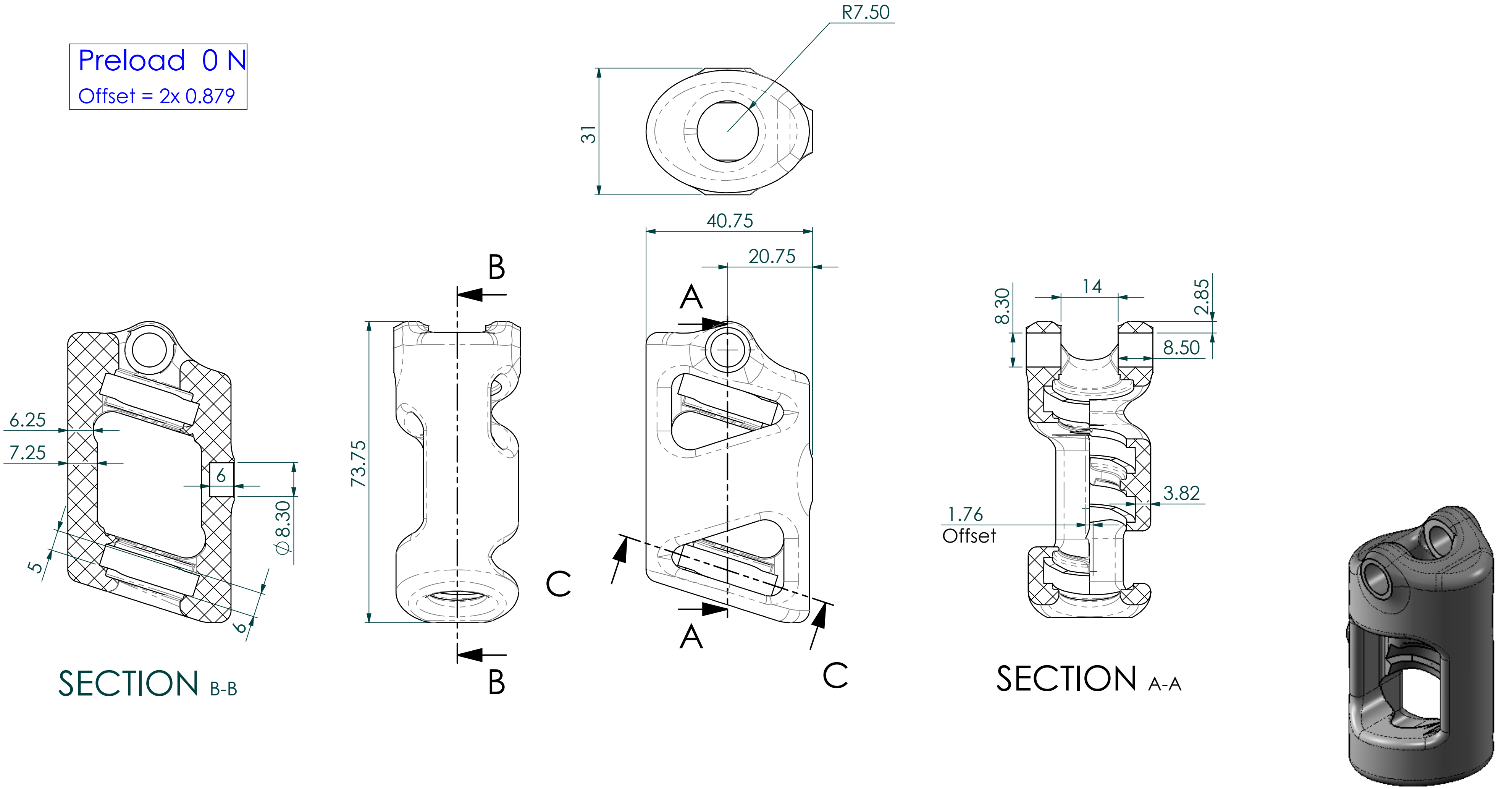
R7.50
31
40.75
20.75
B
B
A
A
C
C
6.25
7.25
6
ϕ8.30
5
6
73.75
14
8.30
2.85
8.50
3.82
1.76
Offset
SECTION B-B
SECTION A-A

PICTORIAL VIEW

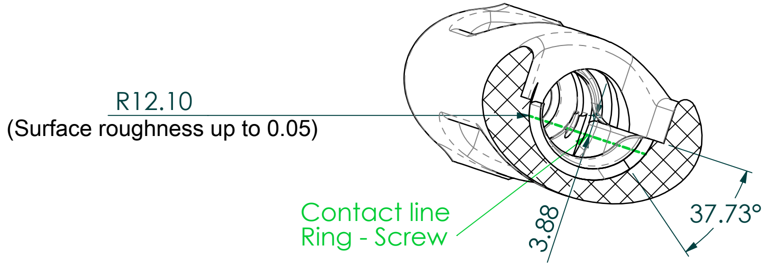
R12.10
(Surface roughness up to 0.05)
Contact line
Ring - Screw
3.88
37.73°

SECTION C-C

Scale 1:1		**Date** 10/01/2018	**Tolerances according to** UNI ISO 8015
Unit mm	**Mass** 31 gram		
Drawn E. Heijmink (elco.heijmink@iit.it)		**Model Ref.** RS0023H	**General tolerances UNI EN 22768-1 / 22768-2** Dimensional Tolerance class - Geometric Tolerance class -
Name RingScrew Nut			**Roughness**
			Material Mat.: DuraForm PA12 Treatment: None
IIT Italian Institute of Technology		formaat A3	**Undim. Rounds** R = 0.2 **Undim. Chamfers** 0.5 x 45

APPENDIX IV
CONCEPTS EXPERIMENTAL SETUP

Screw devices are used in many different applications and so in loading situations. Therefore it is not straight forward to define the test scenario the experimental setup should create. As described in section V-B any coaxial loading that can deliver up to 800N of thrust force fits the requirements.

Concept 1, Double rocker setup

Setup using a rocker (grey) as a load. The motion of the screw(pink) is amplified by the arrangement of the rocker, creating an inertia load. By changing the acceleration the full range of force and speed combinations can be achieved without changing the setup. The driving motor (orange) is connected to the frame (yellow) with an torque sensor (purple) measuring the reaction torque of the motor.

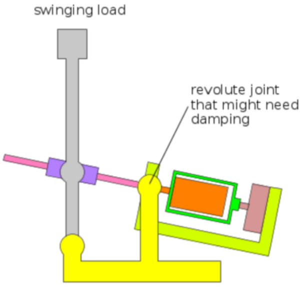

Advantages

- Al loadings possible without changes
- Backdrivability experiments possible.
- Mechanically simple setup
- Only coaxial forces on screw
- Attractive demonstration

Disadvantages

- Moving electronics (wires)
- Many factors contribute to load
- High speed moving parts (safety)

Concept 2, Stationary rocker setup

Setup using a rocker (grey) as a load. The motion of the screw(pink) is amplified by the arrangement of the rocker, creating an inertia load. By changing the acceleration the full range of force and speed combinations can be achieved without changing the setup. The driving motor (orange) is connected to the frame (yellow) with an torque sensor (purple) measuring the reaction torque of the motor.

- 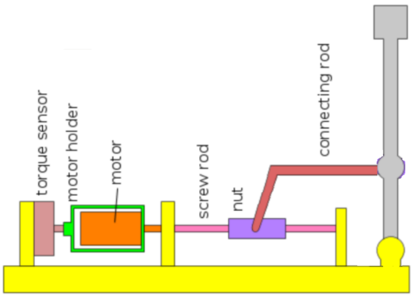
torque sensor
motor holder
motor
screw rod
nut
connecting rod

Advantages

- Al loadings possible without changes
- Backdrivability experiments possible
- Mechanically simple setup
- Attractive demonstration

Disadvantages

- Non coaxial forces on screw
- Many factors contribute to load
- High speed moving parts (safety)

Concept 3, gravity load setup

Setup using a weight (grey) as a load. The motion of the screw(pink) coupled to a weight that gets lifted, creating a gravity load. By changing the weight the full range of force and speed combinations can be achieved but the setup has to be altered. The driving motor (orange) is connected to the frame (yellow) with an torque sensor (purple) measuring the reaction torque of the motor.

- 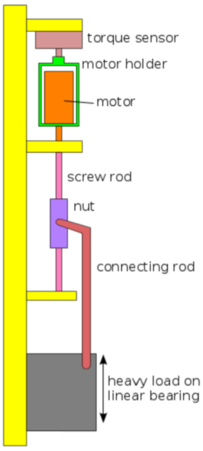
torque sensor
motor holder
motor
screw rod
nut
connecting rod
heavy load on linear bearing

Advantages

- Backdrivability experiments possible
- Mechanically simple setup
- Only coaxial forces on screw
- Easy to determine load
- Steady state experiments possible

Disadvantages

- High speed hard to reach (inertia)
- Changes needed for different loads
- Heavy setup
- Load only pulling

Concept 4, active load

Setup using a second motor as a load. The motion of the screw (pink) to a timer belt that is actuates and braked by a second motor, creating an active load. By controlling the motor all force and speed combinations can be actively defined. The driving motor (orange) is connected to the frame (yellow) with an torque sensor (purple) measuring the reaction torque of the motor.

- 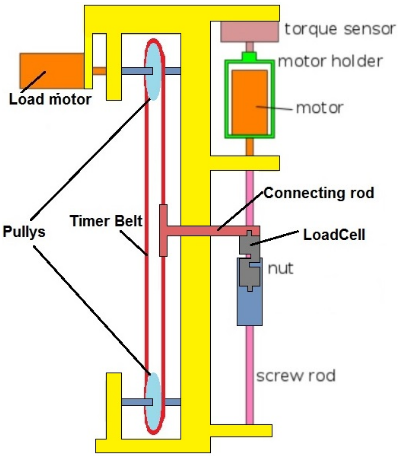
torque sensor
motor holder
Load motor
motor
Connecting rod
Pullys
Timer Belt
LoadCell
nut
screw rod

Advantages

- Backdrivability experiments possible
- Al loadings possible without changes
- Only coaxial forces on screw
- Easy to variate load
- Steady state experiments possible

Disadvantages

- Higher cost, (double electronics)
- Hard to control
- Cogging of the motors

Concept 5, linear damper load

Setup using a damper as a load. The motion of the screw (pink) to a linear hydraulic damper as a load, creating an speed dependant load. By selecting an controllable damper most force and speed combinations can be defined. The driving motor (orange) is connected to the frame (yellow) with an torque sensor (purple) measuring the reaction torque of the motor.

- 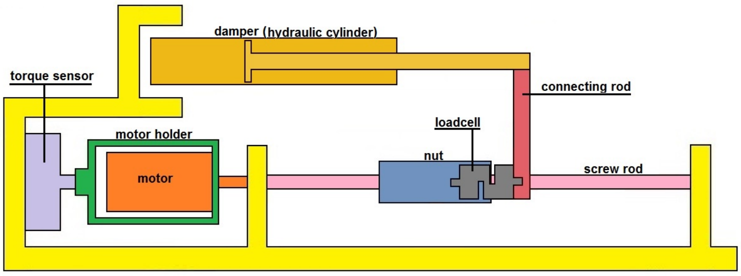
damper (hydraulic cylinder)
torque sensor
connecting rod
loadcell
motor holder
nut
motor
screw rod

Advantages

- Only coaxial forces on screw
- Easy to control
- Steady state experiments by default
- Save (brakes automatically)
- load easy to define

Disadvantages

- Backdrivability experiments not possible
- low force high speed not possible

APPENDIX V
DETAILED RESULTS BEARING FRICTION EXPERIMENTS

This appendix contains extra information and results from the bearing friction experiments described in section V-B.2.

A. *Influence of heat on the bearing friction*

The temperature has an influence on factors like preload and viscosity of the lubrication of a bearing. Therefore changes in temperature can influence the efficiency of a bearing. Although all experiments have been conducted in a controlled room temperature of $20\deg$ celsius, the bearings generate heat themselves resulting in large temperature changes.

To identify this effect of self heating on the energy loss in these bearings an experiment is conducted. In this experiment a bearing that is completely on $20°$ Celsius is operated three times at a high speed for 15 seconds with brakes of 15 seconds in between. This is per formed at various speeds al showing a similar results. In figure 28 a heat experiment at $5000 RPM$ is shown where the tree runs are aligned.

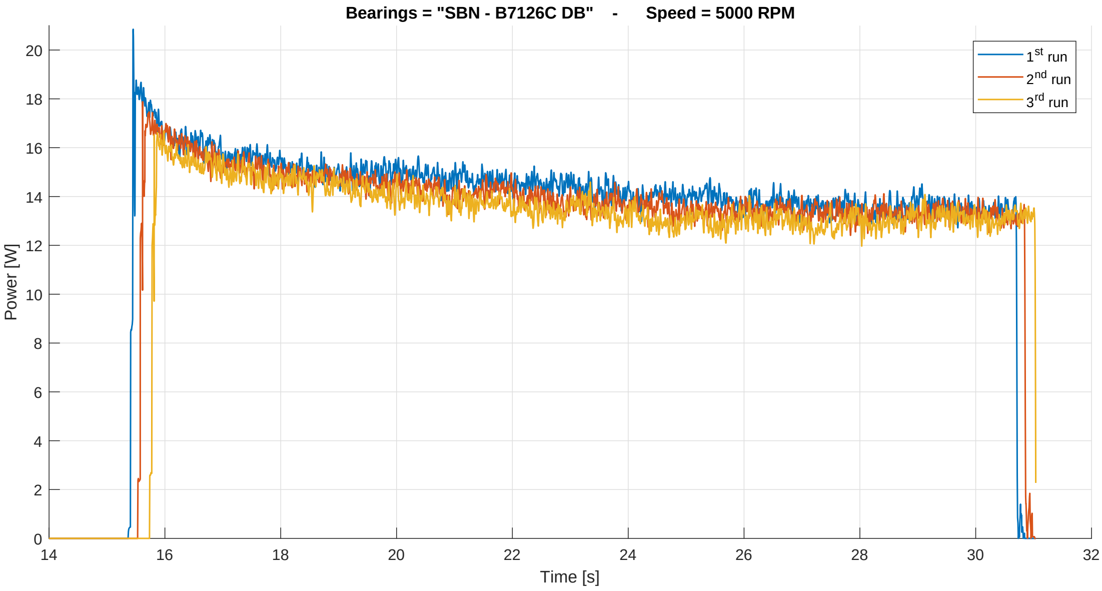

Fig. 28. In this graph the effect of self heating on the energy loss of a bearing is shown. It can be observed that some heat is stored in the bearing after 15s, reducing the initial friction peak. After 5 seconds no big difference in energy observes, while after 10 seconds an complete steady state can be seen.

B. *Bearing friction*

The experimental setup shown in Figure 19 holds the ring screw with a set of angular contact bearings. The energy loss in these bearings will contribute to the measured energy loss in the experiments. To be able to subtract these energy loss from the measurements and so find the efficiency of the ring screw, the energy loss in these bearings is accurately identified.

This subsection presents the more detailed results from the experiments described in section V-B.2.

As indicated by the lines six experiments have been conducted in series, each with a axial load on the bearings of $1N, 100N, 200N, 400N, 600N, 1N$. Where the 1N experiment has been conduced twice to find changes in the results over time. These experiments have been plotted over each other in figure 29. Each of these experiments operate the bearings at 6 speeds which are: $2000RPM, -2000RPM, 4000RPM, -4000RPM, 6000RPM, -6000RPM, 8000RPM, -8000RPM$. So in total all combinations of these forces and speeds result in 64 measured conditions. Al of these conditions have been performed 3 times for a minimum of 10 seconds with a sample rate at $1KHz$.

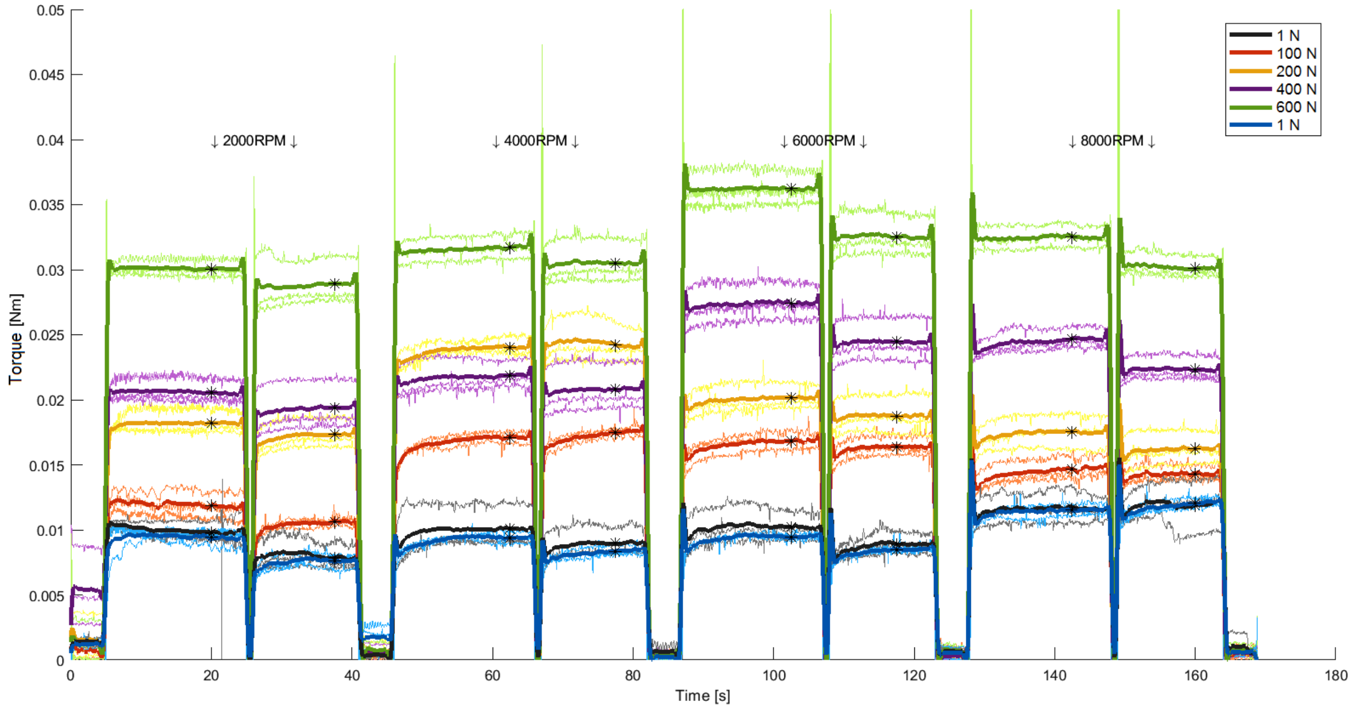

Fig. 29. In this graph the measured bearing friction torque is shown. The thin light lines represent the raw data, where the thick lines represent the filtered mean of the three experiments. It can be seen that the friction torque is mainly influenced by the load and barley by the speed. It can also be seen that counter clockwise (second 10s steps) reults in a lower friction torque than clockwise (first 15s steps).

It is knows that the friction torque can be predicted using formula 27. To find the values of A, B, C and D the data of Figure 29 is fitted on Equation 27. The black stars in the plots in figure 29 indicate the used data points for this data fitting. The created fit using the matlab toolbox is shown in Figure 30.

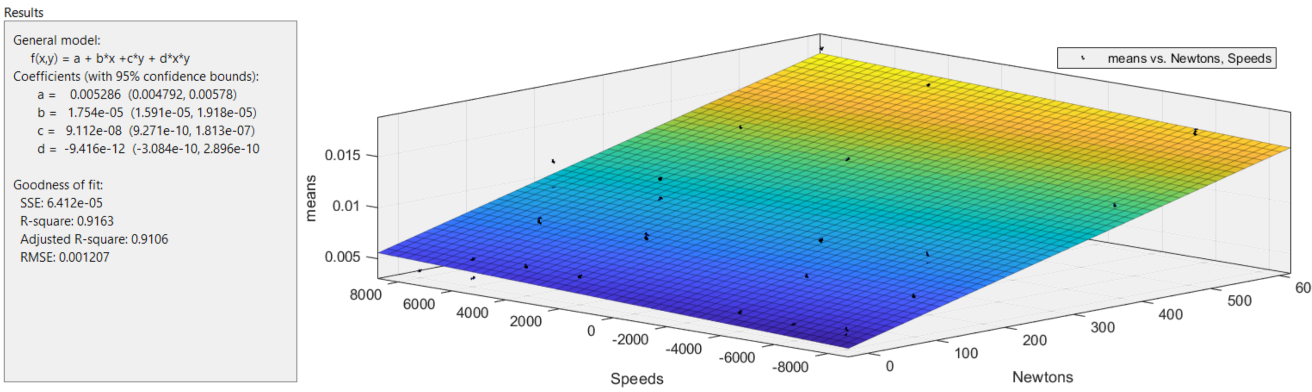

Results

General model:
f(x,y) = a + b*x +c*y + d*x*y
Coefficients (with 95% confidence bounds):
a = 0.005286 (0.004792, 0.00578)
b = 1.754e-05 (1.591e-05, 1.918e-05)
c = 9.112e-08 (9.271e-10, 1.813e-07)
d = -9.416e-12 (-3.084e-10, 2.896e-10)

Goodness of fit:
SSE: 6.412e-05
R-square: 0.9163
Adjusted R-square: 0.9106
RMSE: 0.001207

Fig. 30. The fit made of the experimental data on the friction torque equation. The back points, floating around the plane, indicate the experimental data where the plane represents the made fit.

APPENDIX VI
RESULTS RING SCREW VELOCITY EXPERIMENT

This appendix shows the raw data from the maximal velocity experiments described in section VI.

A. Resonance of screw rod

The experiment presented in this subsection aims to identify the resonance frequently of the screw rod. The resonance frequency of the screw rod could be reached for the screw rod constraind in a ”fixed- simple” configuration, given the maximum velocity of the driving motor. Therefore the constraints of the screw have been changed to ”fixed - free” Lowering the resonance frequency of the screw rod. Figure 31 shows the measurements of this experiment where the screw rod is step-by-step raised till resonance could be observed. Besides visual results, an raise in consumed power could be observed at the resonance frequency.

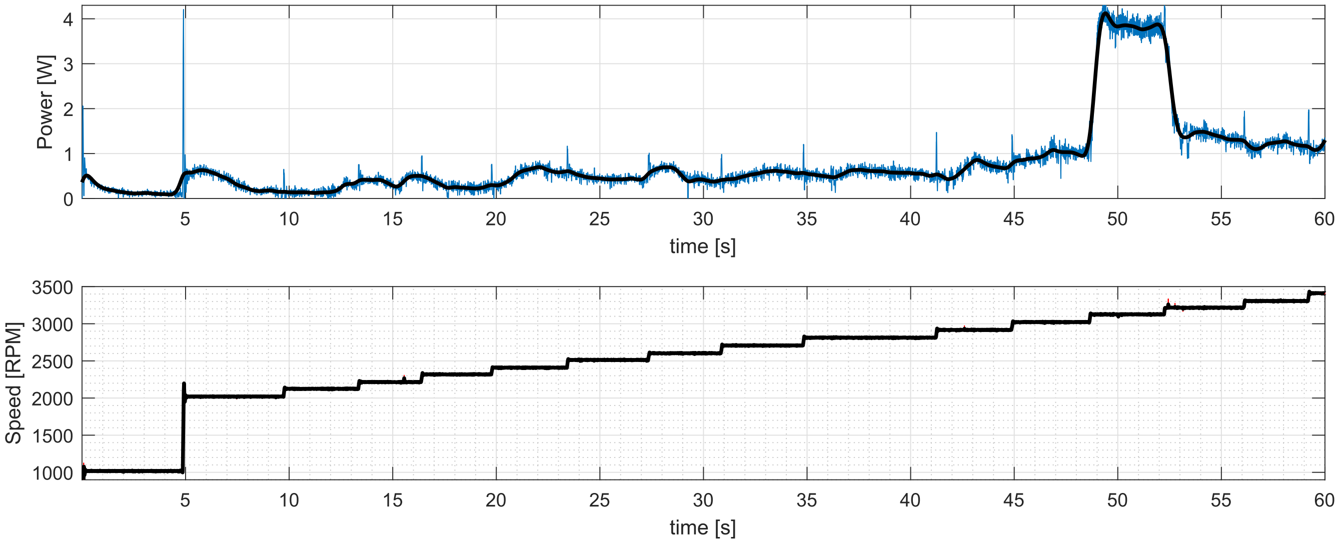

Fig. 31. In this figure an increase of power consumption can be seen at the resonance frequency. This occurs at a speed of $3100 RPM$

B. *Ring screw operation at 16500 RPM*

The experiment presented in this subsection aims to find unexpected failure modes of the ring screw up to its maximum speed. Therefore the ring screw has been operated to the speed of $16500 RPM$. The limited acceleration of the electronics limits the maximum velocity for reliable efficiency experiments to $8000 RPM$. To avoid this issue this experiment does not make use of the driving electronics to reach its top speed. The screw is driven by constant force springs and accelerated over the full lenght of the screw. The acceleration ends at a speed of $16500 RPM$ where the nut reaches the end stops and quickly decelerates. The measurements of this experiments can be found is Figure 33.

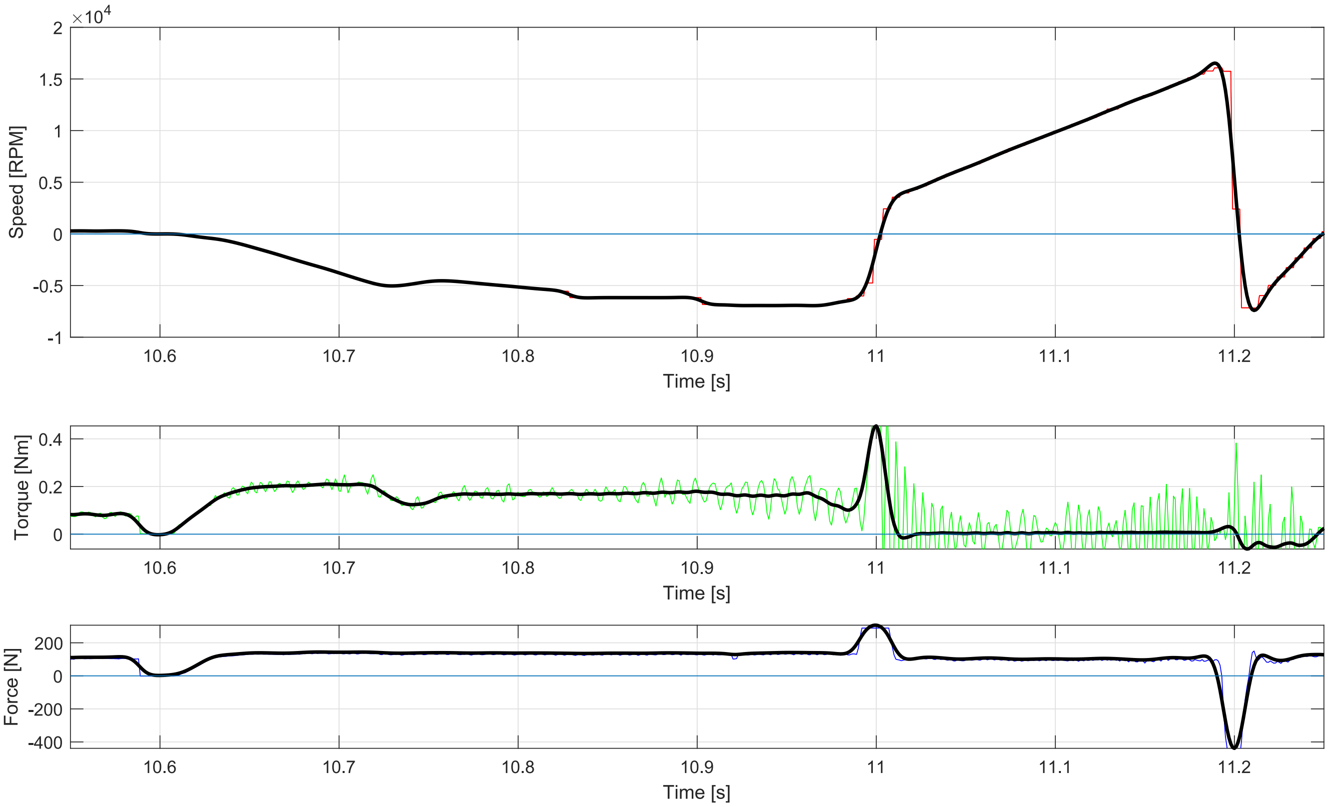

Fig. 32. Ring screw reaching 16500 RPM

APPENDIX VII
EXTRA DATA EFFICIENCY EXPERIMENTS

This appendix shows the raw data, similar to the data presented in Figure 21, for all other measurement points presented in Figure 22. Further more a plot comparing the experimental efficiency with the predicted efficiency of subsection III-D is presented.

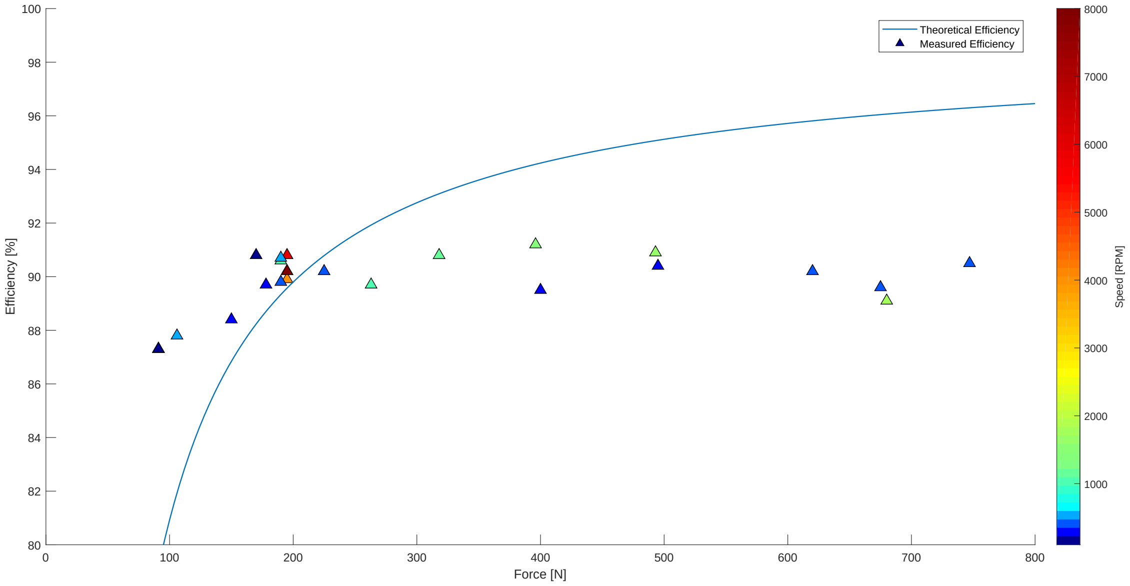

Fig. 33. Experimental data (△) of the ring screw compared with the predicted efficiency.

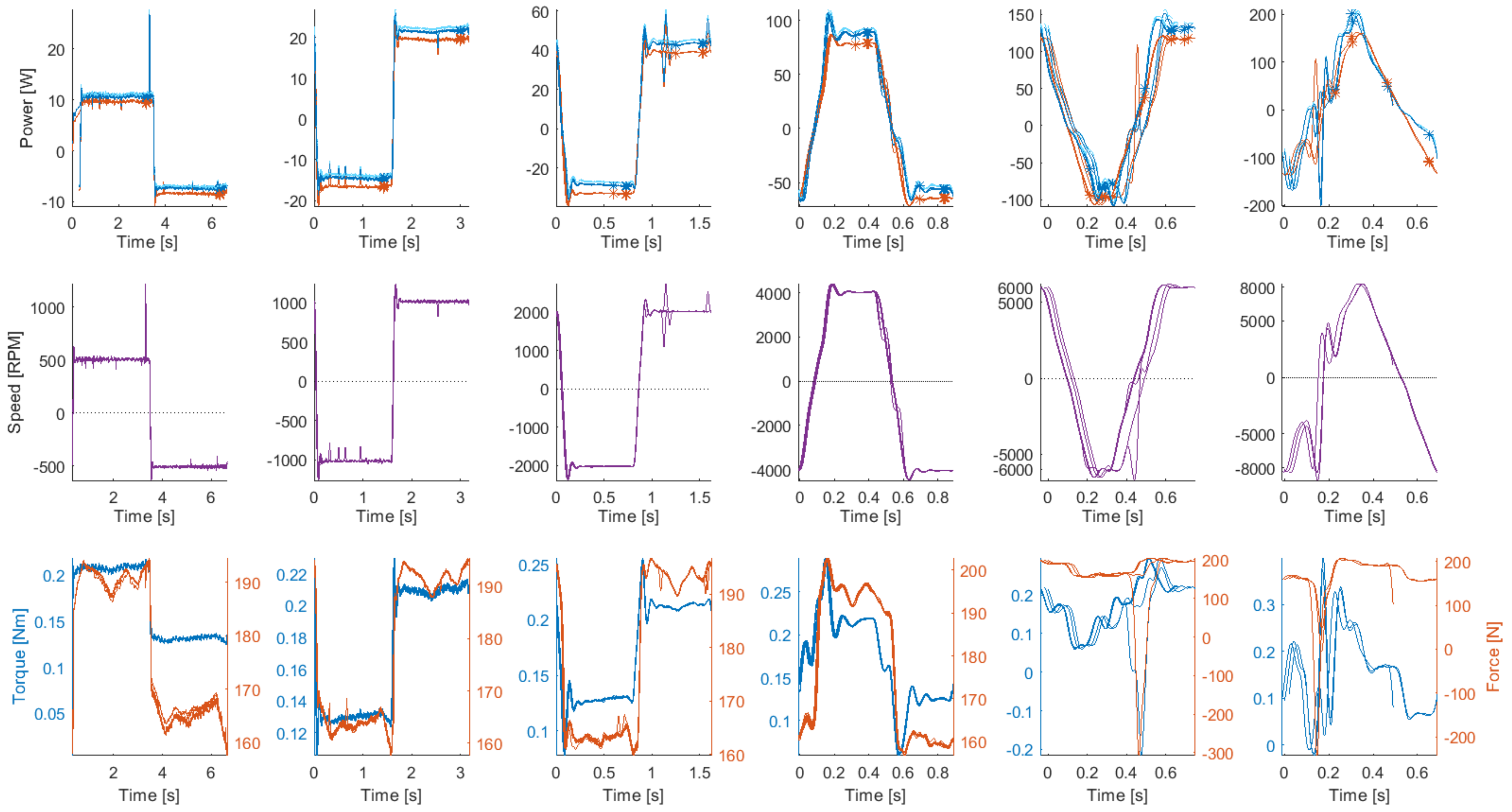
Ring Screw - Load: CFS 180N

Ball Screw - Load: CFS 180N

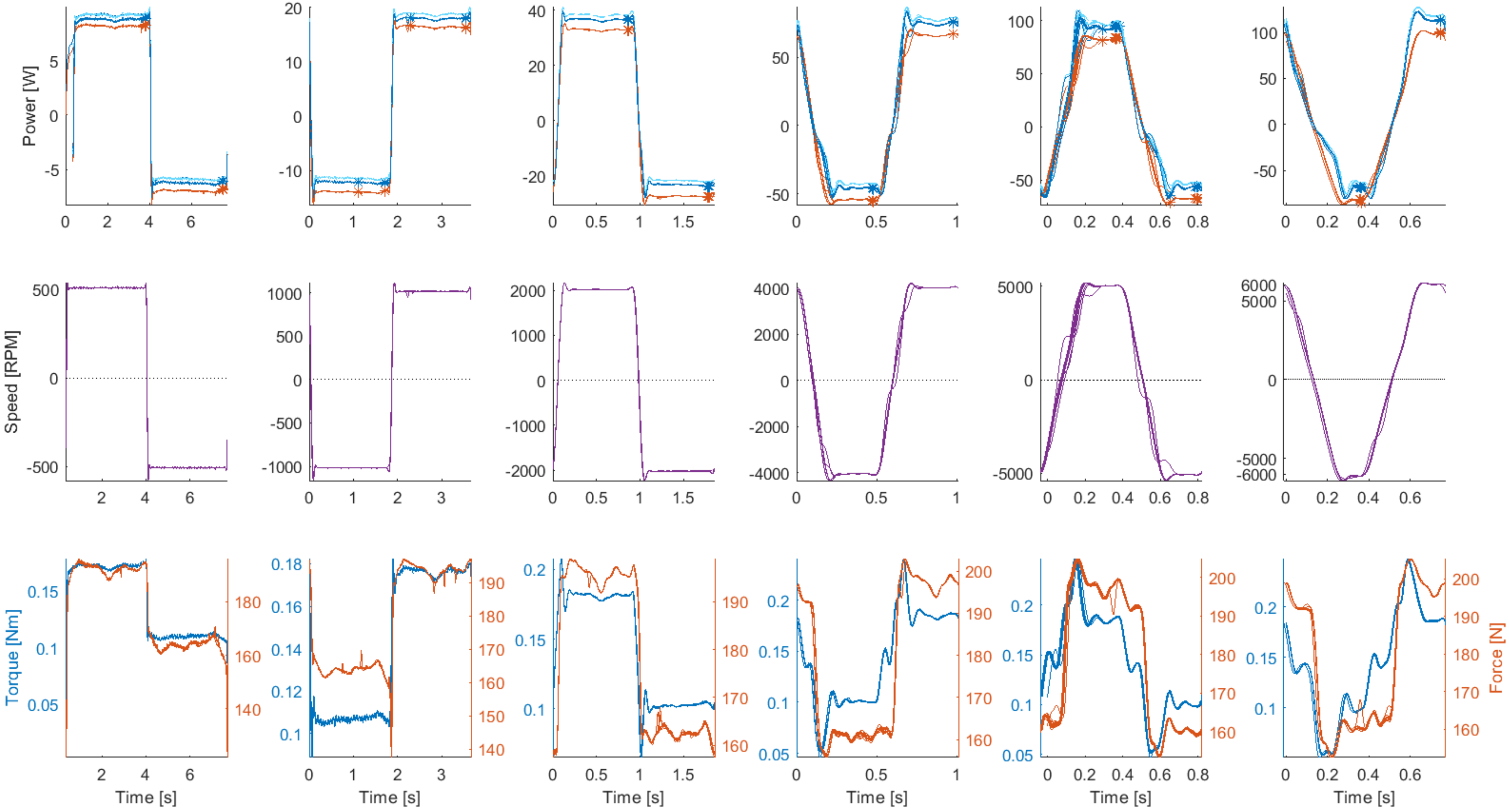

Ring Screw - Load: Damper low

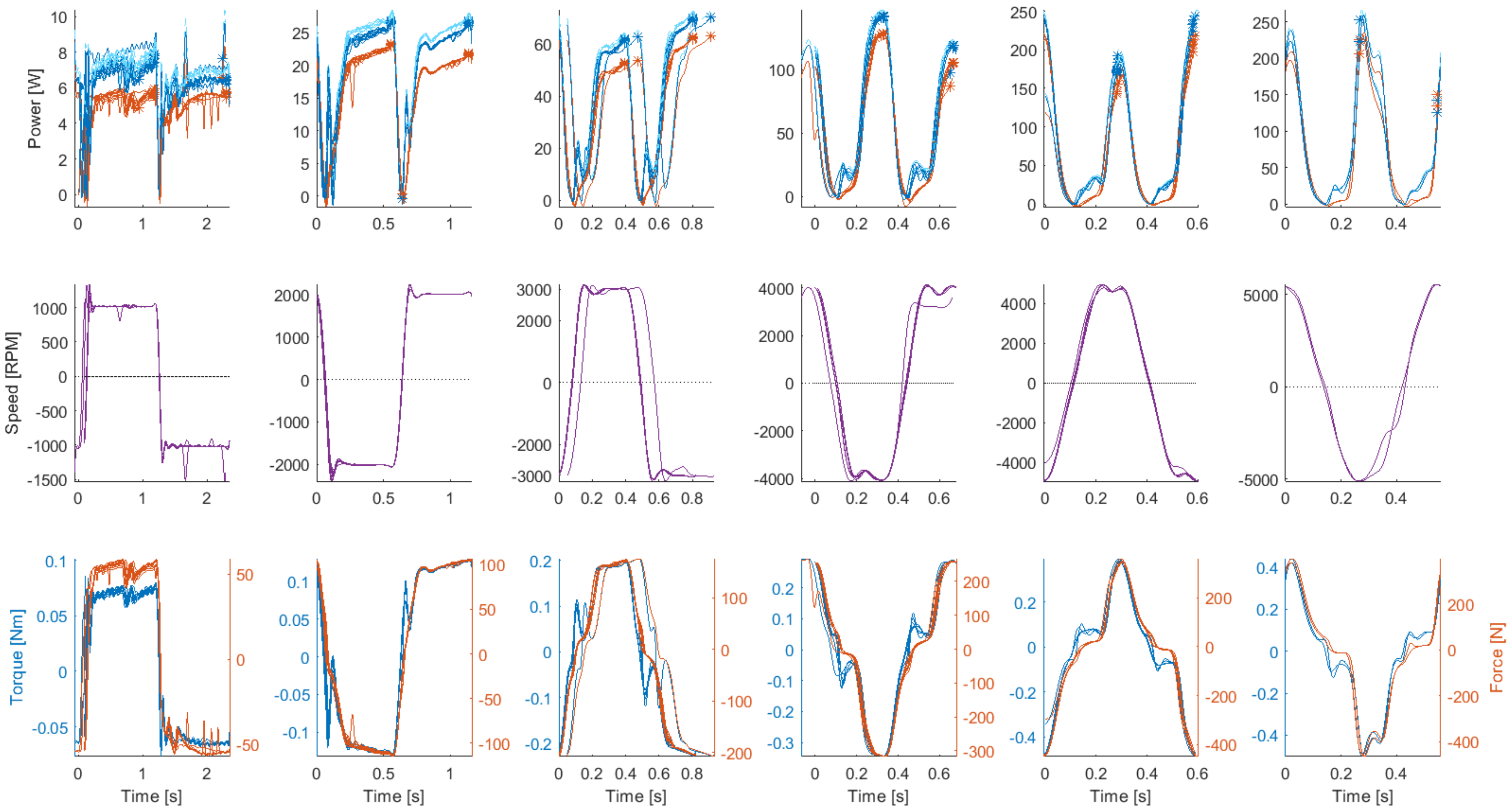

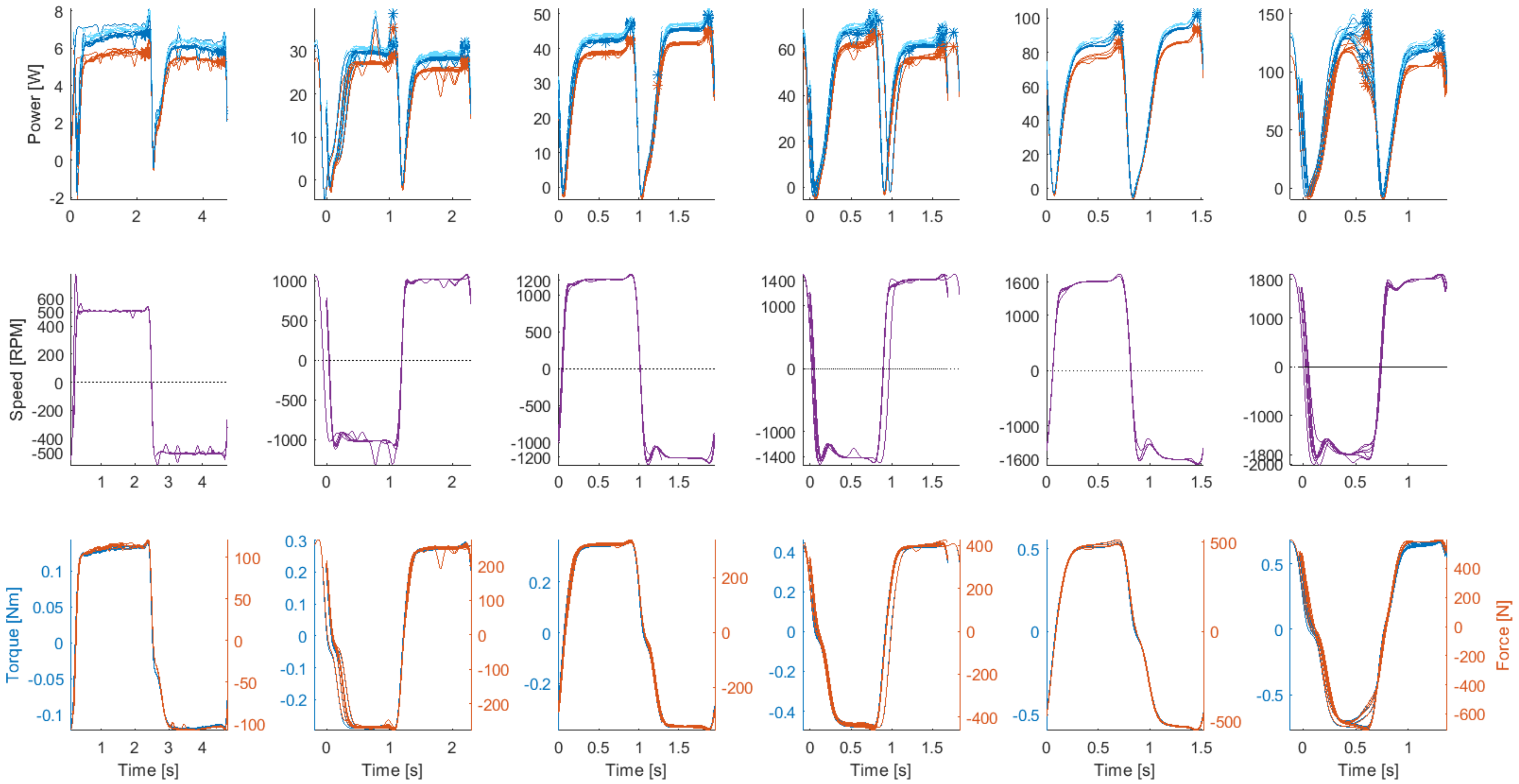

Ring Screw - Load: Damper

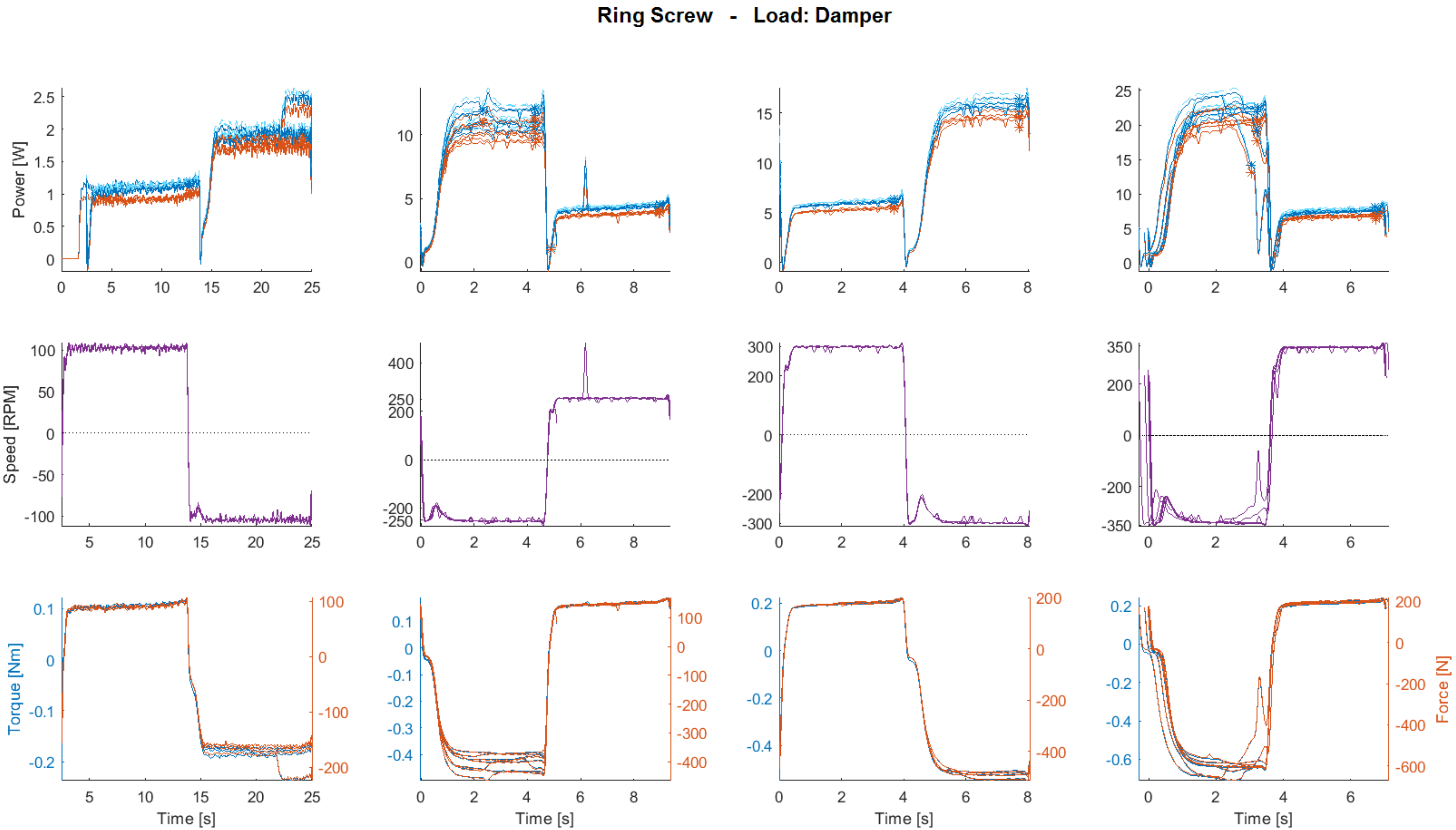
Ring Screw - Load: Damper
Power [W]
Speed [RPM]
Torque [Nm]
Force [N]
Time [s]
Time [s]
Time [s]
Time [s]
0
0.5
1
1.5
2
2.5
5
10
15
20
25
100
50
-50
-100
400
250
200
-200
-250
300
-300
350
-350
0.1
-0.1
-0.2
-0.3
-0.4
0.2
-0.6
-400
-600

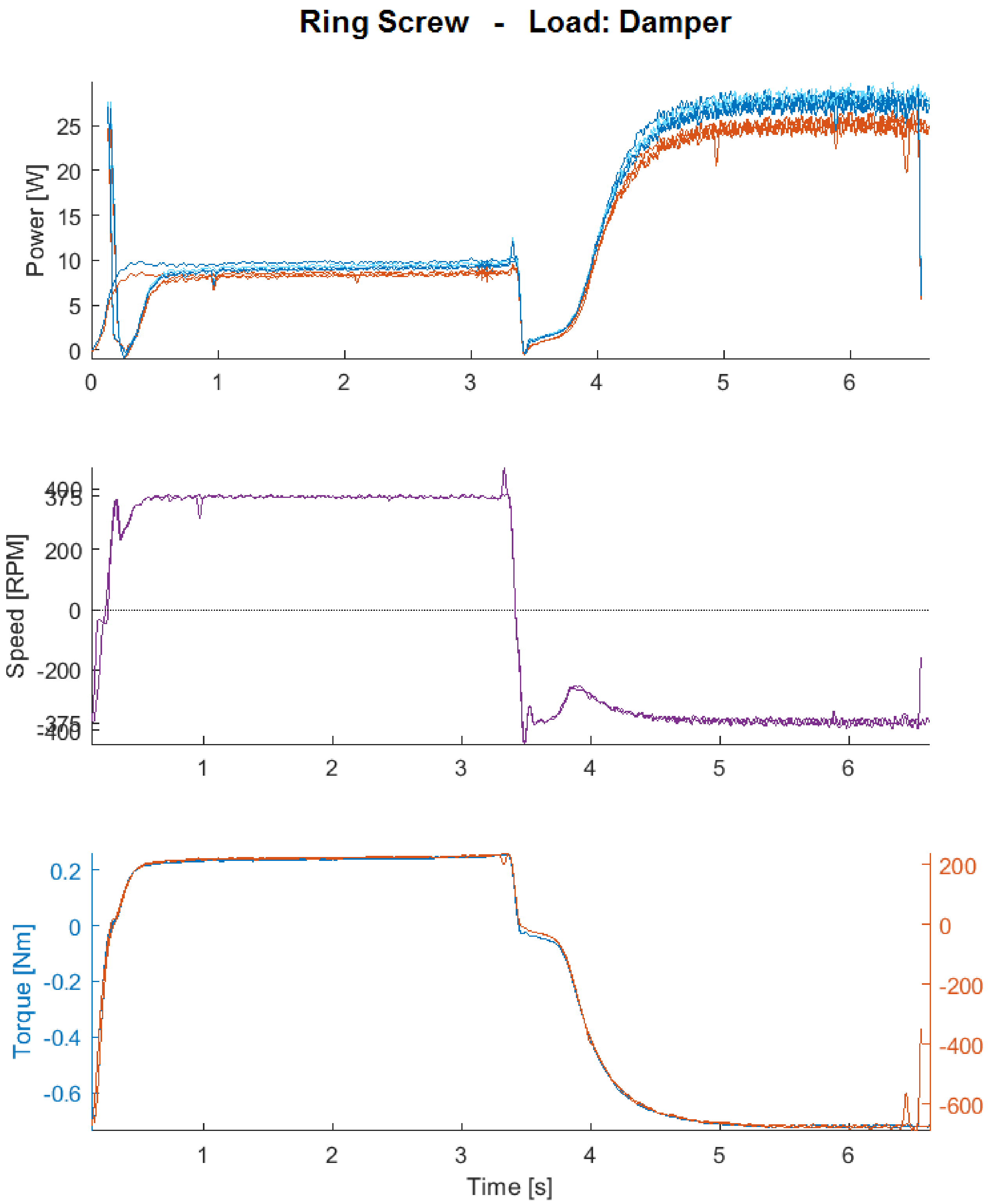
Ring Screw - Load: Damper
Power [W]
25
20
15
10
5
0
0
1
2
3
4
5
6
Speed [RPM]
400
375
200
0
-200
-375
-400
1
2
3
4
5
6
Torque [Nm]
0.2
0
-0.2
-0.4
-0.6
200
0
-200
-400
-600
1
2
3
4
5
6
Time [s]

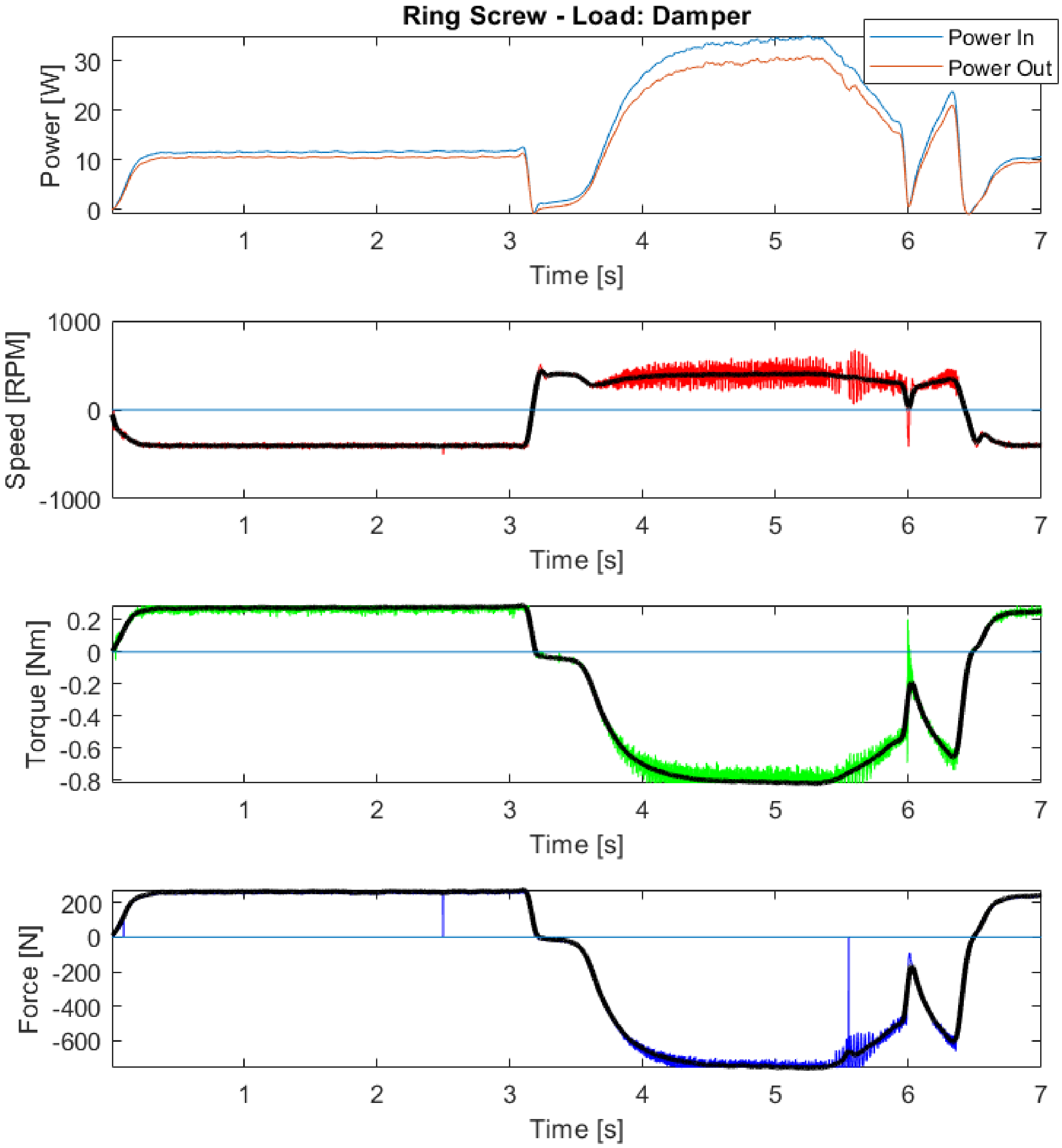
Ring Screw - Load: Damper
Power In
Power Out
Power [W]
30
20
10
0
Speed [RPM]
1000
0
-1000
Torque [Nm]
0.2
0
-0.2
-0.4
-0.6
-0.8
Force [N]
200
0
-200
-400
-600
1
2
3
4
5
6
7
Time [s]

Ball Screw - Load: Damper

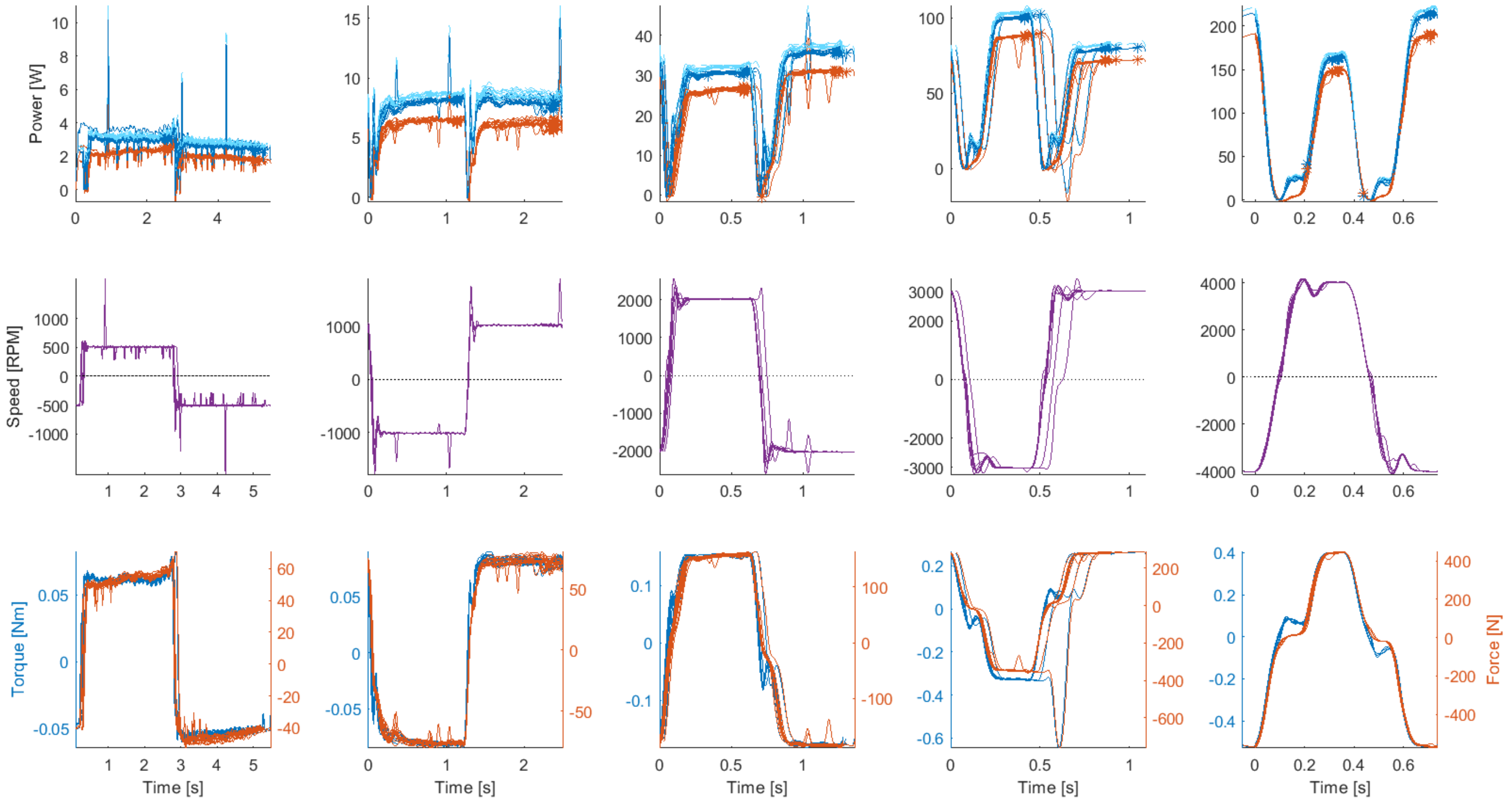

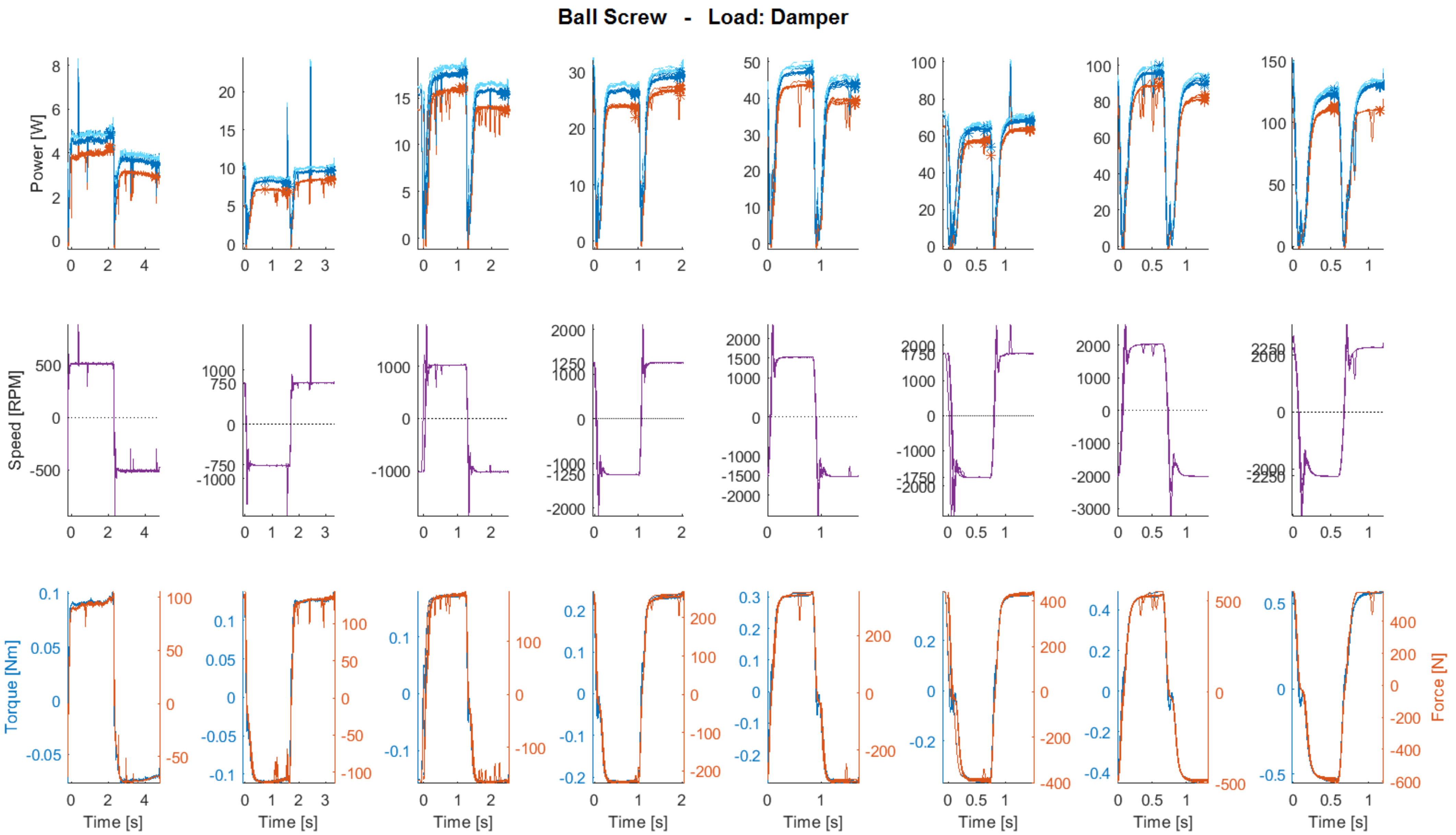Ball Screw - Load: Damper
Power [W]
8 6 4 2 0
20 15 10 5 0
15 10 5 0
30 20 10 0
50 40 30 20 10 0
100 80 60 40 20 0
100 80 60 40 20 0
150 100 50 0
0 2 4
0 1 2 3
0 1 2
0 1 2
0 1
0 0.5 1
0 0.5 1
0 0.5 1
Speed [RPM]
500 0 -500
1000 750 0 -750 -1000
1000 0 -1000
2000 1250 1000 0 -1000 -1250 -2000
2000 1500 1000 0 -1000 -1500 -2000
2000 1750 1000 0 -1000 -1750 -2000
2000 1000 0 -1000 -2000 -3000
2250 2000 0 -2000 -2250
Torque [Nm]
Force [N]
0.1 0.05 0 -0.05
100 50 0 -50
0.1 0.05 0 -0.05 -0.1
100 50 0 -50 -100
0.1 0 -0.1
100 0 -100
0.2 0.1 0 -0.1 -0.2
200 100 0 -100 -200
0.3 0.2 0.1 0 -0.1 -0.2
200 0 -200
0.2 0 -0.2
400 200 0 -200 -400
0.4 0.2 0 -0.2 -0.4
500 0 -500
0.5 0 -0.5
400 200 0 -200 -400 -600
Time [s]

Ball Screw - Load: Damper

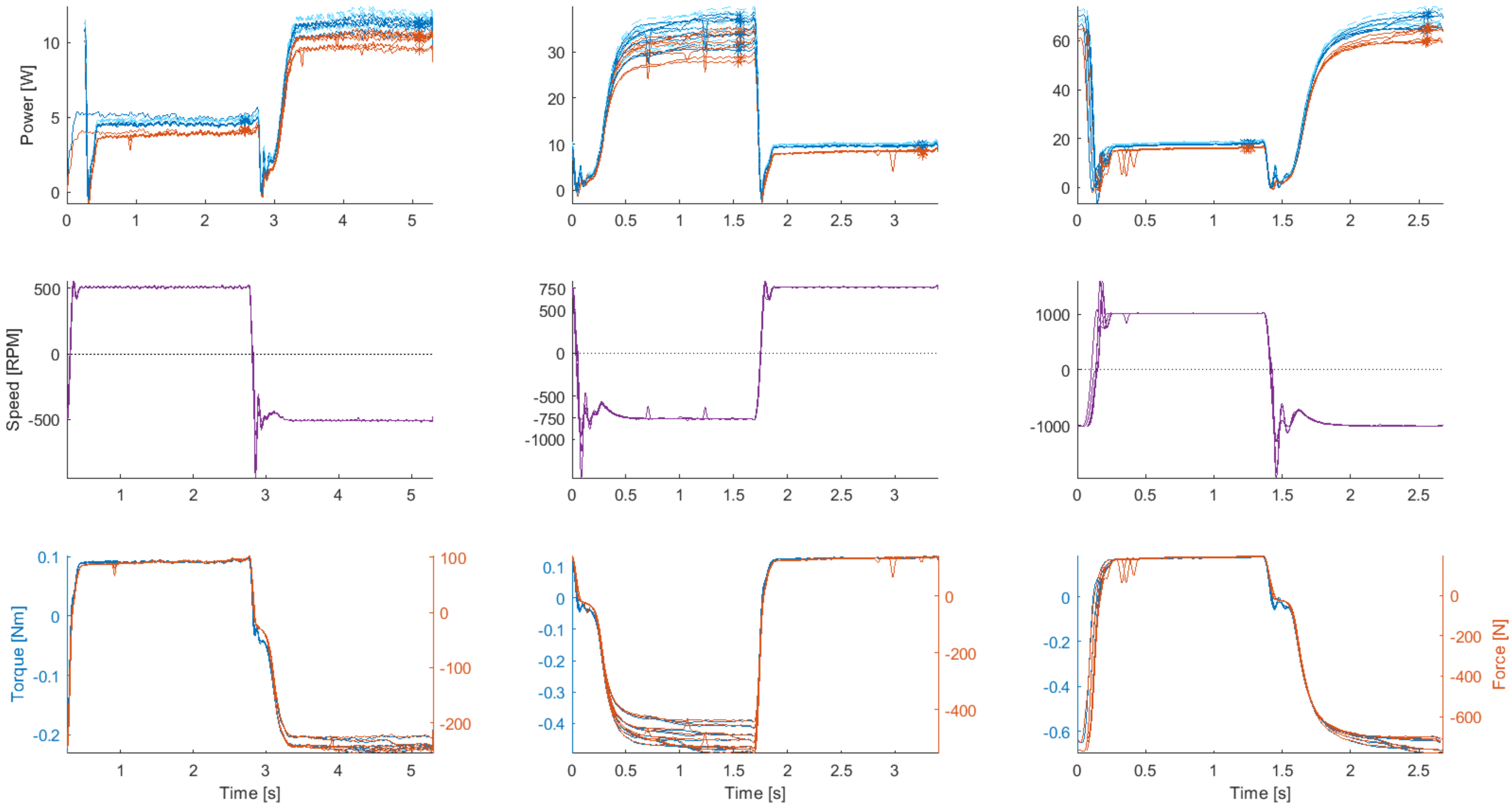

APPENDIX VIII
MECHANICAL DETAILS EXPERIMENTAL SETUP

This appendix shows al mechanical details of the the experimental setup developed to evaluate the performance of the ring screw. This mechanical setup was described in subsection V-B and selected out of the concepts presented in appendix IV. In the next pages the mechanical drawings of all custom parts can be found.

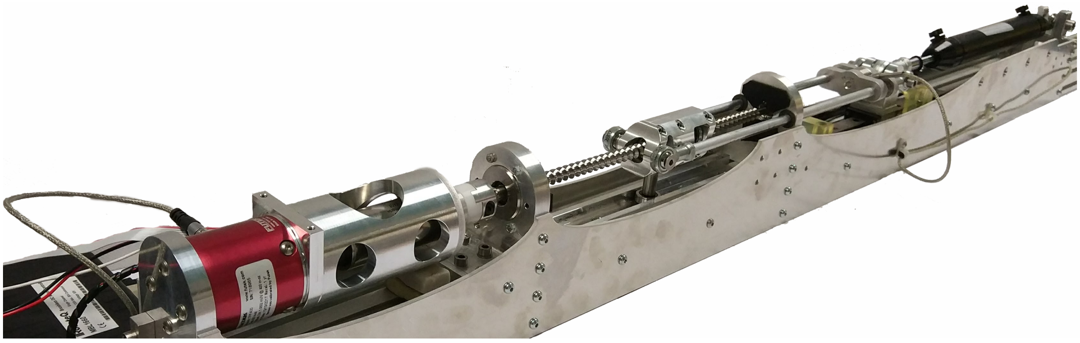

Fig. 34. The test rig, developed in this work to evaluate the performance of the ring screw. It's able to measure high efficiencies accurately while being able to generate load forces over $800N$ and rotational velocities over $15.000RPM$.

Load

A adjustable hydraulic damper (ACE DVC-32-150) is used as a main load for the experimental evaluation. This damper is able to deliver thrust forces from $42N$ up to $2,000N$ and therefore suitable for all experiments. A picture of this damper in the setup can be seen in Figure 35. However the force is always speed related and so high speed experiments with low forces are not possible. Furthermore this speed dependence makes it unable to perform back-driving experiments. Therefore so called constant force springs (CFS) are used for low force experiments at high speeds and for back drive experiments. A picture of this CFS can be seen in Figure 35.

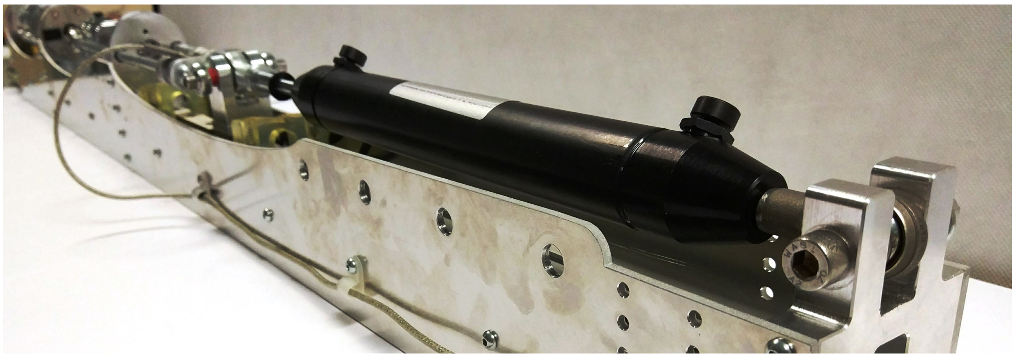

(a)

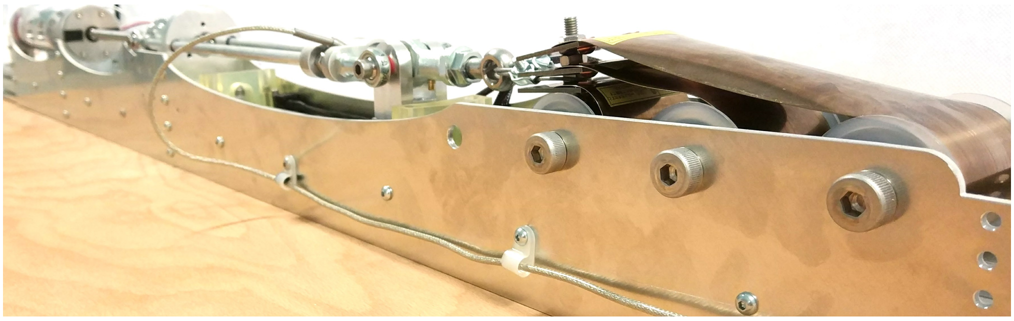

(b)

Fig. 35. Picture showing the test rig with two different loads. a) The adjustable hydraulic damper b) three constant force springs of 60N each.

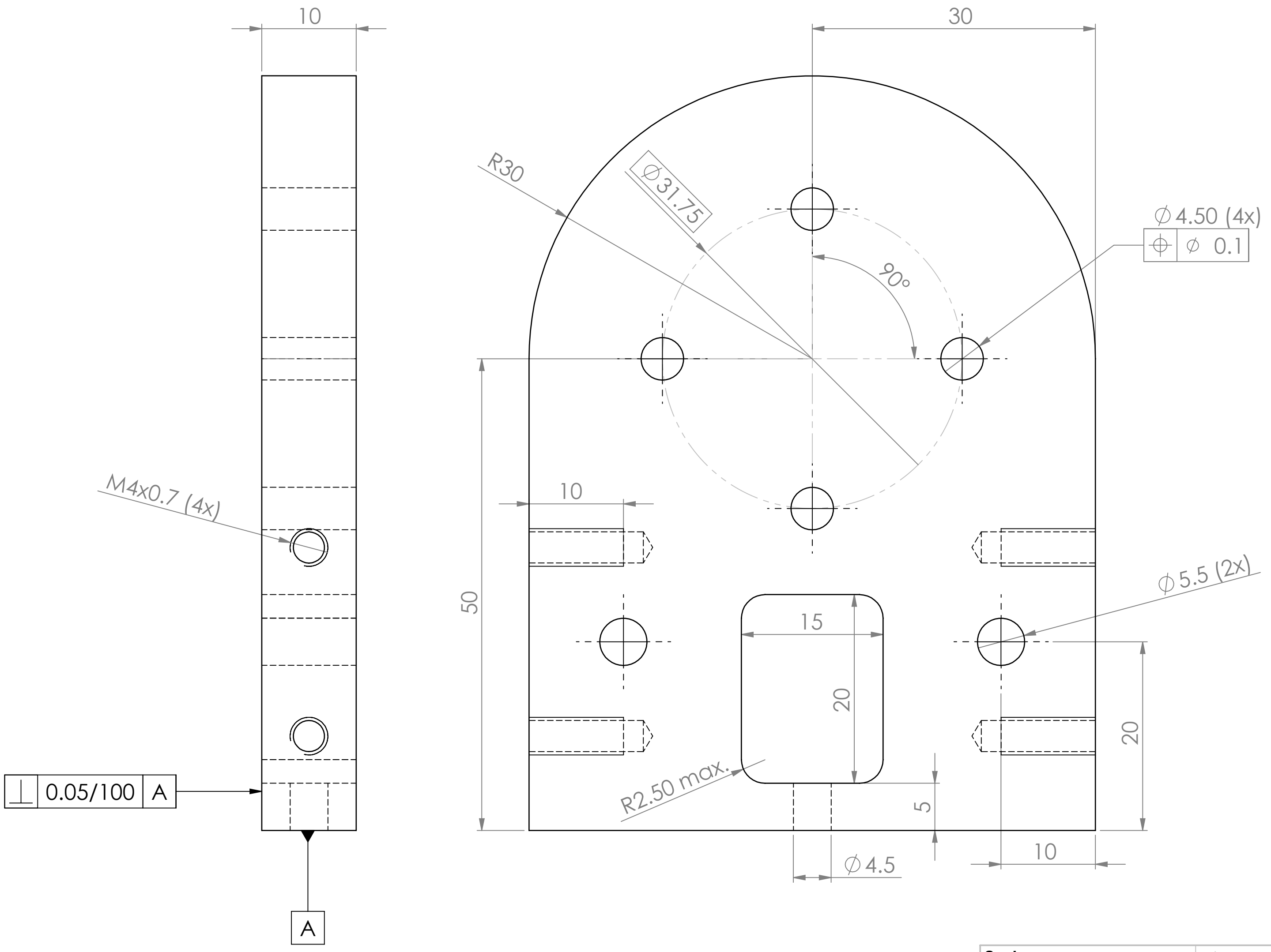
10
30
R30
⌀31.75
90°
⌀4.50 (4x)
⌖ ⌀ 0.1
M4x0.7 (4x)
10
50
⌀5.5 (2x)
15
20
20
R2.50 max.
5
10
⌀4.5
⊥ 0.05/100 A
A

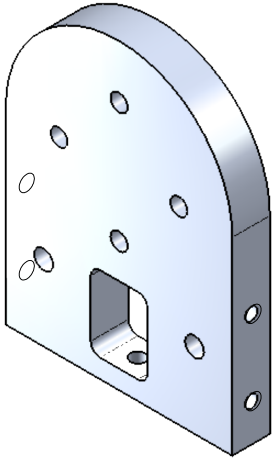

NOTE: BREAK SHARP EDGES

Scale 2:1		**Date** 22/09/2017	**Tolerances according to** UNI ISO 8015
Unit mm	**Mass** 111 gram		
Drawn E. Heijmink		**Model Ref.** TR-MF-002	**General tolerances UNI EN 22768-1 / 22768-2** Dimensional Tolerance class - m Geometric Tolerance class - H
Name Torque Sensor Support			**Roughness** 1.6
			Material Material: AL7075 Treatment: None
IIT Italian Institute of Technology		formaat A3	**Undim. Rounds** R = 0.1
			Undim. Chamfers 0.5 x 45

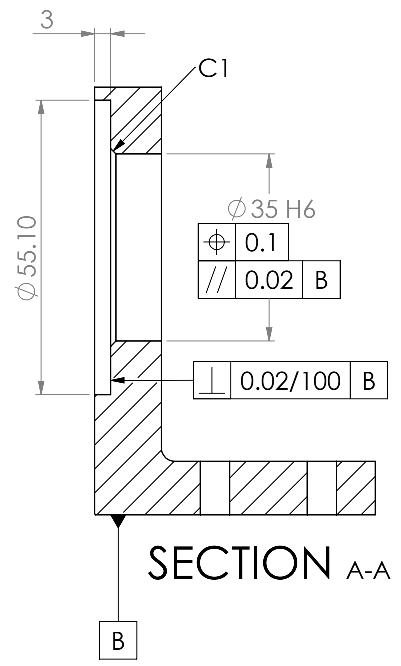
3
C1
Ø55.10
Ø35 H6
⌖ 0.1
// 0.02 B
⊥ 0.02/100 B
B

SECTION A-A

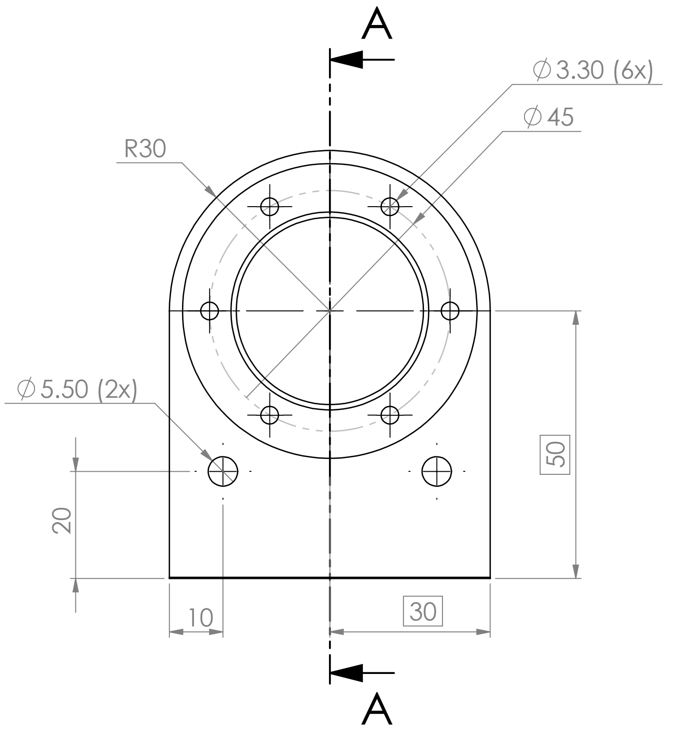
A
Ø3.30 (6x)
Ø45
R30
Ø5.50 (2x)
50
20
10
30
A

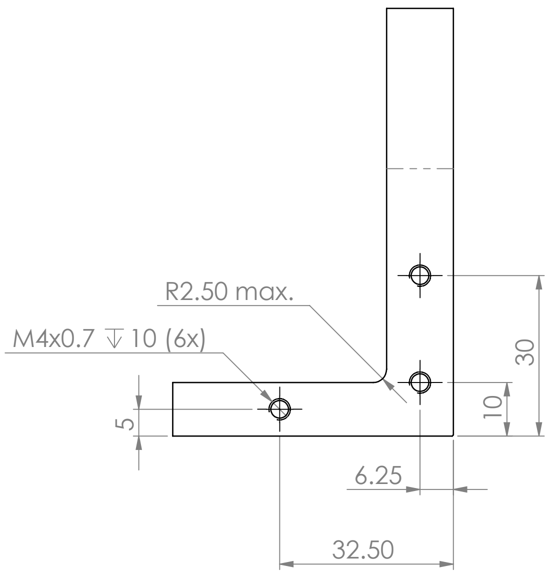
R2.50 max.
M4x0.7 ↧ 10 (6x)
5
30
10
6.25
32.50

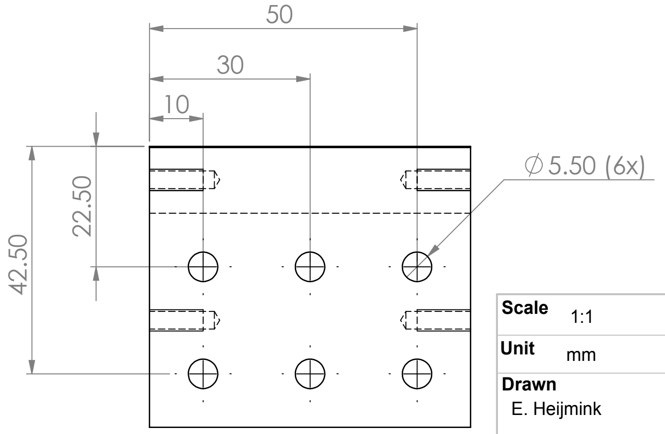
50
30
10
Ø5.50 (6x)
22.50
42.50

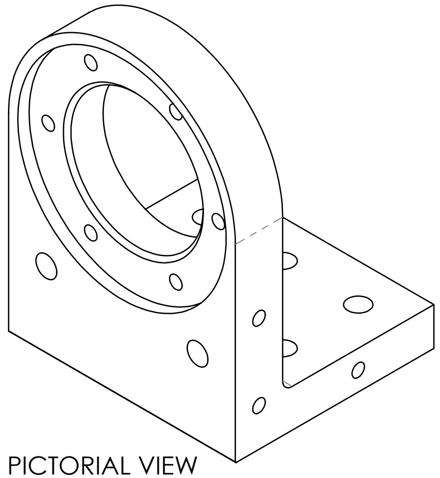

PICTORIAL VIEW

NOTE: BREAK SHARP EDGES

Scale 1:1		**Date** 28/09/2017	**Tolerances according to** UNI ISO 8015
Unit mm	**Mass** 161 gram		
Drawn E. Heijmink		**Model Ref.** TR-MF-003	**General tolerances UNI EN 22768-1 / 22768-2** Dimensional Tolerance class - m Geometric Tolerance class - H
Name Thrust Bearing Support			**Roughness** 1.6
Italian Institute of Technology		formaat A3	**Material** Material: AL7075 Treatment: None **Undim. Rounds** R = 0.2 **Undim. Chamfers** 0.5 x 45

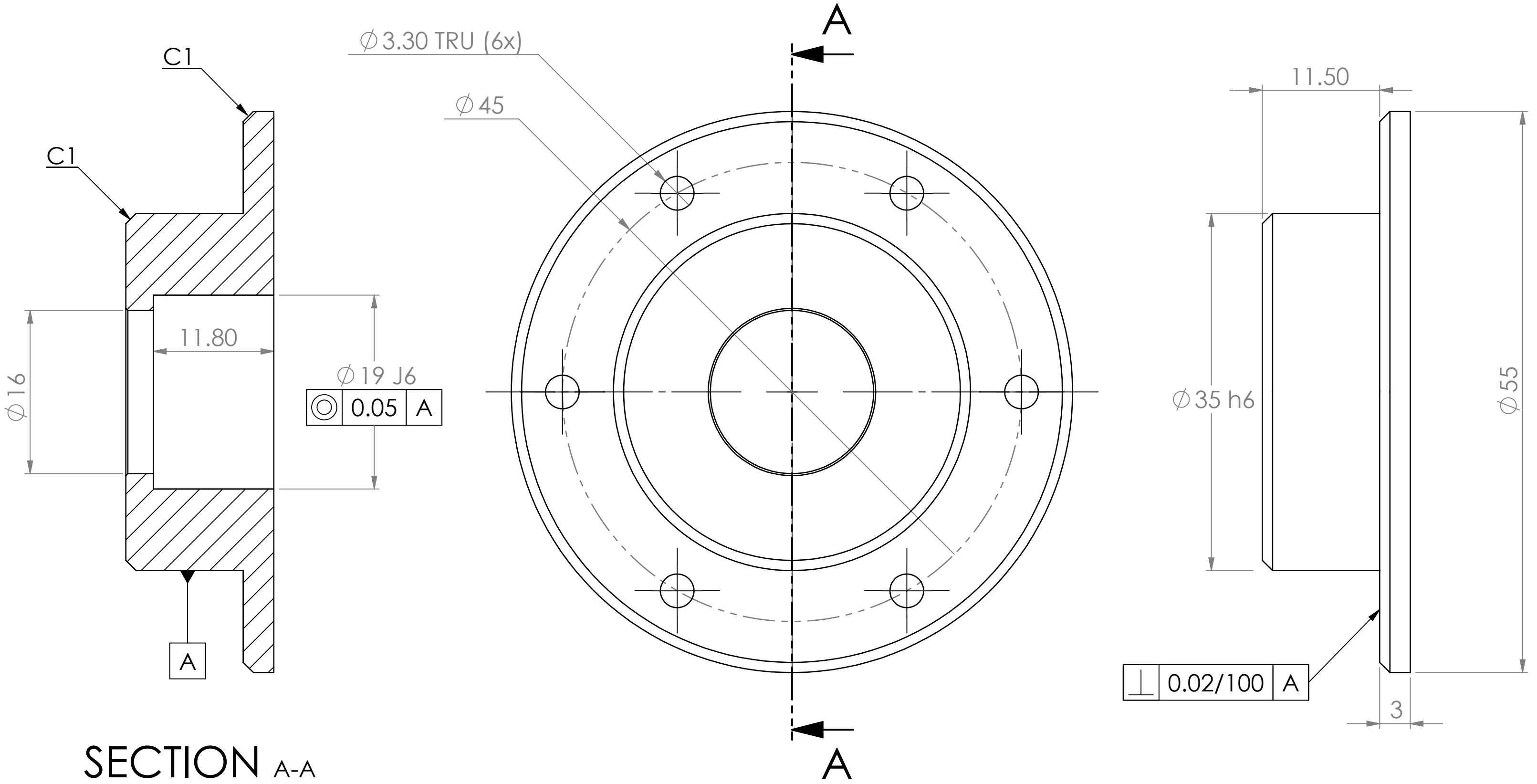
C1
C1
Ø16
11.80
Ø19 J6
◎ 0.05 A
A
Ø3.30 TRU (6x)
Ø45
A
A
11.50
Ø35 h6
Ø55
⊥ 0.02/100 A
3

SECTION A-A

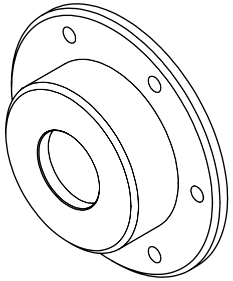

PICTORIAL VIEW

NOTE: BREAK SHARP EDGES

Scale 2:1		**Date** 28/09/2017	**Tolerances according to** UNI ISO 8015
Unit mm	**Mass** 109 gram		
Drawn E. Heijmink		**Model Ref.** TR-MF-004B	**General tolerances UNI EN 22768-1 / 22768-2** Dimensional Tolerance class - f Geometric Tolerance class - H
Name Bearing Adapter B 7126 C			**Roughness** 1.6
			Material Material: STAINLESS STEEL 303 Treatment: None
IIT Italian Institute of Technology		formaat A3	**Undim. Rounds** R = 0.2 **Undim. Chamfers** 0.5 x 45

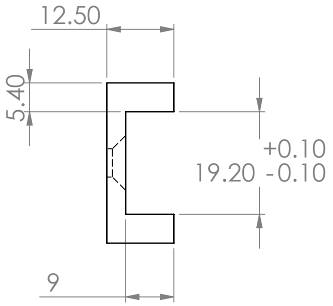
12.50
5.40
+0.10
19.20 -0.10
9

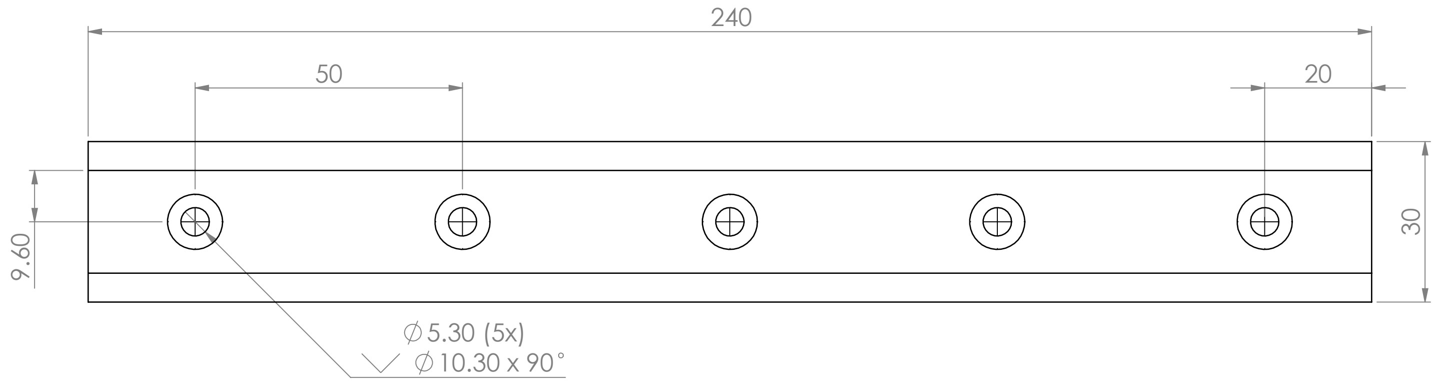
240
50
20
9.60
30
∅5.30 (5x)
∅10.30 x 90°

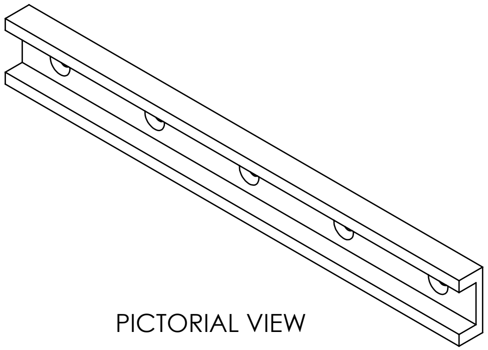

PICTORIAL VIEW

NOTE: BREAK SHARP EDGES

Scale 1:1		**Date** 16/10/2017	**Tolerances according to** UNI ISO 8015
Unit mm	**Mass** 373 gram		
Drawn E. Heijmink		**Model Ref.** TR-MF-005	**General tolerances UNI EN 22768-1 / 22768-2** Dimensional Tolerance class - m Geometric Tolerance class - H
Name Track Roller Rail			**Roughness** 1.6
			Material Material: STAINLESS STEEL 303 Treatment: None
IIT Italian Institute of Technology		formaat A3	**Undim. Rounds** R = 0.2
			Undim. Chamfers 0.5 x 45

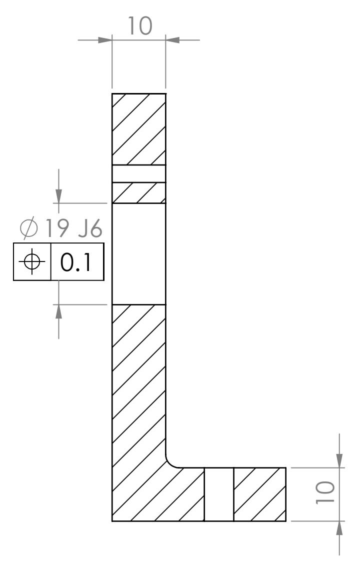
10
⌀19 J6
⌖ 0.1
10

SECTION A-A

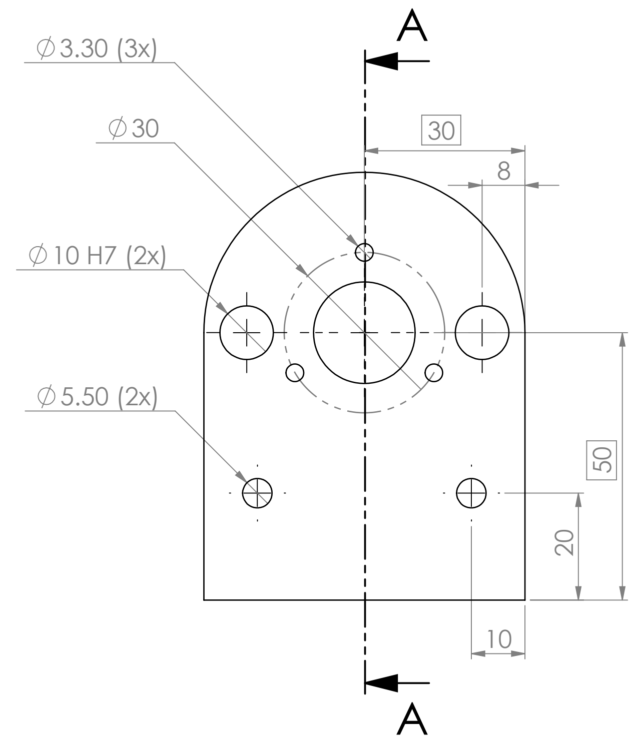
A
⌀3.30 (3x)
⌀30
⌀10 H7 (2x)
⌀5.50 (2x)
30
8
50
20
10
A

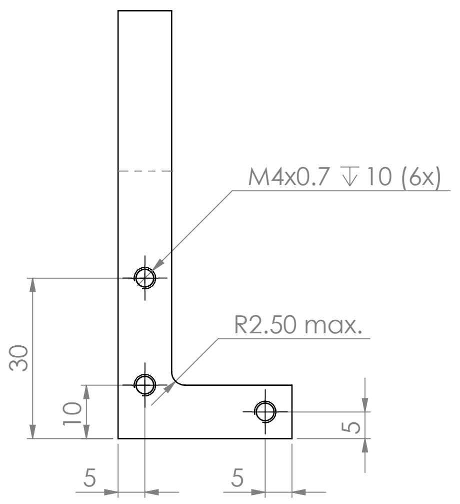
M4x0.7 ↧ 10 (6x)
R2.50 max.
30
10
5
5
5

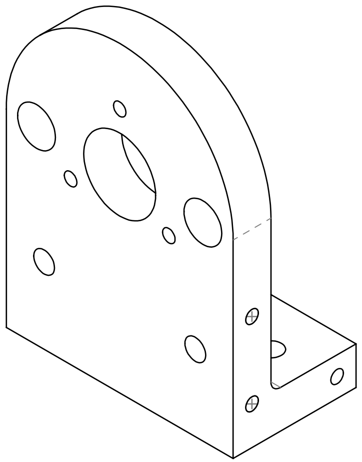

PICTORIAL VIEW

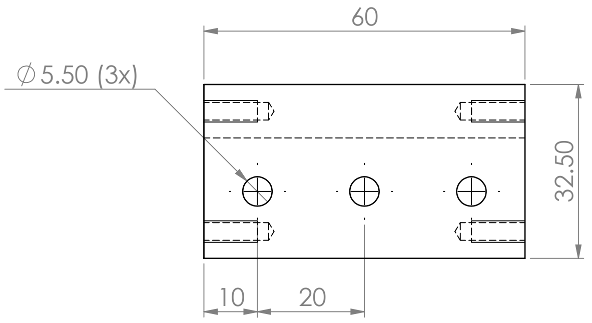
60
⌀5.50 (3x)
32.50
10
20

NOTE: BREAK SHARP EDGES

Scale 1:1
Date 25/09/2017
Tolerances according to
UNI ISO 8015
Unit mm
Mass 138 gram
Drawn E. Heijmink
Model Ref. TR-MF-006
General tolerances UNI EN 22768-1 / 22768-2
Dimensional Tolerance class - m
Geometric Tolerance class - H
Name
End Bearing Support
Roughness 1.6
Material
Material: AL7075
Treatment: None
IIT
Italian Institute of Technology
formaat
A3
Undim. Rounds
R = 0.2
Undim. Chamfers
0.5 x 45

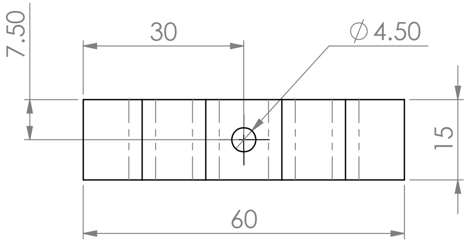
7.50
30
∅4.50
15
60

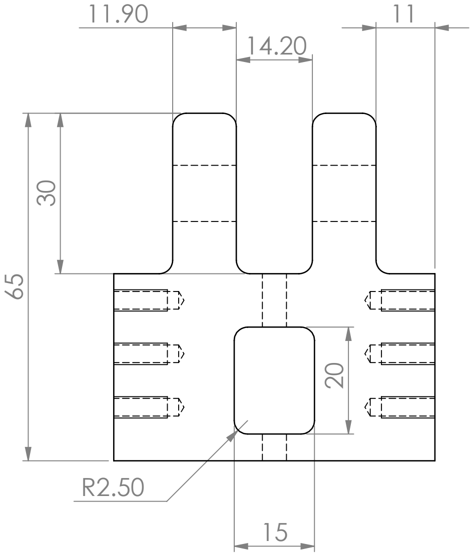
11.90
14.20
11
30
65
20
R2.50
15

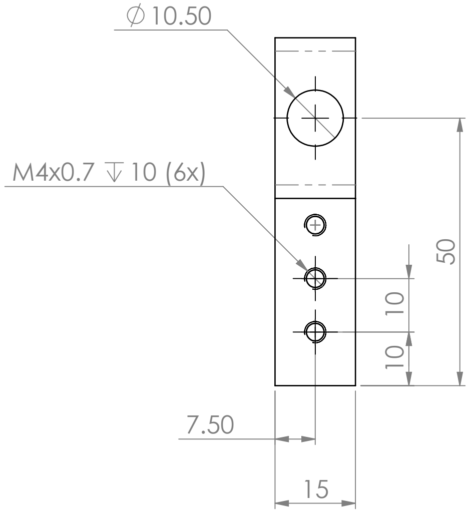
∅10.50
M4x0.7 ↧ 10 (6x)
50
10
10
7.50
15

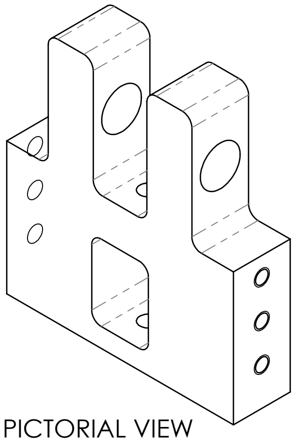

PICTORIAL VIEW

NOTE: BREAK SHARP EDGES

Scale 1:1		**Date** 27/09/2017	**Tolerances according to** UNI ISO 8015
Unit mm	**Mass** 94 gram		
Drawn E. Heijmink		**Model Ref.** TR-MF-007	**General tolerances UNI EN 22768-1 / 22768-2** Dimensional Tolerance class - m Geometric Tolerance class - K
Name Load Support			**Roughness** 3.2
			Material Material: AL7075 Treatment: None
IIT Italian Institute of Technology		formaat A3	**Undim. Rounds** R = 0.2
			Undim. Chamfers 0.5 x 45

MACHINE TO CAD
(LASERCUT)

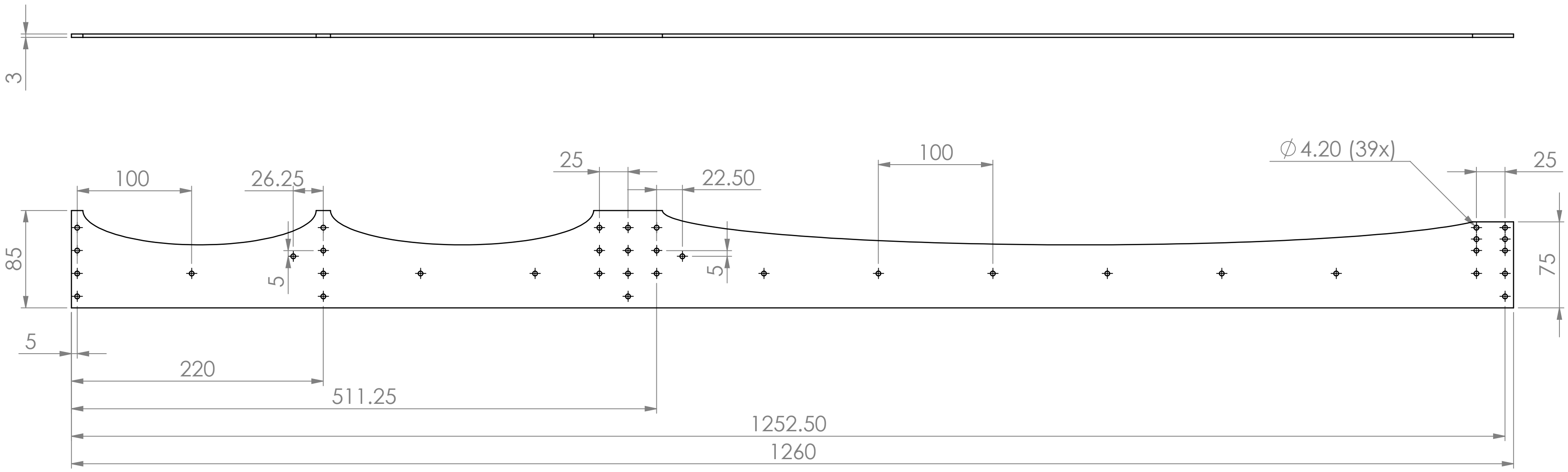
3
100
26.25
25
22.50
100
∅ 4.20 (39x)
25
85
5
5
75
5
220
511.25
1252.50
1260

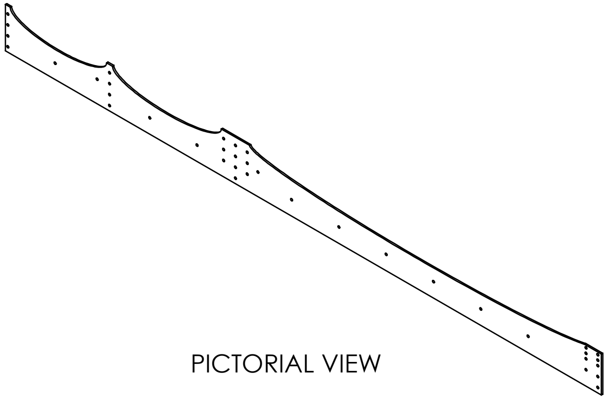

PICTORIAL VIEW

NOTE: BREAK SHARP EDGES

Scale 1:4
Date 28/09/2017
Unit mm
Mass 640 gram
Drawn E. Heijmink
Model Ref. TR-MF-008

Tolerances according to
UNI ISO 8015

General tolerances UNI EN 22768-1 / 22768-2
Dimensional Tolerance class - m
Geometric Tolerance class - H

Name
Side Plate

Roughness 3.2

Material
Material: Aluminium
Treatment: None

Undim. Rounds
R = 0.2

Undim. Chamfers
0.5 x 45

formaat
A3

Italian Institute of Technology

MACHINE TO CAD
(LASERCUT)

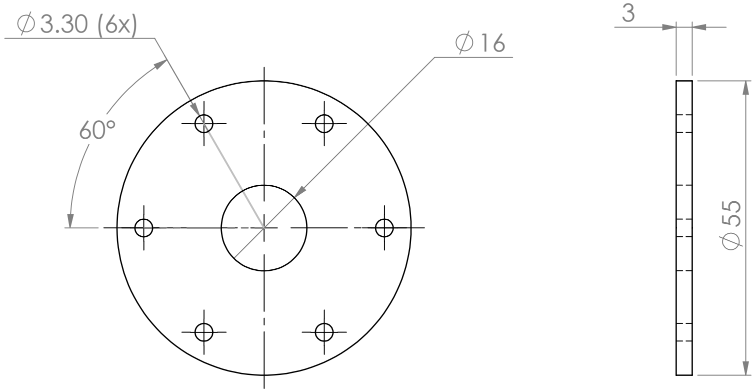

NOTE: BREAK SHARP EDGES

Scale 1:1		**Date** 27/09/2017	**Tolerances according to** UNI ISO 8015
Unit mm	**Mass** 51 gram		
Drawn E. Heijmink	**Model Ref.** TR-MF-010		**General tolerances UNI EN 22768-1 / 22768-2** Dimensional Tolerance class - m Geometric Tolerance class - K
Name Thrust Bearing Lock Plate			**Roughness** 3.2
			Material Material: STAINLESS STEEL Treatment: None
IIT Italian Institute of Technology	formaat A3		**Undim. Rounds** R = 0.2
			Undim. Chamfers 0.5 x 45

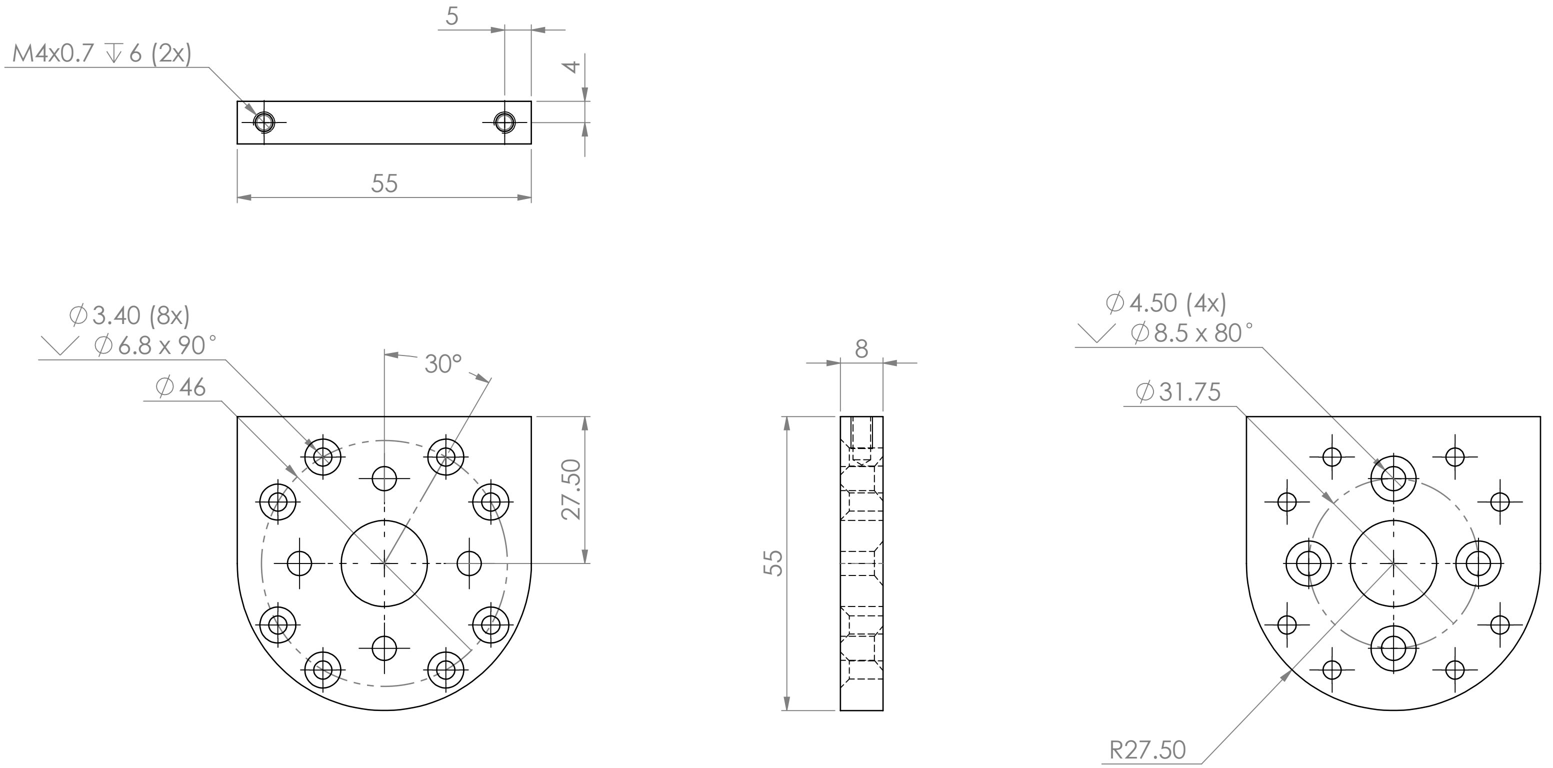
M4x0.7 ↧ 6 (2x)
5
4
55
⌀3.40 (8x)
⌵ ⌀6.8 x 90°
30°
⌀46
27.50
8
55
⌀4.50 (4x)
⌵ ⌀8.5 x 80°
⌀31.75
R27.50

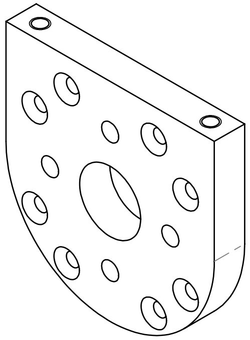

PICTORIAL VIEW

NOTE: BREAK SHARP EDGES

Scale 1:1		**Date** 25/09/2017	**Tolerances according to** UNI ISO 8015
Unit mm	**Mass** 50 gram		
Drawn E. Heijmink		**Model Ref.** TR-MM-002	**General tolerances UNI EN 22768-1 / 22768-2** Dimensional Tolerance class - f Geometric Tolerance class - K
Name Motor House Sensor Side		**Roughness** 1.6	**Material** Material: AL7075 Treatment: None
IIT Italian Institute of Technology	formaat A3	**Undim. Rounds** R = 0.2	**Undim. Chamfers** 0.5 x 45

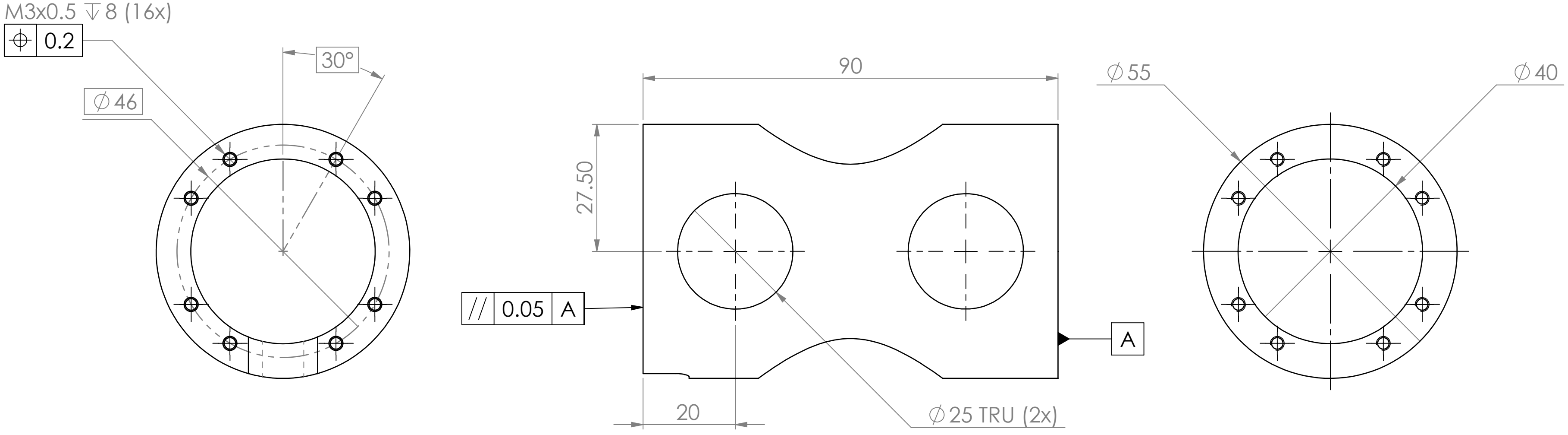
M3x0.5 ↧ 8 (16x)
⌖ 0.2
30°
⌀ 46
90
27.50
// 0.05 A
A
20
⌀ 25 TRU (2x)
⌀ 55
⌀ 40

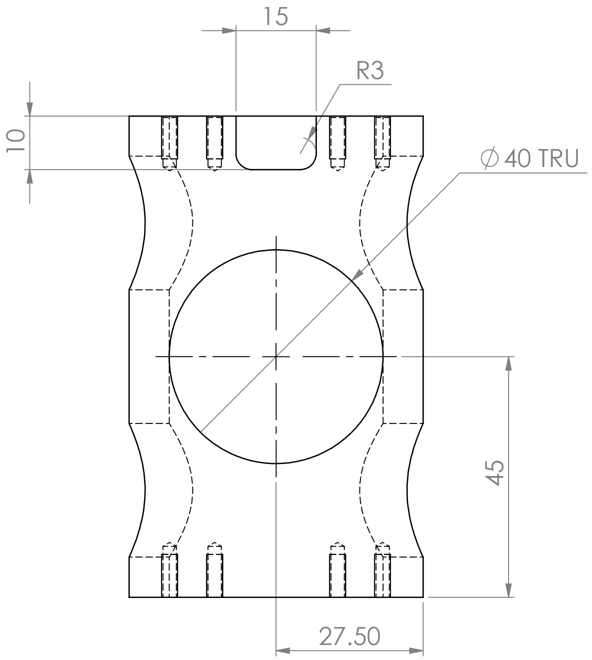
15
R3
10
⌀ 40 TRU
45
27.50

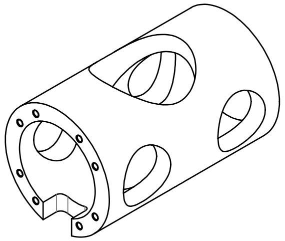

PICTORIAL VIEW

NOTE: BREAK SHARP EDGES

Scale 1:1	⌖	**Date** 25/09/2017	**Tolerances according to** UNI ISO 8015
Unit mm	**Mass** 167 gram		
Drawn E. Heijmink		**Model Ref.** TR-MM-003	**General tolerances UNI EN 22768-1 / 22768-2** Dimensional Tolerance class - C Geometric Tolerance class - K
Name Motor House Tube			**Roughness** 1.6
			Material Material: AL7075 Treatment: None
IIT Italian Institute of Technology		formaat A3	**Undim. Rounds** R = 0.2 **Undim. Chamfers** 0.5 x 45

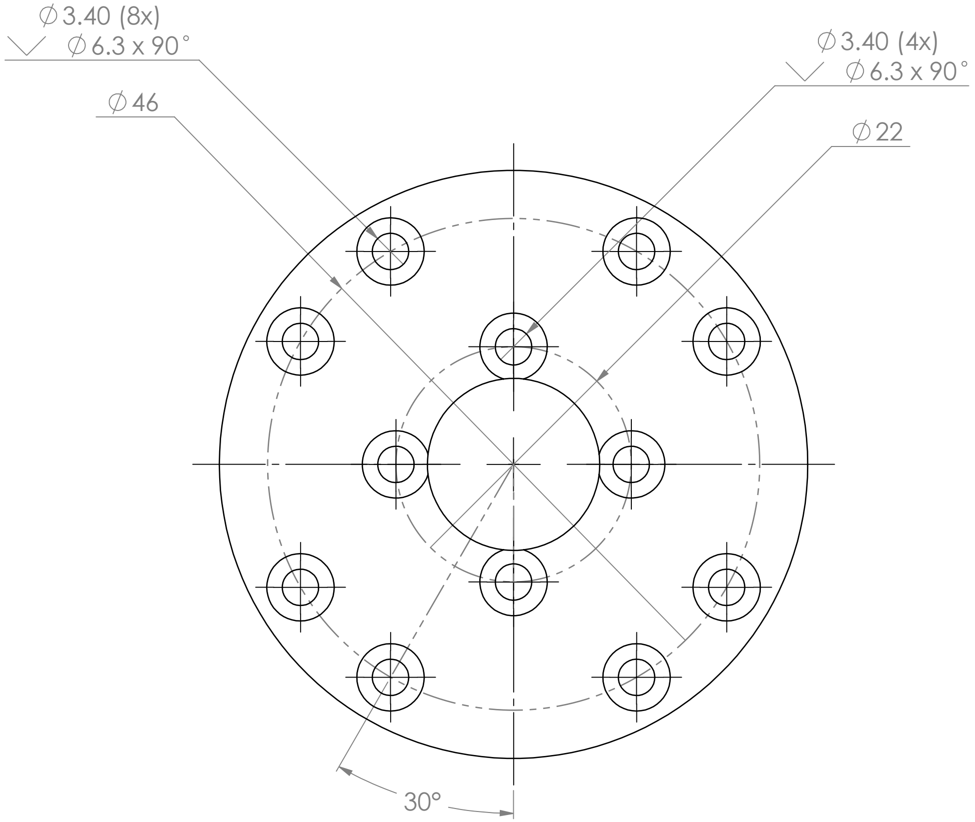

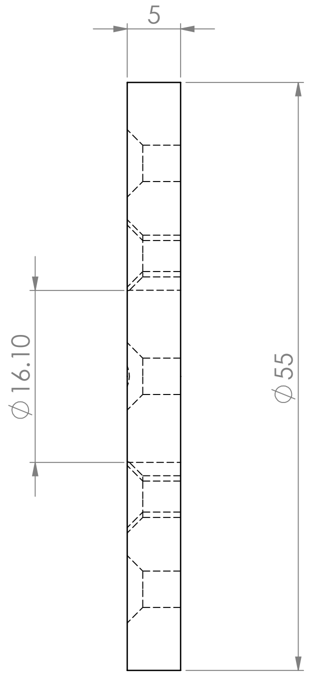

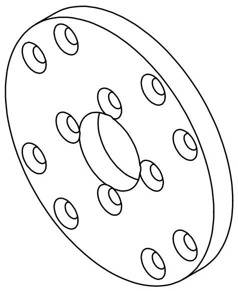

PICTORIAL VIEW

NOTE: BREAK SHARP EDGES

Scale 2:1		**Date** 28/09/2017	**Tolerances according to** UNI ISO 8015
Unit mm	**Mass** 27 gram		
Drawn E. Heijmink		**Model Ref.** TR-MM-002	**General tolerances UNI EN 22768-1 / 22768-2** Dimensional Tolerance class - f Geometric Tolerance class - H
Name Motor House Motor Side			**Roughness** 1.6
			Material Material: AL7075 Treatment: None
IIT Italian Institute of Technology		formaat A3	**Undim. Rounds** R = 0.2
			Undim. Chamfers 0.5 x 45

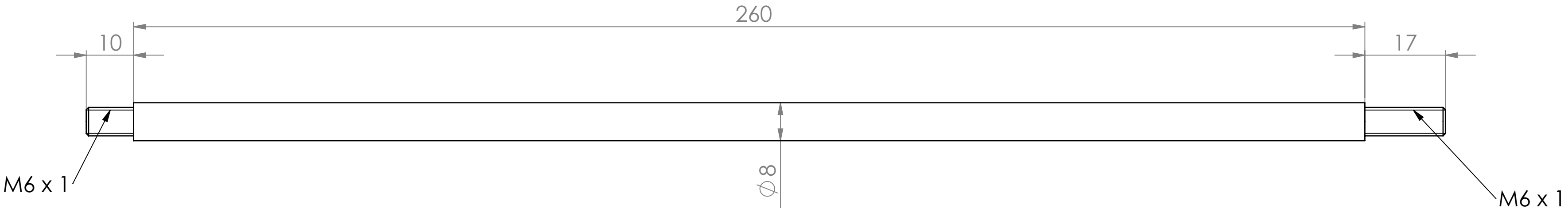

NOTE: BREAK SHARP EDGES

Scale 1:1		**Date** 27/09/2017	**Tolerances according to** UNI ISO 8015
Unit mm	**Mass** 37 gram		
Drawn E. Heijmink		**Model Ref.** TR-MM-005	**General tolerances UNI EN 22768-1 / 22768-2** Dimensional Tolerance class - m Geometric Tolerance class - K
Name Load Bridge Rod			**Roughness** 1.6
Italian Institute of Technology		formaat A3	**Material** Material: AL7075 Treatment: None
			Undim. Rounds R = 0.2
			Undim. Chamfers 0.5 x 45

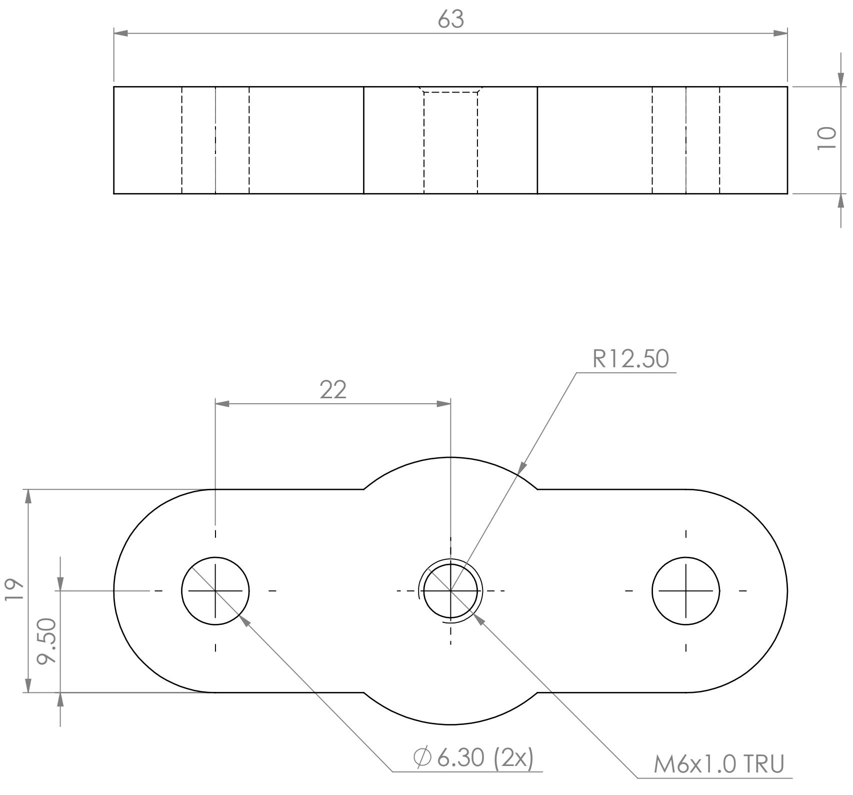

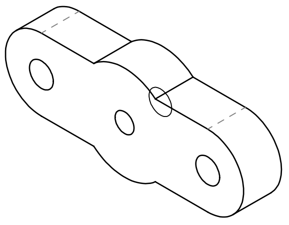

PICTORIAL VIEW

NOTE: BREAK SHARP EDGES

Scale 2:1		**Date** 27/09/2017	**Tolerances according to** UNI ISO 8015
Unit mm	**Mass** 86 gram		
Drawn E. Heijmink	**Model Ref.** TR-MM-006		**General tolerances UNI EN 22768-1 / 22768-2** Dimensional Tolerance class -m Geometric Tolerance class - K
Name Load Bridge Sensor Con.			**Roughness** 3.2
			Material Material: AL7075 Treatment: None
IIT Italian Institute of Technology	formaat A3		**Undim. Rounds** R = 0.2 **Undim. Chamfers** 0.5 x 45

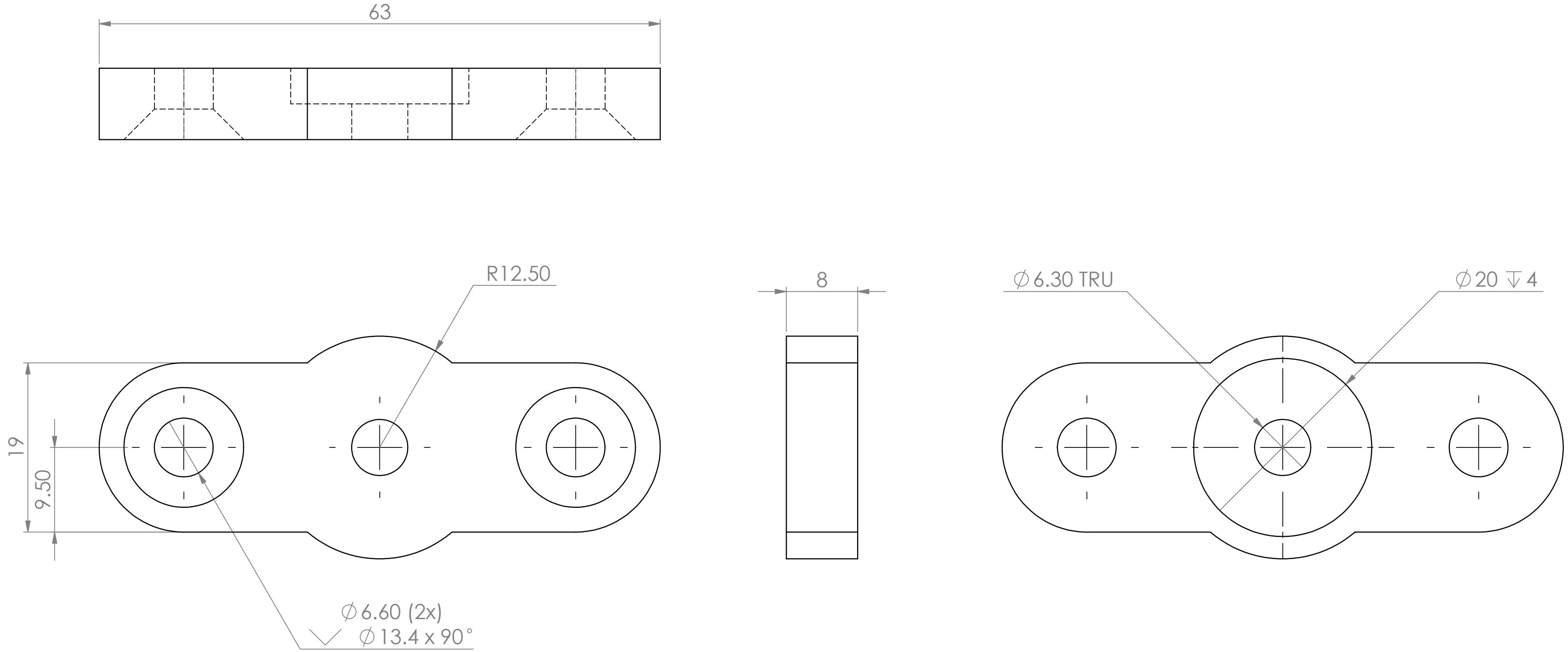

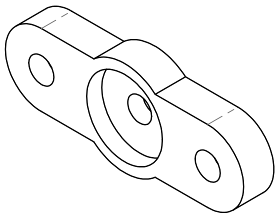

PICTORIAL VIEW

NOTE: BREAK SHARP EDGES

Scale 2:1

Date 27/09/2017

Unit mm

Mass 56 gram

Drawn E. Heijmink

Model Ref. TR-MM-007

Tolerances according to
UNI ISO 8015

General tolerances UNI EN 22768-1 / 22768-2
Dimensional Tolerance class -m
Geometric Tolerance class - K

Name

Sensor Rod End con.

Roughness 3.2

Material
Material: AL7075
Treatment: None

Undim. Rounds
R = 0.2

Undim. Chamfers
0.5 x 45

IIT
Italian Institute of Technology

formaat
A3

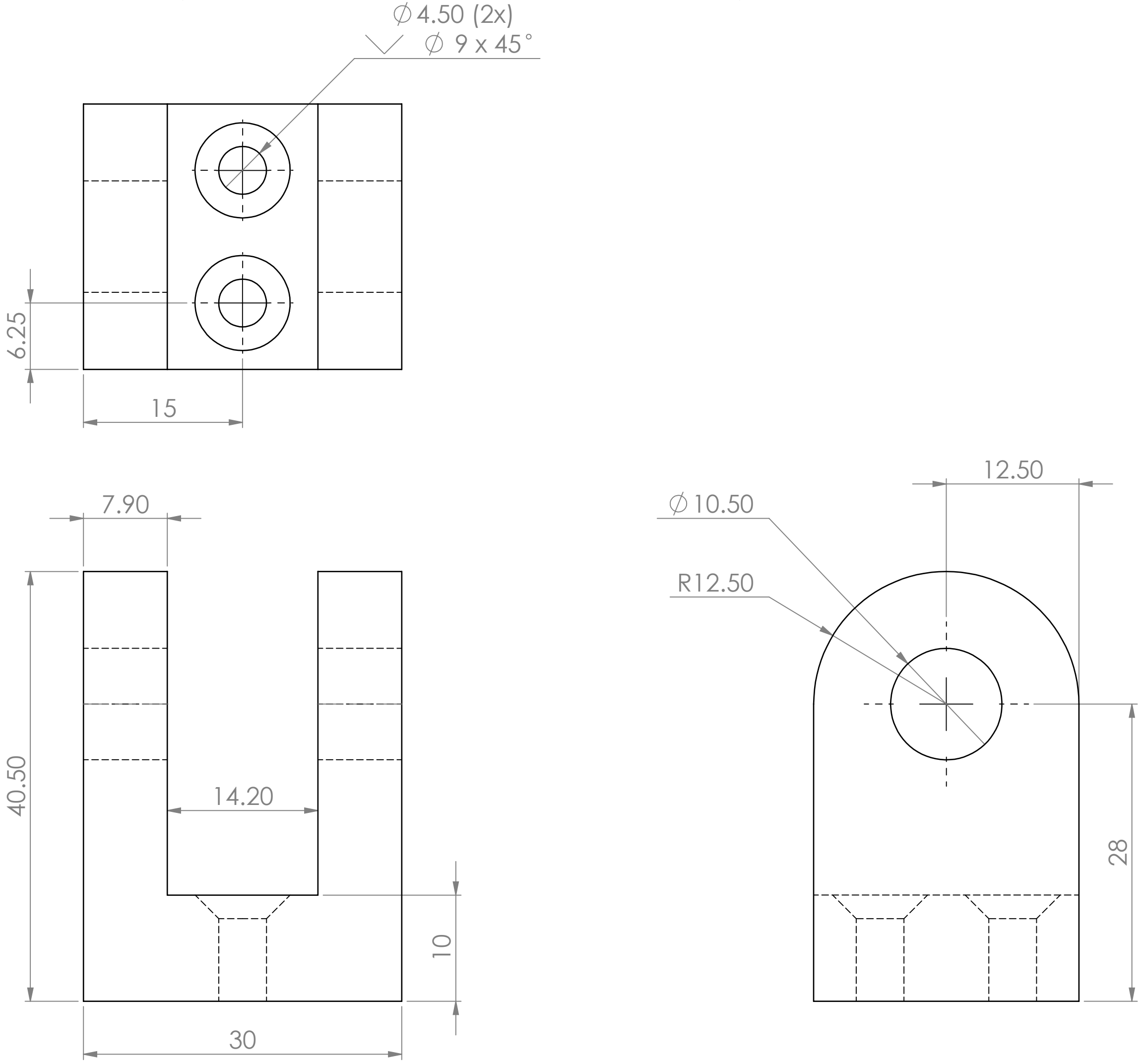
∅4.50 (2x)
∅ 9 x 45°
6.25
15
7.90
40.50
14.20
10
30
∅10.50
R12.50
12.50
28

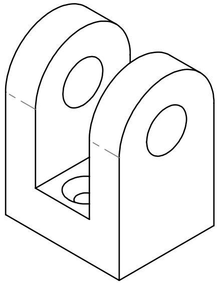
PICTORIAL VIEW

NOTE: BREAK SHARP EDGES

Scale 2:1	⊕	**Date** 26/09/2017	**Tolerances according to** UNI ISO 8015
Unit mm	**Mass** 45 gram		
Drawn E. Heijmink		**Model Ref.** TR-MM-008	**General tolerances UNI EN 22768-1 / 22768-2** Dimensional Tolerance class -m Geometric Tolerance class - K
Name Load Clevis			**Roughness** 3.2 **Material** Material: AL7075 Treatment: None
IIT Italian Institute of Technology		formaat A3	**Undim. Rounds** R = 0.2 **Undim. Chamfers** 0.5 x 45

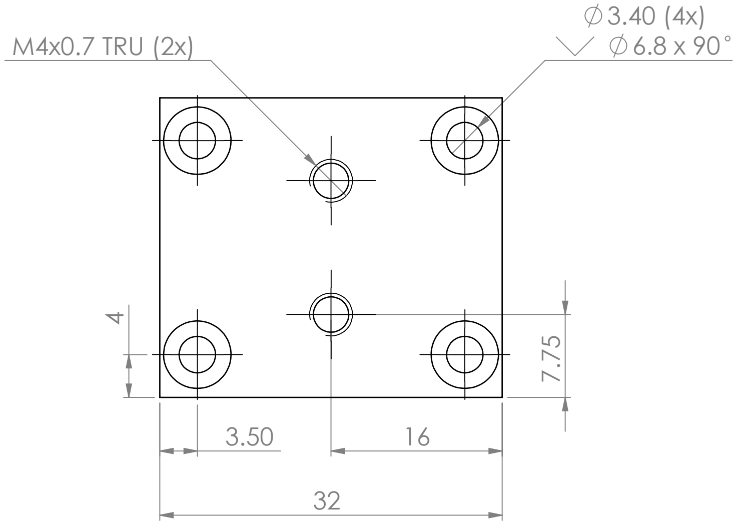

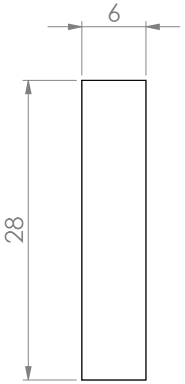

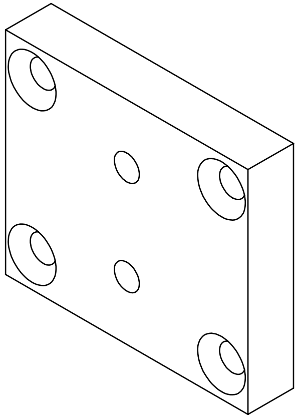

PICTORIAL VIEW

NOTE: BREAK SHARP EDGES

Scale 2:1		**Date** 26/09/2017	**Tolerances according to** UNI ISO 8015
Unit mm	**Mass** 13 gram		
Drawn E. Heijmink		**Model Ref.** TR-MM-009	**General tolerances UNI EN 22768-1 / 22768-2** Dimensional Tolerance class -m Geometric Tolerance class - K
Name Load Clevis Base Plate			**Roughness** 3.2
			Material Material: AL7075 Treatment: None
IIT Italian Institute of Technology		formaat A3	**Undim. Rounds** R = 0.2
			Undim. Chamfers 0.5 x 45

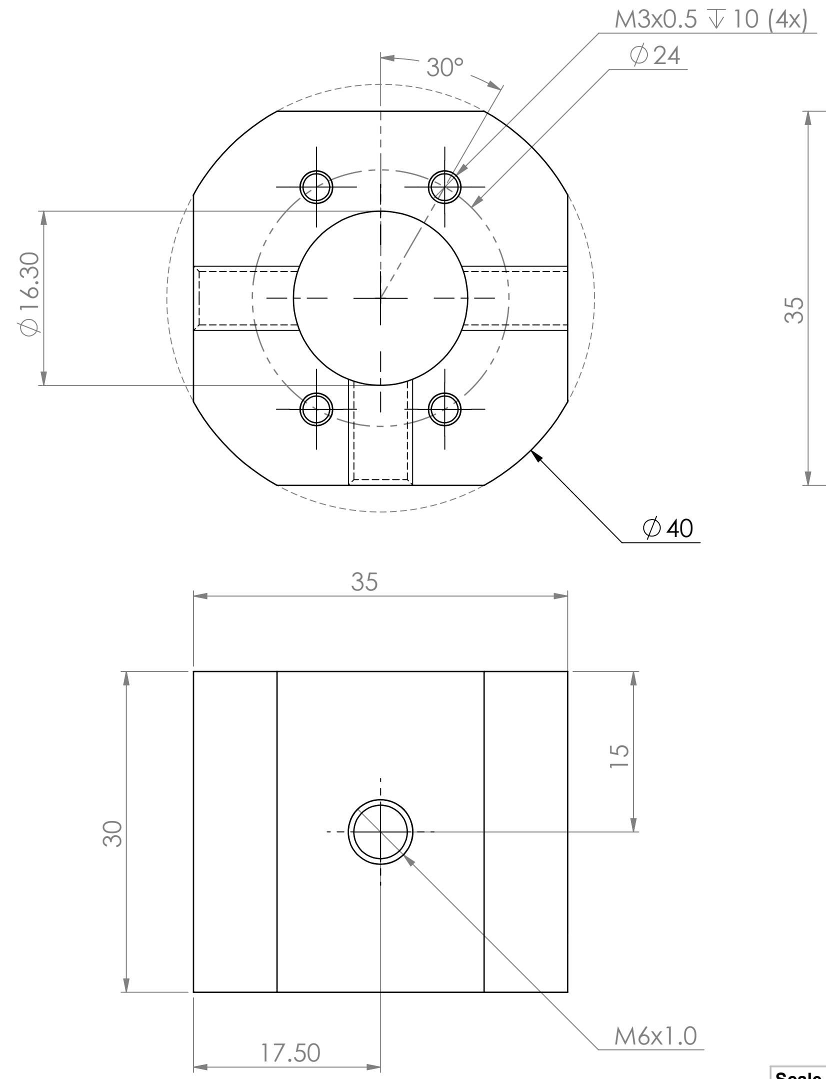
M3x0.5 ↧ 10 (4x)
⌀24
30°
⌀16.30
⌀40
7.50
M6x1.0 (2x)
17.50
35
35
15
30
M6x1.0
17.50

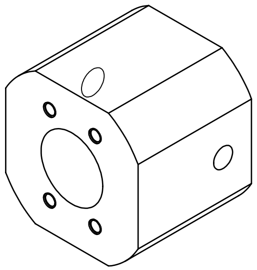

PICTORIAL VIEW

NOTE: BREAK SHARP EDGES

Scale 2:1		**Date** 27/09/2017	**Tolerances according to** UNI ISO 8015
Unit mm	**Mass** 75 gram		
Drawn E. Heijmink	**Model Ref.** TR-MM-010B		**General tolerances UNI EN 22768-1 / 22768-2** Dimensional Tolerance class -f Geometric Tolerance class - K
Name Ball Screw Nut Connector			**Roughness** 3.2
			Material Material: AL7075 Treatment: None
IIT Italian Institute of Technology	formaat A3		**Undim. Rounds** R = 0.2 **Undim. Chamfers** 0.5 x 45

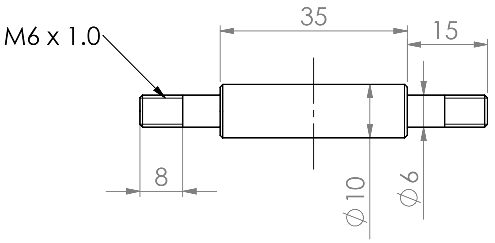

NOTE: BREAK SHARP EDGES

Scale 1:1		**Date** 27/09/2017	**Tolerances according to** UNI ISO 8015
Unit mm	**Mass** 29 gram		
Drawn E. Heijmink		**Model Ref.** TR-MM-013	**General tolerances UNI EN 22768-1 / 22768-2** Dimensional Tolerance class - m Geometric Tolerance class - K
Name Load Clevis Axis			**Roughness** 1.6
			Material Material: STAINLESS STEEL Treatment: None
IIT Italian Institute of Technology		formaat A3	**Undim. Rounds** R = 0.2
			Undim. Chamfers 0.5 x 45

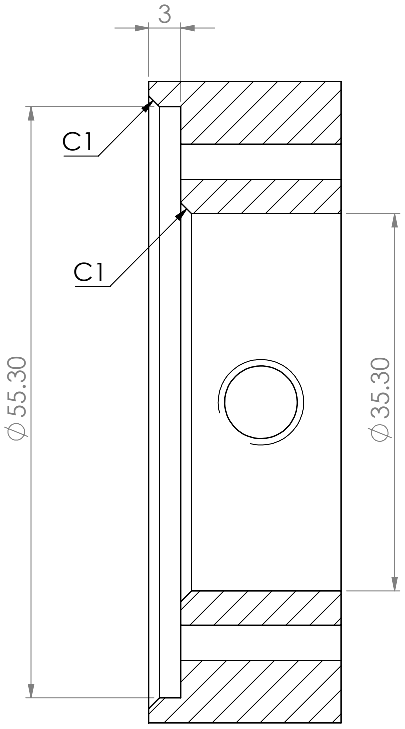
3
C1
C1
Ø55.30
Ø35.30

SECTION B-B

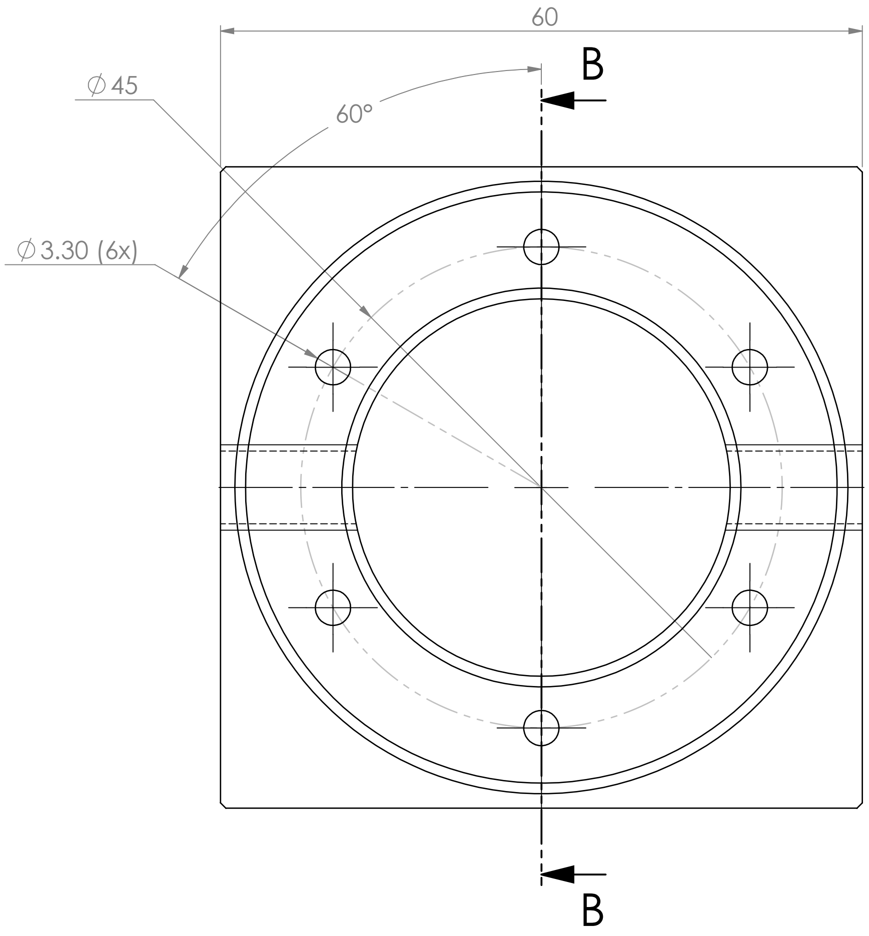
60
B
Ø45
60°
Ø3.30 (6x)
B

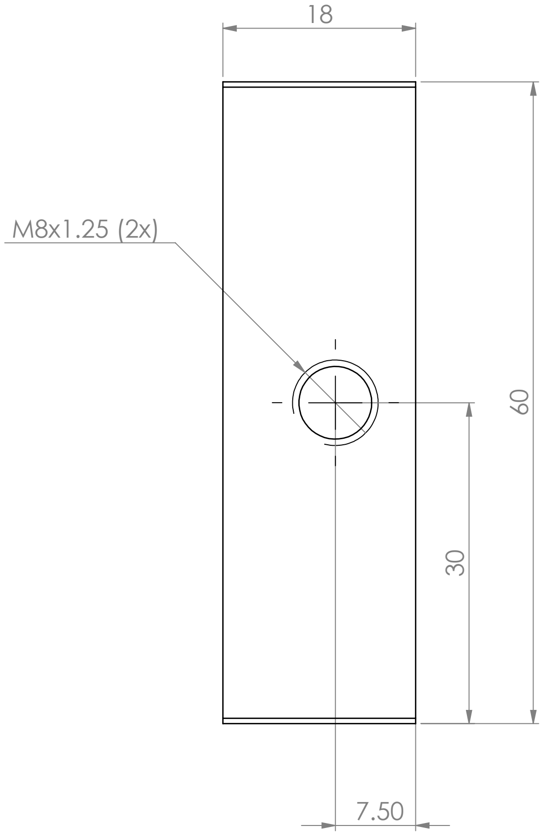
18
M8x1.25 (2x)
60
30
7.50

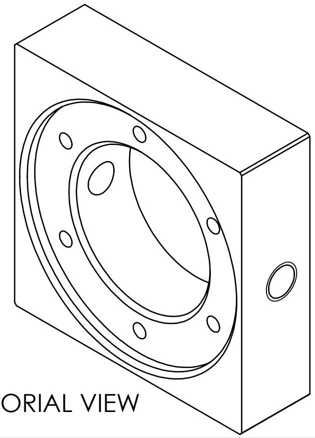

PICTORIAL VIEW

NOTE: BREAK SHARP EDGES

Scale 2:1
Date 27/09/2017
Tolerances according to
UNI ISO 8015
Unit mm
Mass 330 gram
Drawn E. Heijmink
Model Ref. TR-BT-002
General tolerances UNI EN 22768-1 / 22768-2
Dimensional Tolerance class - m
Geometric Tolerance class - K
Name

Pully's Adaper link

Roughness 1.6
Material
Material: STAINLESS STEEL
Treatment: None
Undim. Rounds
R = 0.2
Undim. Chamfers
0.5 x 45

IIT
Italian Institute of Technology

formaat
A3

MACHINE TO CAD
(LASERCUT)

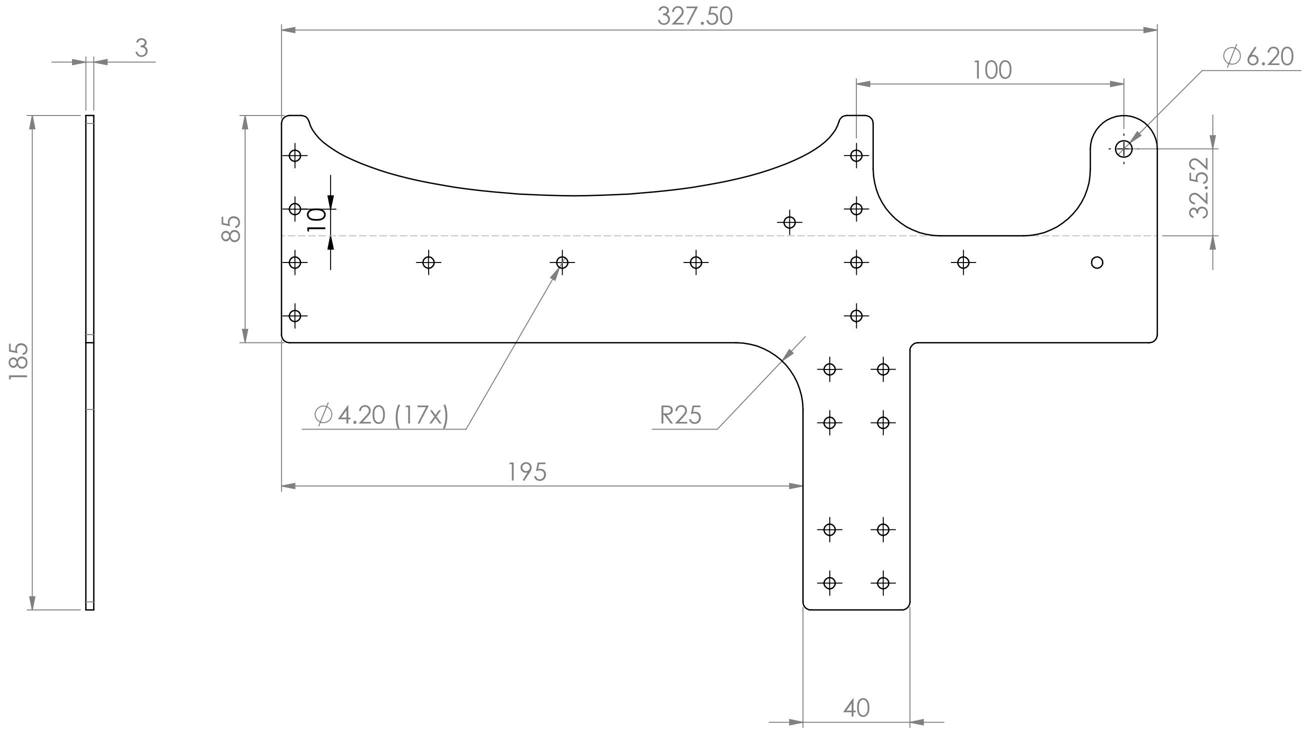

NOTE: BREAK SHARP EDGES

Scale 1:2		**Date** 28/09/2017	**Tolerances according to** UNI ISO 8015
Unit mm	**Mass** 190 gram		
Drawn E. Heijmink		**Model Ref.** TR-BT-007	**General tolerances UNI EN 22768-1 / 22768-2** Dimensional Tolerance class - m Geometric Tolerance class - K
Name Side Plate Bearingtest			**Roughness** 3.2
			Material Material: Aluminium Treatment: None
IIT Italian Institute of Technology		formaat A3	**Undim. Rounds** R = 3
			Undim. Chamfers 0.5 x 45

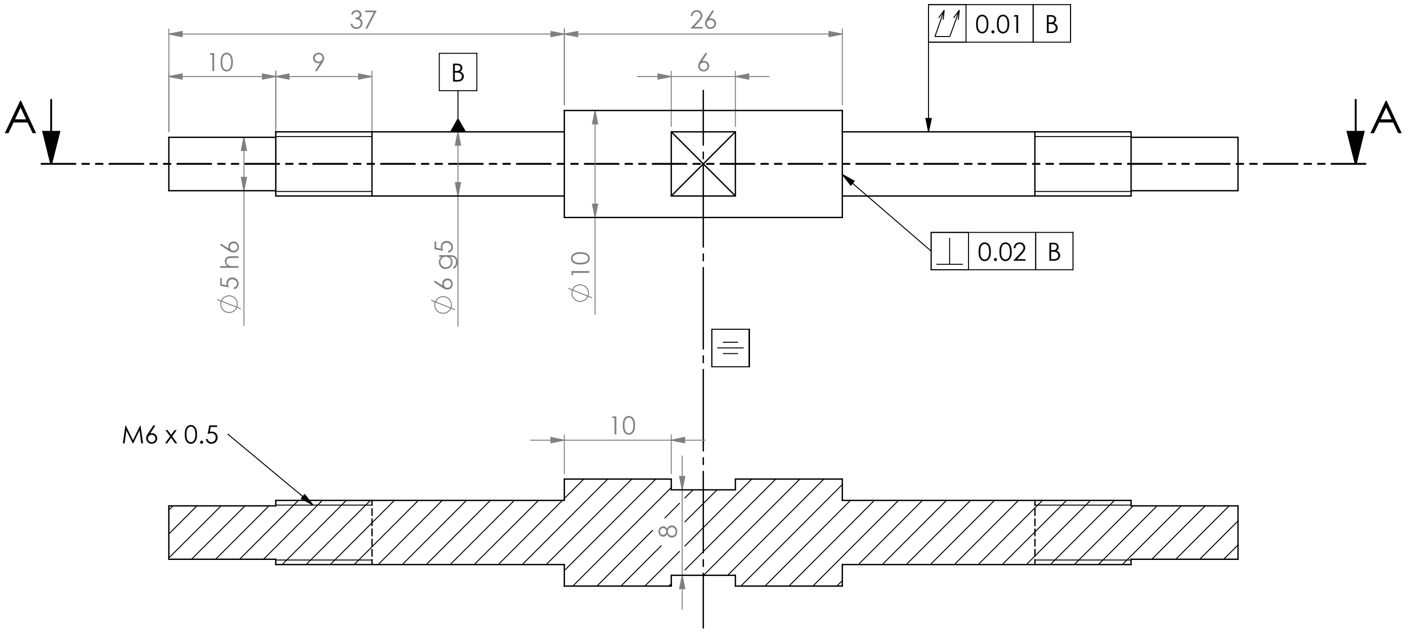

SECTION A-A

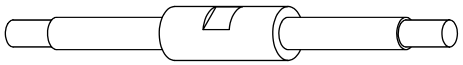

Pictorial view

NOTE: BREAK SHARP EDGES

Scale 2:1
Date 23/02/2018
Unit mm
Mass 31 gram
Drawn E. Heijmink
Model Ref. TR-BT-008B
Tolerances according to UNI ISO 8015
General tolerances UNI EN 22768-1 / 22768-2
Dimensional Tolerance class - m
Geometric Tolerance class - K

Name
Bearing Exp. Axis

Roughness 1.6

Material
Matetrial: STAINLESS STEEL
Treatment: None

Undim. Rounds
R = 0.2

Undim. Chamfers
0.5 x 45

IIT
Italian Institute of Technology

formaat A3

APPENDIX IX
ELECTRONICS EXPERIMENTAL SETUP

Besides the mechanical design of the experimental setup described in section V-B the selected electronics define the performance of the test rig. This appendix therefore presents the most essential electronics.

Application	Part	Details
Controlling & logging	Micro controller	Teensy 3.6
Actuation	Electric motor driving the screw Motor controller	Maxon EC-4pole 30 200W 24V motor MBL1660A. Brushless DC Motor controler, 60V 80A
Mesuring	Encoder on Motor Torque sensor on Motor Force sensor on Load Analogue amplifiers for Futec sensors	Maxon Encoder MR, type ML, 500cpr, 3ch Futec TFF400 Reaction Torque Sensor, 2.8Nm Futec LCM300 Loadcell, 250 lb (1112N) Custom, Gain = 501, see Fig 36

Schematics of Analogue amplifier for Futec sensors

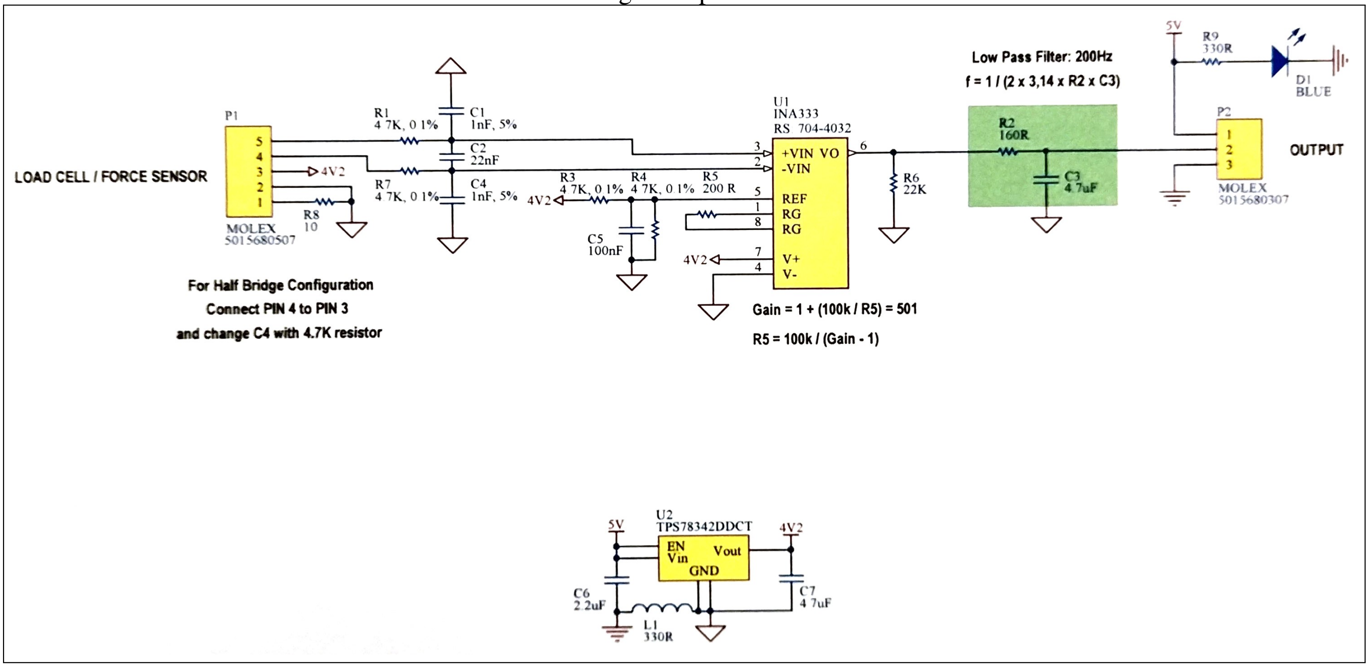
LOAD CELL / FORCE SENSOR
P1
5
4
3
2
1
4V2
MOLEX
5015680507
R8
10
R1
4.7K, 0.1%
C1
1nF, 5%
C2
22nF
R7
4.7K, 0.1%
C4
1nF, 5%
R3
4.7K, 0.1%
R4
4.7K, 0.1%
R5
200 R
4V2
C5
100nF
For Half Bridge Configuration
Connect PIN 4 to PIN 3
and change C4 with 4.7K resistor
U1
INA333
RS 704-4032
+VIN VO
-VIN
REF
RG
RG
V+
V-
3
2
5
1
8
7
4
6
4V2
Gain = 1 + (100k / R5) = 501
R5 = 100k / (Gain - 1)
R6
22K
Low Pass Filter: 200Hz
f = 1 / (2 x 3,14 x R2 x C3)
R2
160R
C3
4.7uF
5V
R9
330R
D1
BLUE
P2
1
2
3
OUTPUT
MOLEX
5015680307
U2
TPS78342DDCT
5V
EN
Vin
Vout
GND
4V2
C6
2.2uF
L1
330R
C7
4.7uF

Fig. 36. Schematics of the analogue amplifiers used for the force and torque sensors. A first order low pass filter is added before and after the amplifier. The first to avoid saturation of the amplifier, while the second is to avoid saturation of the analogue to digital converter (ADC). Furthermore a voltage regulator is added to supply a stable voltage to the sensors.

Circuit board

The use of analogue signals makes the connections vulnerable for signal loss and noise. There fore a custom Printed circuit board (PCB) is designed and made to connect all electronics to the micro controller as can be seen in figure 37. Compared to other solutions like the direct soldering or the use of a breadboard a PCB allows for easy debugging, low nice and more reliable connections. The schematics of these PCB is added on the next page.

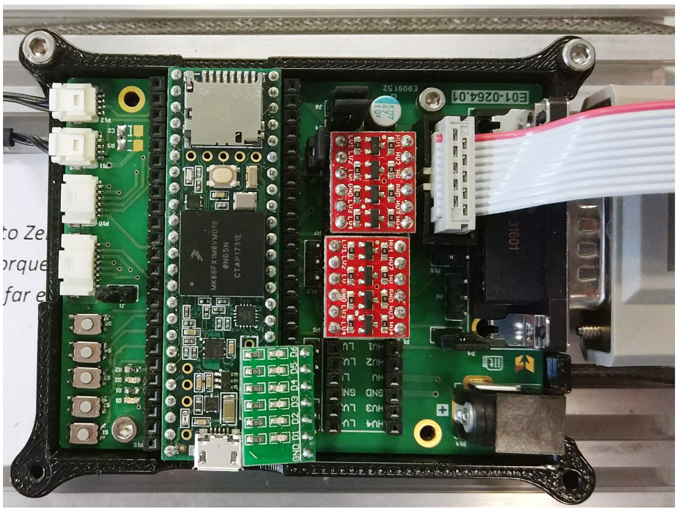

Fig. 37. Picture showing the developed PCB. This PCB connects all electronics to the micro controller. The use of a PCB ensures good low noise connections for the analogue signals.

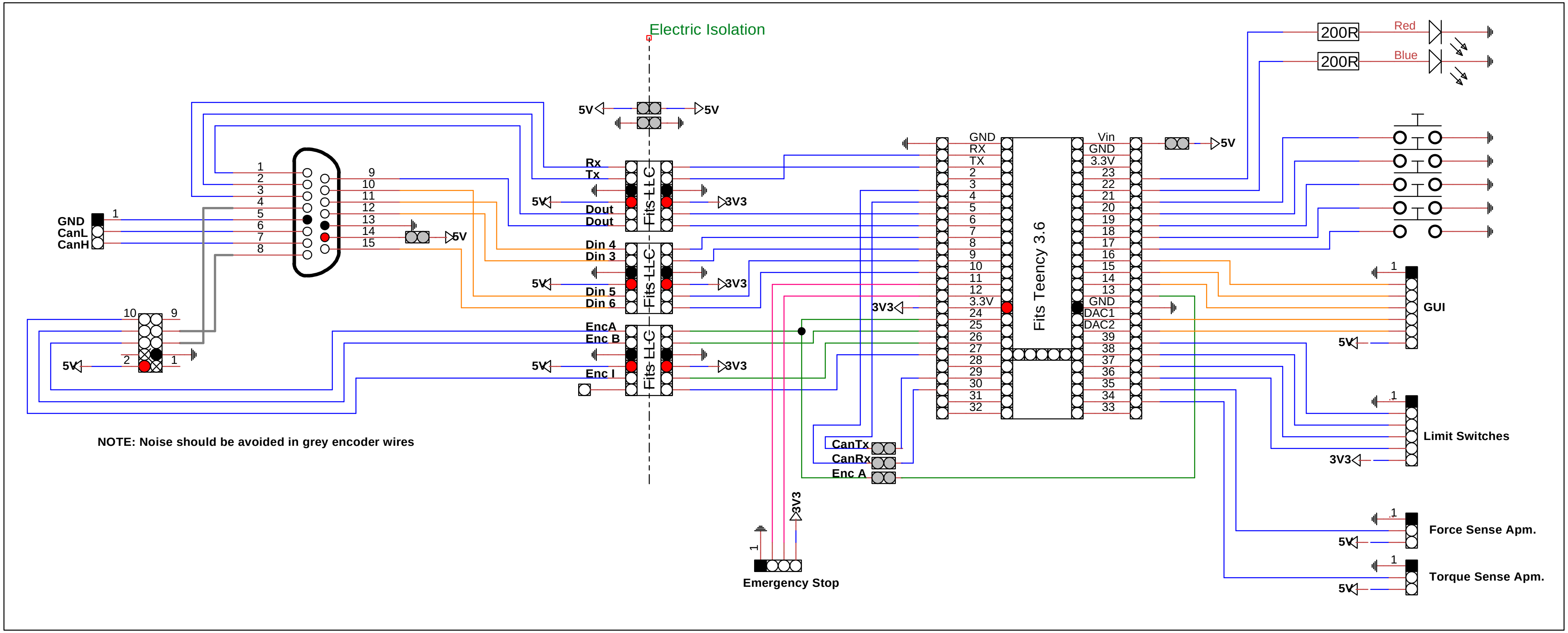

Electric Isolation
5V
5V
Rx
Tx
5V
Dout
Dout
3V3
Fits LLC
Din 4
Din 3
5V
Din 5
Din 6
3V3
Fits LLC
EncA
Enc B
5V
Enc I
3V3
Fits LLC
GND
CanL
CanH
1
1
2
3
4
5
6
7
8
9
10
11
12
13
14
15
5V
10
9
2
1
5V
GND
RX
TX
2
3
4
5
6
7
8
9
10
11
12
3.3V
24
25
26
27
28
29
30
31
32
Fits Teency 3.6
Vin
GND
3.3V
23
22
21
20
19
18
17
16
15
14
13
GND
DAC1
DAC2
39
38
37
36
35
34
33
3V3
5V
CanTx
CanRx
Enc A
3V3
1
Emergency Stop
200R
Red
200R
Blue
1
GUI
5V
1
Limit Switches
3V3
1
Force Sense Apm.
5V
1
Torque Sense Apm.
5V

NOTE: Noise should be avoided in grey encoder wires

3x1 female header

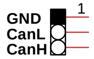

GND
CanL
CanH
1

5x2 male header

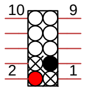

1 N.C.
2 V_{CC}
3 GND
4 N.C.
5 Channel $\bar{A}$
6 Channel A
7 Channel $\bar{B}$
8 Channel B
9 Channel $\bar{I}$ (Index)
10 Channel I (Index)

DB-15

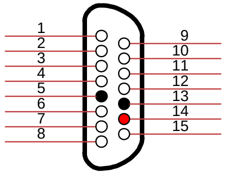

1
2
3
4
5
6
7
8
9
10
11
12
13
14
15

1 Dout
2 TX
3 RX
4 Enc A
5 GND
6 CanL
7 CanH
8 Enc B
9 Dout
10 Din 5
11 Din 4
12 Din 3 (PWM)
13 GND
14 5V
15 Din 6

2x 5x1 female header
to fit SparkFun Logic Lev. Converter
BOB-12009

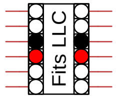

2x 24x2 female header
to fit Teency 3.6
with extra row of female headers

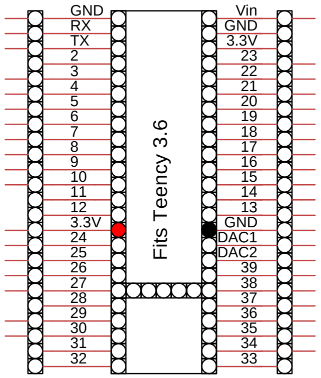

GND
RX
TX
2
3
4
5
6
7
8
9
10
11
12
3.3V
24
25
26
27
28
29
30
31
32
Fits Teency 3.6
Vin
GND
3.3V
23
22
21
20
19
18
17
16
15
14
13
GND
DAC1
DAC2
39
38
37
36
35
34
33

Jumper (2x1 male header)

e.g. Molex

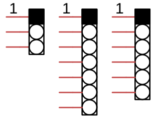

Title
Ring-Screw main PCM

Author
Elco Heijmink
IIT

File
C:\Users\elco\Dropbox\RingS ... RS-MC-PCB.dsn

Document

Revision
1.5

Date
29-01-2018

Sheets
1 of 1